



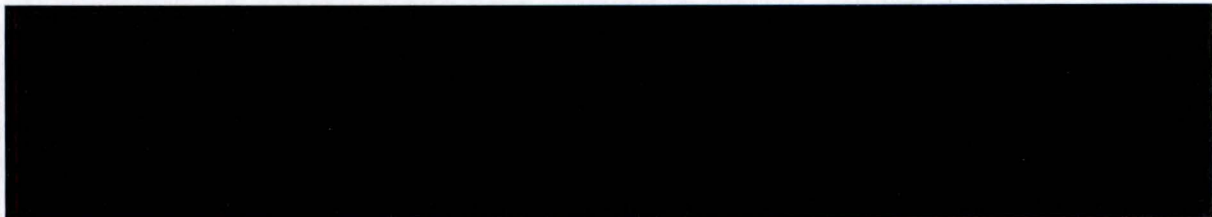
30441R00031
Revision B

REACTOR-BASED MOLYBDENUM-99 SUPPLY SYSTEM PROJECT

MO-99 TARGET ASSEMBLY NUCLEAR DESIGN FOR ONCE-THROUGH OPERATION

Prepared by General Atomics
for the U.S. Department of Energy/National Nuclear Security
Administration and Nordion Canada Inc.

Cooperative Agreement DE-NA0002773



GA Project 30441
WBS 1110



REVISION HISTORY

Revision	Date	Description of Changes
A	26AUG 16	Initial Release
B	19JAN17	Revised to incorporate design changes due to redefinition of MURR limiting core conditions

POINT OF CONTACT INFORMATION

PREPARED BY:			
Name	Position	Email	Phone
Hangbok Choi	Engineer	Hangbok.Choi@ga.com	858-909-5236
APPROVED BY:			
Name	Position	Email	Phone
B. Schleicher	Chief Engineer	Bob.Schleicher@ga.com	858-455-4733
K. Murray	Project Manager	Katherine.Murray@ga.com	858-455-3272
K. Partain	Quality Engineer	Katherine.Partain@ga.com	858-455-3225

DESIGN CONTROL SYSTEM DESCRIPTION

<input type="checkbox"/>	R & D	DISC	QA LEVEL	SYS
<input type="checkbox"/>	DV&S			
<input checked="" type="checkbox"/>	DESIGN			
<input type="checkbox"/>	T&E			
<input type="checkbox"/>	NA	N	II	N/A

TABLE OF CONTENTS

REVISION HISTORY	II
POINT OF CONTACT INFORMATION	II
DESIGN CONTROL SYSTEM DESCRIPTION	II
ACRONYMS	X
1 INTRODUCTION.....	1
1.1 Scope of Work.....	1
1.2 Comparison of RB-MSS with Other System.....	2
1.3 Physics Design and Analysis Methods.....	3
1.3.1 Criticality and neutron flux calculation	3
1.3.2 Depletion calculation	3
1.3.3 ⁹⁹ Mo production calculation	3
2 PHYSICS DESIGN REQUIREMENTS.....	4
2.1 Design Requirements.....	4
2.1.1 Nominal flux and power distribution of the core.....	4
2.1.2 Reactivity effect due to target rod loading	5
2.1.3 Target rod burnup and management.....	5
2.1.4 Reactivity control system.....	5
2.2 MURR Technical Specifications	5
2.3 Physics Design and Analysis Model.....	6
2.3.1 MURR reference core model.....	7
2.3.2 Target assembly loading analysis	12
2.4 Physics Design Computer Codes.....	13
2.4.1 MCNP6 model	13
2.4.2 MCODE and ORIGEN2 model	14
2.4.3 Analytic formulation of Mo-99 production	14
3 DETERMINATION OF TARGET LOADING PATTERN	17
3.1 Target Rod Model Description.....	18
3.1.1 Target assembly dimensions.....	19
3.1.2 Material compositions.....	20
3.1.3 Target assembly MCNP6 model.....	21
3.2 Target Assembly Loading Pattern	24
3.2.1 Selection of bounding values for control blade position	25
3.2.2 Selection of target rod position	26
3.2.3 [REDACTED]	27
3.3 Target Assembly at Reference Position	30
4 PHYSICS PERFORMANCE OF TARGET ASSEMBLY.....	30
4.1 Target Assembly Criticality.....	32
4.2 Impact of Target Assembly Loading on MURR Core	32
4.2.1 Reactivity insertion due to target assembly loading	32
4.2.2 MURR core power peaking due to target assembly loading	33
4.2.3 Core reactivity characteristics.....	35
4.2.4 Kinetic parameters.....	36
4.3 Target Assembly Flux and Power Distribution	37
4.3.1 Base target assembly loading	37
4.3.2 Staggered target assembly loading.....	41

4.3.3	Partial Target Assembly Loading.....	49
4.4	Sensitivity to Control Blade Position for Base Target Assembly Loading	52
4.4.1	Sensitivity of non-critical core cases.....	52
4.4.2	Sensitivity of critical core cases.....	59
4.4.3	Limiting core configuration.....	61
4.4.4	Sensitivity to regulating rod position	62
4.5	Uncertainty Analysis.....	62
4.5.1	Sensitivity calculations.....	63
4.5.2	Total uncertainties of the limiting core performance parameters.....	65
4.6	Target Material Depletion	66
4.7	Structural Component Heating	68
4.7.1	Steady-state structural component heating	68
4.7.2	Post-shutdown structural component heating	70
5	VALIDATION OF METHODS USED IN PHYSICS DESIGN	71
5.1	Validation for Computational Methods and Calculations at MURR	72
5.2	Validation of MURR Control Blade Depletion Model	79
5.3	Advanced Test Reactor Criticality Benchmark Problem.....	89
5.4	Verification of Physics Method for Estimating ⁹⁹ Mo Production.....	92
6	SUMMARY.....	94
7	REFERENCES.....	96
	APPENDIX A MURR FUEL ELEMENT PEAKING FACTORS.....	A-1
	APPENDIX B TARGET ASSEMBLY LINEAR POWER	B-1

LIST OF FIGURES

Figure 2-1.	MURR main chamber	7
Figure 2-2.	MURR core layout	8
Figure 2-3.	MURR map for fuel elements and reflector regions	9
Figure 2-4.	Typical MURR control blade travel during full power operation.....	11
Figure 2-5.	MURR control blade travel during 1/13/2014 and 9/15/2015	11
Figure 2-6.	MCNP6 physics model for the target assembly loading pattern.....	12
Figure 3-1.	Target assembly schematic.....	17
Figure 3-2.	MCNP6 model of the reference target assembly at axial mid-plane.....	22
Figure 3-3.	22
Figure 3-4.	Vertical view of the target assembly	23
Figure 3-5.	Horizontal view of the target rod model	23
Figure 3-6.	Vertical view of the target rod model	24
Figure 3-7.	Target rod numbers and positions.....	24
Figure 3-8.	Axial power distribution of the peak power rod for the maximum burnup core	28

Figure 3-9. Azimuthal power distribution of the peak power node for the maximum burnup core	28
Figure 3-10. Axial power distribution of the peak power rod for the extreme burnup core.....	29
Figure 3-11. Azimuthal power distribution of the peak power node for the extreme burnup core	29
Figure 4-1. Target rod 6 axial neutron flux distribution in position 5A for the base loading	38
Figure 4-2. Target rod 17 axial neutron flux distribution in position 5B for the base loading	38
Figure 4-3. Target assembly azimuthal neutron flux distribution for the base loading	39
Figure 4-4. Power envelope of the base loading for the extreme burnup core	40
Figure 4-5. Power envelope of the base loading for the maximum burnup core	40
Figure 4-6. Target assembly pellet linear power distribution for the base loading	41
Figure 4-7. Target rod 6 axial neutron flux for the staggered loading with fresh assembly in 5A42	
Figure 4-8. Target rod 17 axial neutron flux for the staggered loading with fresh assembly in 5A.....	42
Figure 4-9. Target assembly azimuthal neutron flux for the staggered loading with fresh assembly in 5A.....	43
Figure 4-10. Target rod 6 axial neutron flux for the staggered loading with fresh assembly in 5B.....	43
Figure 4-11. Target rod 17 axial neutron flux for the staggered loading with fresh assembly in 5B.....	44
Figure 4-12. Target assembly azimuthal neutron flux for the staggered loading with fresh assembly in 5B.....	44
Figure 4-13. Power envelope of the staggered loading for the extreme burnup core (fresh target in 5A).....	46
Figure 4-14. Power envelope of the staggered loading for the maximum burnup core (fresh target in 5A).....	46
Figure 4-15. Target assembly pellet linear power distribution for the staggered loading (fresh target in 5A).....	47
Figure 4-16. Power envelope of the staggered loading for the extreme burnup core (fresh target in 5B).....	47
Figure 4-17. Power envelope of the staggered loading for the maximum burnup core (fresh target in 5B).....	48
Figure 4-18. Target assembly pellet linear power distribution for the staggered loading (fresh target in 5B).....	48
Figure 4-19. Target rod 6 axial neutron flux for the partial loading	49

Figure 4-20. Target rod 17 axial neutron flux for the partial loading	50
Figure 4-21. Target assembly azimuthal neutron flux for the partial loading	50
Figure 4-22. Power envelope of the partial loading for the extreme burnup core	51
Figure 4-23. Power envelope of the partial loading for the maximum burnup core.....	51
Figure 4-24. Target assembly pellet linear power distribution for the partial loading	52
Figure 4-25. Variation of target power vs. control blade position	54
Figure 4-26. Variation of peak linear power vs. control blade position	54
Figure 4-27. Variation of driver fuel peaking factor vs. control blade position.....	55
Figure 4-28. MURR control blade age tilt vs age distribution.....	61
Figure 4-29. Estimation of weekly ⁹⁹ Mo production for different loading patterns.....	67
Figure 4-30. Estimation of the target assembly power during 2-week operation	68
Figure 5-1. A detailed MCNP model of the MURR core	72
Figure 5-2. A depiction of the generalized information flow in the modified MONTEBURNS simulation for predicting hot startup ECPs	75
Figure 5-3. A plot of the predicted ECP vs. actual initial critical height	77
Figure 5-4. Cross sectional view of the MURR core	79
Figure 5-5. Axial and radial discretization in the bottom 4" of the MURR MCNP control blade model.....	82
Figure 5-6. Control blade ¹⁰ B reaction rates for; mixed fuel core; 1971 graphite reflector; critical (CB at 17 inches).....	84
Figure 5-7. Control blade ¹⁰ B reaction rates for; mixed fuel core; 2008 graphite reflector; critical (CB at 17 inches).....	84
Figure 5-8. k_{eff} deviations from critical vs. control blade burnup history for fresh control blades and those blades with depletion history modeled.....	86
Figure 5-9. Bottom half-inch radial depletion profiles for control blade number 5-08.....	87
Figure 5-10. Bottom half-inch radial depletion profiles for control blade number 5-08.....	87
Figure 5-11. Axial ¹⁰ B atom density profiles for different residence times for control blade number 5-08	88
Figure 5-12. Comparison of MURR and ATR fuel elements	90
Figure 5-13. MCNP model of ATR core	91

LIST OF TABLES

Table 2-1. Definition of MURR core burnup	10
Table 2-2. Nominal process yield of ⁹⁹ Mo production	16
Table 2-3. Nominal process time of ⁹⁹ Mo production	16
Table 3-1. Pellet parameters (cold dimensions)	19
Table 3-2. Target rod parameters (cold dimensions)	19
Table 3-3. Target assembly parameters	20
Table 3-4. Chemical specification of uranium metal	20
Table 3-5. Chemical composition (wt%) of materials for physics model	21
Table 3-6. Critical control blade position	25
Table 3-7. Expected control blade travelling range for target-loaded core	25
Table 3-8. Sensitivity to the target rod position (2 fresh target assemblies)	27
Table 3-9. Reference target rod loading with critical CB position	30
Table 4-1. K_{eff} and reactivity insertion values for single target assembly	33
Table 4-2. MURR core power peaking due to target assembly loading	33
Table 4-3. MURR fuel element F5 power peaking factors	34
Table 4-4. Reactivity coefficients of core with two fresh target assemblies	35
Table 4-5. Reactivity device worth with two target assemblies	36
Table 4-6. Kinetic parameters of the core with and without target assemblies	37
Table 4-7. Calculated target power level and linear power	39
Table 4-8. Calculated target power level and pellet linear power of the staggered loading	45
Table 4-9. Calculated target power level and pellet linear power of the partial loading	49
Table 4-10. Sensitivities of target assembly power and core peaking factors for the base loading	53
Table 4-11. Sensitivities of target assembly power and core peaking factors for the staggered loading (5A)	56
Table 4-12. Sensitivities of target assembly power and core peaking factors of the staggered loading (5B)	57
Table 4-13. Sensitivities of target assembly power and core peaking factors for the partial loading	58
Table 4-14. Control blade age model for critical core conditions	59
Table 4-15. Sensitivity of target assembly power and peaking factors for the critical core of the base loading	60
Table 4-16. Effect of regulating rod position on target power and peak linear power	62

Table 4-17. Material impurities for uncertainty analysis	63
Table 4-18. Uncertainty of core eigenvalue due to simulation and manufacturing	64
Table 4-19. Uncertainty of target power due to simulation and manufacturing	64
Table 4-20. Uncertainty of peak linear power due to simulation and manufacturing	65
Table 4-21. Total uncertainty of the performance parameter	66
Table 4-22. Target material composition and burnup for the average burnup core	67
Table 4-23. Component radiation heating of the maximum burnup core	69
Table 4-24. Spatial distribution of Be reflector radiation heating for the maximum burnup core	69
Table 4-25. Spatial distribution of Be reflector radiation heating for the minimum burnup core	70
Table 5-1. A comparison of predicted initial critical rod height vs. actual at the MURR	76
Table 5-2. A Comparison of the predicted ECP vs recorded rod height data for an actual hot startup from an unscheduled-shutdown event	78
Table 5-3. A Comparison of the predicted ECP vs recorded rod height data for an actual failed hot startup from an unscheduled-shutdown event	78
Table 5-4. Deviations for the estimated k_{eff} values from critical for the case with fresh control blades (from feasibility study) and with depleted blades	85
Table 5-5. Comparison of MURR and ATR core characteristics	89
Table 5-6. ATR criticality benchmark calculation	92
Table 5-7. Comparison of ^{235}U cross sections	93
Table A-1. MURR fuel element 1 peaking factor for the maximum burnup core (CB=44 cm) ..	A-2
Table A-2. MURR fuel element 2 peaking factor for the maximum burnup core (CB=44 cm) ..	A-3
Table A-3. MURR fuel element 3 peaking factor for the maximum burnup core (CB=44 cm) ..	A-4
Table A-4. MURR fuel element 4 peaking factor for the maximum burnup core (CB=44 cm) ..	A-5
Table A-5. MURR fuel element 5 peaking factor for the maximum burnup core (CB=44 cm) ..	A-6
Table A-6. MURR fuel element 6 peaking factor for the maximum burnup core (CB=44 cm) ..	A-7
Table A-7. MURR fuel element 7 peaking factor for the maximum burnup core (CB=44 cm) ..	A-8
Table A-8. MURR fuel element 8 peaking factor for the maximum burnup core (CB=44 cm) ..	A-9
Table A-9. MURR fuel element 1 peaking factor for the extreme burnup core (CB=30 cm) ...	A-10
Table A-10. MURR fuel element 2 peaking factor for the extreme burnup core (CB=30 cm) .	A-11
Table A-11. MURR fuel element 3 peaking factor for the extreme burnup core (CB=30 cm) .	A-12
Table A-12. MURR fuel element 4 peaking factor for the extreme burnup core (CB=30 cm) .	A-13
Table A-13. MURR fuel element 5 peaking factor for the extreme burnup core (CB=30 cm) .	A-14
Table A-14. MURR fuel element 6 peaking factor for the extreme burnup core (CB=30 cm) .	A-15
Table A-15. MURR fuel element 7 peaking factor for the extreme burnup core (CB=30 cm) .	A-16

Attachment 6

Table A-16. MURR fuel element 8 peaking factor for the extreme burnup core (CB=30 cm). A-17
Table B-1. Target assembly linear power for the maximum burnup core (CB=44 cm) B-2
Table B-2. Target assembly linear power for the average burnup core (CB=40 cm)..... B-3
Table B-3. Target assembly linear power for the minimum burnup core (CB=30 cm) B-4
Table B-4. Target assembly linear power for the extreme burnup core (CB=30 cm)..... B-5



ACRONYMS

Acronym	Description
ANL	Argonne National Laboratory
ANS	American Nuclear Society
ANSI	American National Standards Institute
ASME	American Society of Mechanical Engineers
ATR	Advanced Test Reactor
Be	Beryllium
BOC	Beginning Of Cycle
BOL	Beginning Of Life
CB	Control Blade
CHF	Critical Heat Flux
CHFR	Critical Heat Flux Ratio
cm	Centimeter
ECP	Estimated Critical Position
ENDF	Evaluated Nuclear Data File
EOC	End Of Cycle
EOL	End Of Life
FPD	Full Power Day
GA	General Atomics
GTRI	Global Threat Reduction Initiative
HEU	Highly Enriched Uranium
HM	Heavy Metal
HPC	High Performance Computing
ICSBEP	International Criticality Safety Benchmark Evaluation Project
ID	Inner Diameter
INL	Idaho National Laboratory
IRPhEP	International Reactor Physics Experiment Evaluation Project
JENDL	Japanese Evaluated Nuclear Data Library
k_{eff}	Effective multiplication factor
kW(t)	Kilo Watt Thermal
LEU	Low enriched uranium

Acronym	Description
LOFA	Loss Of Flow Accident
LP	Linear Power
LWR	Light Water Reactor
MCNP	Monte Carlo N-Particle
MCODE	MCNP-ORIGEN Depletion Program
MIT	Massachusetts Institute of Technology
MITR	MIT Nuclear Research Reactor
MoO ₂ Cl ₂	Moly Oxy Chloride
MURR	University of Missouri Research Reactor
MWd	Mega Watt Day
MW(t)	Mega Watt Thermal
NDR	Nuclear Design Report
NNSA	National Nuclear Security Administration
NUREG	Nuclear Regulatory Commission Regulation
pcm	Per Cent Mille
ppm	Part Per Million
RB-MSS	Reactor-Based Mo-99 Supply System
RMS	Root-Mean-Square
Tc	Technetium
UO ₂	Uranium Dioxide
U.S. NRC	United State Nuclear Regulatory Committee
U ₃ O ₈	Tri-uranium octoxide
wt%	Weight Percent
Zircaloy	Zirconium alloy

1 INTRODUCTION

Technetium-99m (^{99m}Tc) is the most commonly used medical isotope today, accounting for about 50,000 medical imaging procedures daily in the United States [Whipple 2009]. ^{99m}Tc is known to be very accurately penetrating into human body, efficiently detected by scintillation instruments, low residual dose to a patient owing to a short half-life (6.01 hours) and flexible in fabricating various tracers depending on diagnostic use. ^{99}Mo is a unique mother isotope of ^{99m}Tc that decays to ^{99m}Tc by β -emission, becomes ^{99}Tc by isomeric transition and stabilizes to ^{99}Ru . ^{99}Mo can be produced through neutron capture reaction of Mo. However, the specific activity of the product is very low because of a small cross section of (n, γ) reaction. On the other hand, nuclear fission is known to be a more favorable method, which provides a high specific activity and massive production, although it requires radioactive waste treatment of all the fission products and actinides.

Due to the expected shortage of ^{99}Mo supply, National Nuclear Security Administration (NNSA) announced a funding opportunity entitled "Low Enriched Uranium (LEU) fission target technology and accelerator technology for demonstration and full-scale production of a reliable, domestic supply of Molybdenum-99 without the use of Highly Enriched Uranium (HEU)." Based on the projected demand of ^{99}Mo , the technology is required to produce 3,000 6-day curies of ^{99}Mo per week, steady state, defined as greater or equal to 48 weeks per year.

1.1 Scope of Work

The Nuclear Design Report (NDR) describes physics design analysis results of the target rod (or pin)/assembly for ^{99}Mo production. Multiple target rods (i.e., assembly) are used as a component of Reactor-based Mo-99 Supply System (RB-MSS) that produces ^{99}Mo via nuclear reactions. The target rods have been specifically designed to be loaded in the reflector region of University of Missouri Research Reactor (MURR).

The physics analyses have been conducted to determine target assembly configuration, target rod and pellet sizes, pellet enrichment, criticality, power distribution and ^{99}Mo production in conjunction with thermal-mechanical and thermal-hydraulic design analyses. This report describes nuclear performance of target assembly and its impact on MURR core performance. This report shall be further used for:

- license amendment application to the United State Nuclear Regulatory Committee (U.S. NRC),
- safety analysis of the target rod/assembly,
- radiation analysis of the target rod/assembly and
- selection of target rod/assembly operational schemes and performance analysis of ^{99}Mo production.

1.2 Comparison of RB-MSS with Other System

The target rod uses LEU to produce ^{99}Mo as a fission product of nuclear reaction and is loaded in the reflector region of MURR with its own cooling system. In order to understand design specifications of RB-MSS target rod, a nuclear device which has similar characteristics, in terms of its configuration and constituent materials, is reviewed and summarized here.

The Massachusetts Institute of Technology (MIT) Nuclear Research Reactor (MITR) fission converter is a nuclear fission device of a higher intensity beam, designed to convert neutrons from the MITR to neutrons with a fission spectrum. The fission converter consists of an array of up to 11 MITR fuel elements arranged on a fuel grid plate located in the fission converter tank. The fission converter design was reviewed by NRC for several design parameters such as criticality, power level and power distribution, which are summarized as follows:

- Subcriticality and self-sustaining chain reaction was evaluated by the Monte Carlo N-Particle (MCNP) code [LANL 2003]. The estimated highest k_{eff} was 0.670, which is low enough to preclude a criticality accident in the converter and is well below the limit established for MITR fuel storage racks ($k_{\text{eff}} < 0.90$). The highest reactivity due to the converter operation is $0.00125 \Delta k/k$, which is within the limit established for the MITR for a movable experiment with a limit of $0.002 \Delta k/k$.
- The highest power level of the fission converter is 251 kW(t) or 316 kW(t) depending on placement of the aluminum block when the reactor power level is 10 MW(t). The licensed power level of MITR is 6 MW(t).
- The hot channel factor of the fission converter was estimated by MCNP under the assumption that all power is deposited in the fuel region. The technical specification requires that the nuclear hot channel factor not exceed 1.53 for the fresh fuel condition to satisfy the safety limits and the limiting safety system settings.

The evaluation concluded that the fission converter facility is a complex experimental facility but it is a subcritical array of fuel and cannot maintain a self-supporting chain reaction like a reactor. In addition, similar to the RB-MSS target assembly, the fission converter cannot perform its irradiation function without the MITR operation. The conclusions were based on acceptance criteria that are stated in several documents, such as NUREG-1537, "Guidelines for Preparing and Reviewing Applications for the Licensing of Non-Power Reactors," and American National Standard ANSI/ANS-15.1-1990, "The Development of Technical Specifications for Research Reactors" (ANS-1 5.1) as applied to experiments [NRC 1999].

1.3 Physics Design and Analysis Methods

The starting point of the physics design is to collect relevant details of engineering design of the target rod, which includes size of the rod, number of target rods, operating conditions, material selection, etc. General Atomics (GA) has conducted independent studies on RB-MSS for various reactor types and target rod/assembly concepts, and narrowed down to a feasible target rod/assembly concept specifically for MURR [Choi 2011, Choi 2015a]. The basic method and computer codes used for physics design are outlined.

1.3.1 Criticality and neutron flux calculation

The physics calculations are conducted by the Monte Carlo code MCNP6 using Evaluated Nuclear Data File (ENDF)/B-VII.1 [Parsons 2012, Conlin 2013] to obtain eigenvalue and neutron flux distribution. The MCNP6 calculations also generate fission energy deposition averaged over a cell (F7 tally) which are used to obtain the driver fuel and target assembly power. Neutron flux averaged over a cell (F4 tally) is used to obtain isotopic cross sections of ^{235}U , ^{238}U , ^{239}Pu and ^{99}Mo using tally multiplier for individual segment of the target rod, i.e., pellet. For the physics calculations, 100 million active source histories ($10,000 \times 10,000$) are used, which gives a standard deviation (1σ) of eigenvalue less than 0.01%.

1.3.2 Depletion calculation

Depletion calculation of the target assembly is conducted by the MCNP-ORIGEN Depletion Program (MCODE) [Xu 2006], which is an open source linkage-program for combining MCNP6 and the one-group depletion code ORIGEN2 [Croff 1980]. In this coupled simulation, MCNP6 generates neutron flux distribution and cross section tables for the target materials, while the ORIGEN2 code performs the depletion calculation using its full burnup chain and the MCNP6 results, followed by updating target materials consistent with MCNP6 format and repeating this process for multiple depletion steps. It is known that the standalone ORIGEN2 calculation has limited applications because of its cross section library generated for conventional Light Water Reactor (LWR) fuel lattice and burnup [NRC 1997]. The MCNP-ORIGEN coupling enables consistent use of the MCNP cross section data for the depletion calculation with much less computing time when compared to a stand-alone MCNP6 burnup calculation.

1.3.3 ^{99}Mo production calculation

The ^{99}Mo production is calculated analytically by the Bateman equation using microscopic cross sections (capture and fission) obtained from MCNP6. In the analytic equation, the variation of ^{99}Mo number density is represented by its production and loss rate, where the production includes fission yields from all actinides while the loss includes decay and neutron capture. The detailed equations are provided in Section 2.4.3.

2 PHYSICS DESIGN REQUIREMENTS

The physics design requirements of the target rod/assembly are different from those of commercial or research reactor fuels. However, there are also similarities between these systems such that both systems use nuclear materials to maintain fission reactions and they should satisfy safety limits during normal and transient operations. The system design requirements are driven from system functions which are as follows:

- The target rods produce ^{99}Mo and other desired fission product isotopes at the required rate when subject to neutron irradiation from in the graphite reflector region of the MURR core.
- The target rods maintain the pellet configuration such that the target rod/assembly is safely sub-critical by itself and such that the coupled target rod/assembly and MURR core are safely controllable by the MURR reactivity control system.

2.1 Design Requirements

The RB-MSS shall use two graphite reflector positions of the MURR for target rod loading to meet the performance production goal. The maximum allowable ^{235}U enrichment of the target material is 19.75 wt%. Before the commercial operation of RB-MSS, prototype target assemblies will be irradiated to demonstrate the ^{99}Mo production process and integrity of the target rod. The ultimate design goals of RB-MSS are:

- The commercial operation shall be capable of delivering 3,000 6-day curies (defined as number of curies 6 days after production) of ^{99}Mo per week in a steady-state mode, given operation of MURR at 10 MW(t) for 152 consecutive hours before shutdown for 16 hours per week.
- The prototype operation shall provide 1,500 6-day curies per week.

The physics design and analysis of the target assembly includes evaluation of the target assembly and MURR core performance as summarized below.

2.1.1 Nominal flux and power distribution of the core

The nominal power of the MURR core is 10 MW(t) with and without target rod loading. Because the target assembly loading in the reflector region affects the nominal power distribution of the MURR core, the perturbation of the neutron flux and power distribution shall be evaluated and shown to acceptable within the MURR operating limits. The limiting operating conditions of the target assembly in terms of the peak linear power and total power shall be used for the cooling system design and safety analysis of the target assembly system.

2.1.2 Reactivity effect due to target rod loading

The reactivity effects due to target assembly loading as a result of postulated accident conditions shall be estimated, which is necessary to evaluate the performance of existing control/safety system. The reactivity effects that should be known for representative core conditions are the fuel temperature coefficient of reactivity, coolant temperature coefficient of reactivity, coolant density effect (partial and full voiding), sub-criticality of the target rods, and reactivity insertion due to target rod loading. The requirements of the reactivity effect are specified in MURR Technical Specifications 3.1, 3.2, 3.8, and 5.3 which are described in Section 2.2.

2.1.3 Target rod burnup and management

The base target operating scheme is [REDACTED] full power continuous irradiation in two reflector positions. Depending on the ^{99}Mo demand, the irradiation time could be either shortened or extended. Detailed (pellet-wise) power distribution and burnup of the target rod shall be estimated and used for thermal/mechanical analysis of the target rod.

5a, d,
e, f

2.1.4 Reactivity control system

The static reactivity worth of the control rods (blades) must be adequate to permit the power to be quickly adjusted to the desired value even with the target assembly loading. The static reactivity insertion characteristics of the control rods shall be estimated. From the safety view point, the dynamic reactivity and dynamic power transients following a reactor trip in response to reactivity excursion are more important. These transients shall be calculated in the Safety Analysis.

2.2 MURR Technical Specifications

MURR Technical Specifications describe the reactivity condition of the reactor and the reactivity worth of control blades and experiments to assure that the reactor can be shut down at all times and to assure that the reactor core safety limits will not be exceeded [MURR 2006]. The limiting conditions for operation, including reactivity limitations, are summarized below.

- (3.1.a) The reactor core excess reactivity above reference core condition shall not exceed $0.098 \Delta k/k$. Here, Technical Specification 1.27 defines the reference core condition as the condition of the core when it is at ambient temperature (cold) and the reactivity worth of xenon is negligible ($< 0.002 \Delta k/k$).
- (3.1.b) The reactor shall be subcritical by a margin of at least $0.02 \Delta k/k$ with the most reactive shim blade and the regulating blade in the fully withdrawn positions.
- (3.2.d) The maximum rate of reactivity insertion for the regulating blade shall not exceed $1.5 \times 10^{-4} \Delta k/k/\text{sec}$.

- (3.2.e) The maximum rate of reactivity insertion for the four (4) shim blades operating simultaneously shall not exceed $3.0 \times 10^{-4} \Delta k/k/\text{sec}$.
- (3.8.a) The absolute value of the reactivity worth of each secured removable experiment shall be limited to $0.006 \Delta k/k$.
- (3.8.b) The absolute value of the reactivity worth of all experiments in the center test hole shall be limited to $0.006 \Delta k/k$.
- (3.8.c) Each movable experiment or the movable parts of any individual experiment shall have a maximum absolute reactivity worth of $0.001 \Delta k/k$.
- (3.8.d) The absolute value of the reactivity worth of each unsecured experiment shall be limited to $0.0025 \Delta k/k$.
- (3.8.e) The absolute value of the reactivity worth of all unsecured experiments which are in the reactor shall be limited to $0.006 \Delta k/k$.
- (5.3.a) The average reactor core temperature coefficient of reactivity shall be more negative than $-6.0 \times 10^{-5} \Delta k/k/^\circ\text{F}$ ($-1.08 \times 10^{-4} (\Delta k/k)/^\circ\text{C}$).
- (5.3.b) The average core void coefficient of reactivity shall be more negative than $-2.0 \times 10^{-3} \Delta k/k/\%$ void.
- (5.3.d) The regulating blade total reactivity worth shall be a maximum of $6.0 \times 10^{-3} \Delta k/k$.

Technical Specification 1.35 defines the secured experiments as follows:

"A secured experiment is any experiment which is rigidly held in place by mechanical means with sufficient restraint to withstand any anticipated forces to which the experiment might be subjected to."

Considering the mechanical structure of the target rods and assemblies of RB-MSS and duration of irradiation in the reactor system, the technical demonstration of RB-MSS has been categorized as a "secured experiment". Therefore, Technical Specifications (3.2.e) and (3.8.b) to (3.8.e) are not relevant to the nuclear design analysis of the target rod/assembly.

2.3 Physics Design and Analysis Model

MURR is a pressurized, reflected, open pool-type, light water moderated and cooled, heterogeneous system designed for operation at a maximum steady-state power level of 10 MW(t). The MURR core consists of eight fuel elements, each having identical physical dimensions. The main chamber of the MURR is shown in Figure 2-1. Staffs of MURR and GA

agreed to use "MURR2015 reflector development MCNP model", dated 2/4/2015, as the reference MCNP model of the MURR core for the target assembly design and safety analysis [GA 2015].

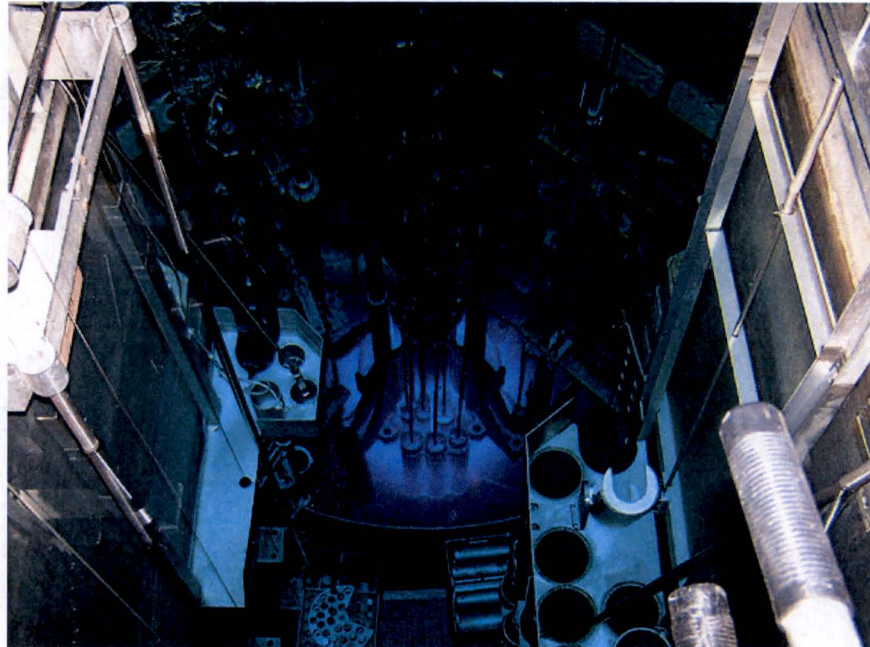


Figure 2-1. MURR main chamber

2.3.1 MURR reference core model

The MURR2015 model describes reactor core and associated facilities that incorporate detailed control blade (CB) geometry and graphite reflectors. The model was established for use in MCNP calculations to obtain the flux profiles and for further use in determining the thermal-hydraulic behavior of the MURR core during upset and accident conditions. In this model, the north-south plane is offset 22.5 degrees clock-wise to facilitate modeling of the individual MURR fuel elements. All annotated descriptions are with respect to this offset axis. Elements of a typical mixed fuel MURR core are considered in this model, i.e., fuel burnup is considered. Also considered are CB age, beryllium (Be) reflector age, reduced water density, and component temperatures. The coolant and pool water densities are 0.98622 and 0.99254 g/cm³, respectively. The horizontal and vertical layouts are shown in Figure 2-2 [McKibben 2006].

The current HEU fuel elements are placed vertically around an annulus between two cylindrical aluminum reactor pressure vessels. The fuel element has 24 curved plates that form a 45-degree arc. The fuel plates are 0.127 cm (0.050 inches) thick. The fuel meat is 0.0508 cm (0.02 inches) thick in each plate and consists of UAl_x aluminide fuel containing uranium with a ²³⁵U enrichment of ~93%. The fuel plates are clad with 0.0381 cm (0.015 inches) of Al-6061 aluminum. The fuel

plates are 64.77 cm (25.5 inches) long, with an active fuel meat length of 60.96 cm (24 inches). The plate and meat width varies by plate with each plate having two unfueled edges that are each 0.3683 cm (0.145 inches) wide.

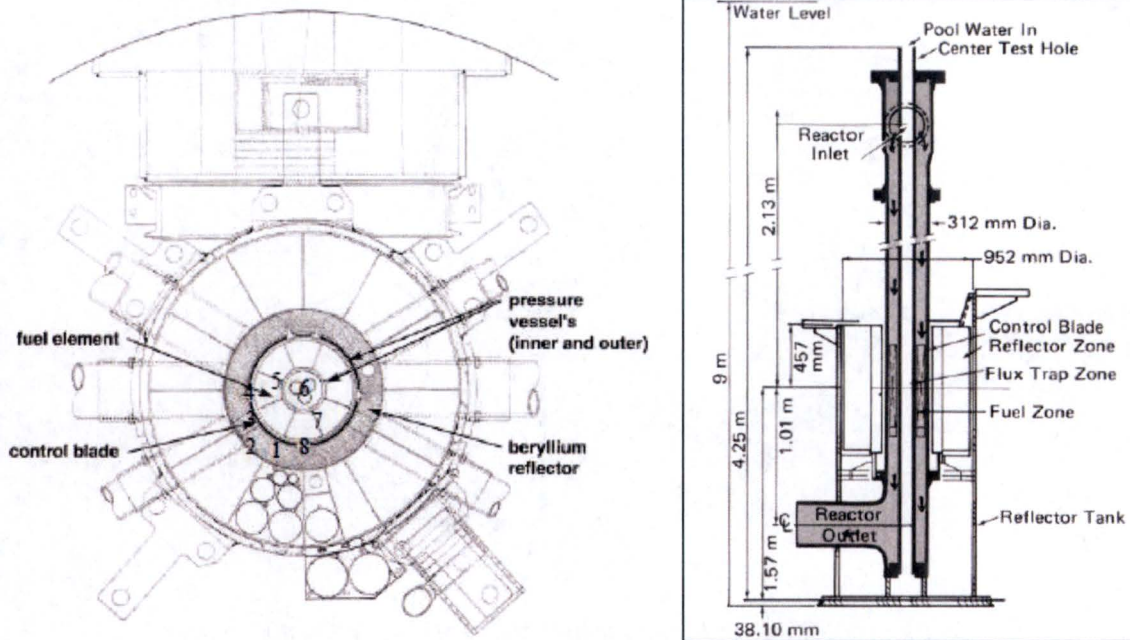


Figure 2-2. MURR core layout

2.3.1.1 Core configuration

The MURR core has a fixed geometry consisting of eight fuel elements, each having identical physical dimensions. The fuel elements are placed vertically around an annulus between two cylindrical aluminum reactor pressure vessels. Cross-sectional views of the MURR reactor core, control blades, reflector, and experimental holes are shown in Figure 2-3.

MURR is currently licensed for a maximum core power of 10 MW(t). This power level provides neutron flux levels in the center flux trap and irradiation positions in the graphite reflector to enable MURR to fulfill its mission of providing experimental and irradiation services to a variety of users. The RB-MSS will install two target assemblies in wedge L (reflector 5A) and N (reflector 5B).

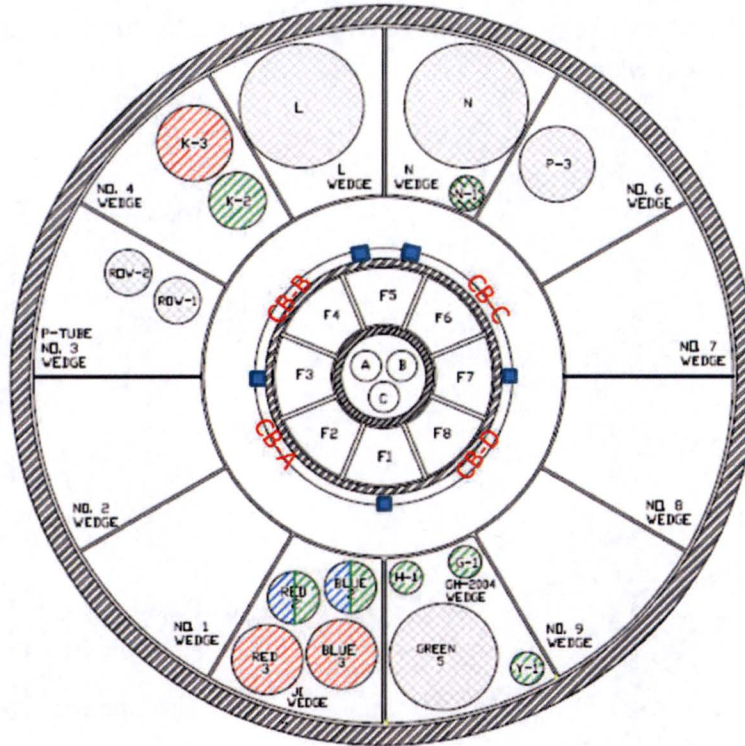


Figure 2-3. MURR map for fuel elements and reflector regions

2.3.1.2 Driver fuel element loading pattern

MURR operates continuously with the exception of a weekly scheduled shutdown. The averaged operation time is approximately 6.33 days (152 hours) per week at full power. A core loading will always consist of four different pairs of elements, with the two elements of each pair loaded opposite of each other in the core. Elements are loaded at beginning-of-cycle (BOC) under xenon-free conditions. Previously irradiated elements are kept in the storage baskets for two or three weeks before being reused in the reactor to allow for decay of the ^{135}Xe . Typically a fuel element will be used in 18 to 20 different core loadings before being retired from the fuel cycle with an average discharge burnup of ~150 Megawatt days (MWd).

Fresh elements are always loaded in core positions F1 or F5. In subsequent cycles, an element will usually be alternated between the two positions (i.e., loaded in first in position F1, then in position F5, etc.). The elements will typically be re-loaded in either of these two positions about 4 or 5 times before being transitioned to positions F3/F7 of the core. After 4 or 5 cycles in the F3/F7 positions, the element is alternated between the F2/F6 positions, and then finally discharged from either the F4/F8 position [Stillman 2013].

Table 2-1 shows the average, minimum, and maximum fuel burnup of the core, which are used for the target design and analysis. The average total core burnup in the equilibrium cycles is roughly 600 MWd. The average burnup of the fuel element is lowest in the F1/F5 positions, followed by F3/F7, F2/F6, and F4/F8. An extreme burnup core concept is also used to represent a core loading pattern that could create the worst power peaking in both the driver and target assemblies. This was a near-maximum burnup core with a fresh and a to-be-discharged element adjacent to each other in the F1 and F8 positions (and F5 and F4), respectively.

Table 2-1. Definition of MURR core burnup

Driver fuel	Extreme burnup core <core_ext>	Minimum burnup core <core_min>	Average burnup core <core_avg>	Maximum burnup core <core_max>
Xenon	Clean	Clean	Equilibrium	Equilibrium
F1	0	0	19	3
F2	117	20	92	122
F3	67	18	60	68
F4	142	142	130	145
F5	0	0	19	3
F6	117	20	92	123
F7	67	18	60	68
F8	142	142	130	144
Core total (MWd)	652	360	600	676

2.3.1.3 Control blade position

Four CBs and one regulating rod are partially inserted in the core during normal operation. The CB position is affected by the driver fuel depletion, CB absorber material depletion, and degradation of reflector material. Figure 2-4 shows a typical estimated critical position (ECP) of CB (tip distance from fully-inserted CB tip position) during full power operation. The ECP was generated for Core 14-03 and Core 14-37 in 2014 for the aged and fresh beryllium reflector, respectively. For the typical operation cycle of MURR core, the control blade reaches its equilibrium height about 48 hours (Day-2 state) after startup and slowly withdraws until the end of cycle (EOC).

During 2014 – 2015 operation, the lowest startup and highest shutdown critical position was recorded at CB position of 32.69 cm and 61.6 cm, respectively [Peters 2016]. These two CB positions are used as bounding values that include various reactor perturbations such as Be

reflector installation, CB replacement and experimental loading/unloading. Figure 2-5 shows CB movement during 19-month operation in 2014 and 2015. The average CB age during this period is 4.7 to 5.7 years.

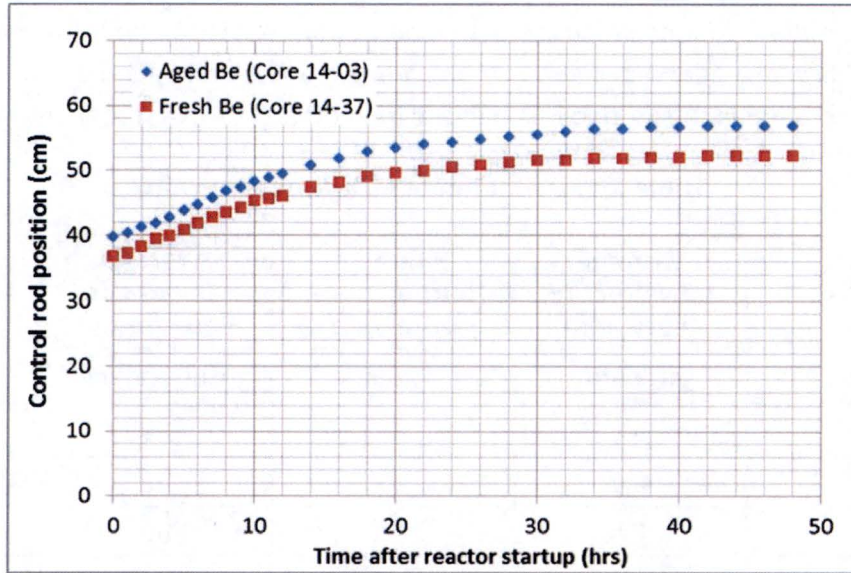


Figure 2-4. Typical MURR control blade travel during full power operation

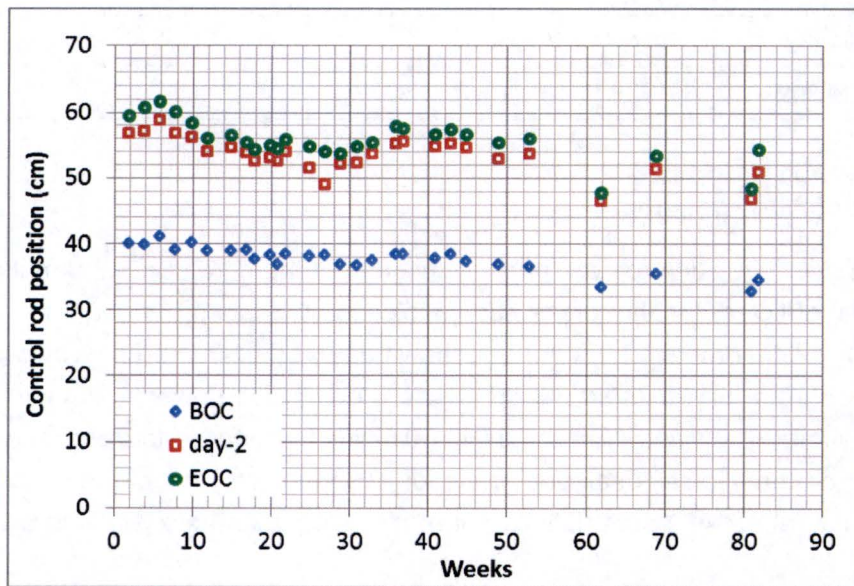


Figure 2-5. MURR control blade travel during 1/13/2014 and 9/15/2015

2.3.2 Target assembly loading analysis

The loading pattern of target rod is to place two sets of 11-rod assembly side-by-side in the graphite reflector 5A and 5B positions of the MURR, shown in Figure 2-6, which are equivalent to Wedge L and N in Figure 2-3. The target assembly loading position was systematically searched such that the peak linear power of the target rod and total target assembly power are within the design limits of the critical heat flux ratio (CHFR) and cooling capability in case of loss of flow accident (LOFA), recommended by the thermal-hydraulic design and safety analysis [Chiger 2016; Bolin 2016].

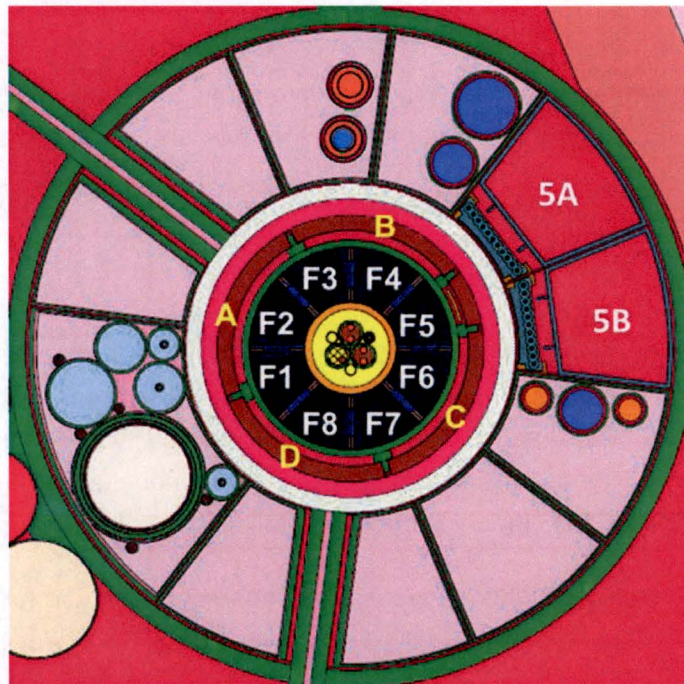


Figure 2-6. MCNP6 physics model for the target assembly loading pattern

In order to accommodate the neutron flux (power) variations of the target due to MURR operating conditions, the analyses of the target loading pattern are conducted as follows:

- Four core burnup states are used to determine CB bounding positions and to assess the core and target assembly performance.
- The core and target assembly performance is evaluated for both the non-critical and critical core conditions according to the CB insertion.
- For all core states, it is assumed that the target material is fresh without impurities to conservatively estimate the target power from the safety analysis view point.

- It is assumed that the Be reflector is fresh to create a higher neutron flux in the target assembly.
- It is assumed that the CB age is tilted such that A & D are fresh and B & C are 8-years old to create a higher power peaking in the target assembly.
- It is assumed that the CB tip position is tilted such that the tip position of B & C is higher than that of A & D by 2.54 cm to create higher power peaking in the target assembly.
- The central flux trap is loaded with sample materials to the maximum reactivity during the operation.
- All the experimental holes are plugged with aluminum and silicon for smaller (Inner diameter (ID) < 2.54 cm) and larger holes (ID > 2.54 cm), respectively.

2.4 Physics Design Computer Codes

2.4.1 MCNP6 model

MCNP6 is a general-purpose Monte Carlo transport code. A variety of nuclear data libraries have been generated for the continuous energy, discrete, multi-group, thermal and dosimetry neutron data [Goorley 2013a; Goorley 2013b]. MCNP6 is used for criticality and neutron flux calculations. In the MURR2015 model, all driver fuel plates are explicitly modeled for fuel meat and cladding of 24×8 fuel plates. The MCNP6 model is briefed as follows:

- A total of 9077 cells and 1362 surfaces are used to construct the full core model.
- Each driver fuel element is modeled by 24 plates with 24 axial numerical meshes. Two axial meshes are grouped into a single material mesh. A total of 2304 materials are defined for the driver fuel.
- The fuel composition have been generated through Argonne National laboratory (ANL)-MURR MCNP model development program of the MURR HEU fuel cycle [Stillman 2012]. The fuel composition consists of ^{234}U , ^{235}U , ^{236}U , ^{238}U , ^{237}Np , ^{238}Pu , ^{239}Pu , ^{240}Pu , ^{241}Pu , ^{242}Pu , ^{241}Am , ^{135}I , ^{135}Xe , ^{149}Pm , and ^{149}Sm and a lumped fission product, which have been obtained by WIMS-ANL [Hanan 1998; Deen 2003; Dionne 2008] and REBUS-3 [Olson 2001] code.
- Each CB (A, B, C and D) is segmented into 292 material zones, resulting a total of 1168 materials.
- Be reflector is modeled by 15 materials (all are fresh).

- All beam tubes, flux trap and experimental holes are explicitly modeled.
- The MCNP6 KCODE option is used for the criticality calculation. A total of 100 million active particles are run for each core simulation.

Validation of MCNP code for predicting critical CB position of MURR was conducted for unscheduled shutdown cores after normal operation as described in Sections 6.1 and 6.2. The deviations between the predictions and actual CB heights are less than 1.0% [Peters 2013]. The validation of CB depletion model was also conducted for a 620 MWD MURR core. The error of core criticality was reduced from 1.1% to 0.41% when the CB depletion model is applied [Peters 2012b]. Additional benchmark test of MCNP6 summarized in Section 6.3 is a criticality calculation of the Advanced Test Reactor (ATR), of which the fuel type, reflector, and coolant are similar to those of MURR, i.e., HEU aluminide fuel, beryllium reflector, and light water coolant [Kim 2005]. The simulation predicts the criticality of the core within 0.2%Δk.

2.4.2 MCODE and ORIGEN2 model

MCODE, as described in Section 1.3.2, is an open source linkage-program for combining MCNP6 and ORIGEN2. The ORIGEN2 code calculates the buildup, decay, and processing of radioactive materials, using the exponential matrix method to solve a large system of coupled linear first-order ordinary differential equations. In this coupled simulation,

- MCNP6 calculates neutron flux distribution and generates cross section tables for the target materials. Each target rod is divided into 50 numerical meshes in the axial direction, while 5 distinct materials are defined vertically for each assembly.
- ORIGEN2 performs the depletion calculation for 10 target materials using its full burnup chain and the cross sections from the MCNP6. The constant neutron flux depletion model is used with time steps automatically selected by the code.
- The target material compositions are updated and fed into MCNP6 for the new flux calculation. The process is repeated for multiple depletion steps.

2.4.3 Analytic formulation of Mo-99 production

The ⁹⁹Mo production is calculated analytically by Bateman equation [Bateman 1910] using microscopic cross sections (capture and fission) obtained from MCNP6. In the analytic equation, the variation of nuclide number density is represented by its production and loss rate. For example, the ²³⁵U, ²³⁸U, and ²³⁹Pu number densities can be written as follows:

$$\frac{dN^5}{dt} = -\sigma_a^5 N^5 \phi \quad (2-1)$$

$$\frac{dN^8}{dt} = -\sigma_a^8 N^8 \varphi \quad (2-2)$$

$$\frac{dN^9}{dt} = \sigma_c^8 N^8 \varphi - \sigma_a^9 N^9 \varphi \quad (2-3)$$

where σ_a^5 , σ_a^8 , σ_a^9 , and σ_c^8 are ^{235}U , ^{238}U , ^{239}Pu absorption cross sections and ^{238}U capture cross section, respectively. Then the number densities at time t under neutron flux φ will be as follows:

$$N^5 = N_0^5 \exp(-\sigma_a^5 \varphi t) \quad (2-4)$$

$$N^8 = N_0^8 \exp(-\sigma_a^8 \varphi t) \quad (2-5)$$

$$N^9 = N_0^9 \exp(-\sigma_a^9 \varphi t) + N_0^8 \left(\frac{\sigma_c^8}{\sigma_a^9 - \sigma_a^8} \right) [\exp(-\sigma_a^8 \varphi t) - \exp(-\sigma_a^9 \varphi t)] \quad (2-6)$$

2.4.3.1 Estimation of ^{99}Mo number density

The ^{99}Mo number density (N^m) in the target pellets during the irradiation period is a balance between ^{99}Mo production from the fission reactions and the loss due to decay and transmutation as follows:

$$\frac{dN^m}{dt} = \gamma^5 \sigma_f^5 N^5 \varphi + \gamma^8 \sigma_f^8 N^8 \varphi + \gamma^9 \sigma_f^9 N^9 \varphi - (\lambda_m + \sigma_a^m \varphi) N^m \quad (2-7)$$

where γ^5 , γ^8 , and γ^9 are ^{99}Mo cumulative yields of ^{235}U (0.06008), ^{238}U (0.06139), and ^{239}Pu (0.05982), respectively. The cumulative yield was obtained from Japanese Evaluated Nuclear Data Library (JENDL)-3 instantaneous fission yield [Nakagawa 2003]. λ_m is a decay constant of ^{99}Mo ($2.92 \times 10^{-6}/\text{sec}$). σ_f^5 , σ_f^8 , σ_f^9 , and σ_a^m are ^{235}U , ^{238}U , ^{239}Pu fission cross section and ^{99}Mo absorption cross section, respectively.

After irradiation, target pins are cooled and sent to the collection system for ^{99}Mo extraction. When extraction starts, the balance of collected ^{99}Mo number density (N^c) is written in terms of collection efficiency (ξ) and decay:

$$\frac{dN^c}{dt} = \xi N^m - \lambda_m N^c \quad (2-8)$$

The verification test of the analytical model has been conducted by ORIGEN2.2 code as summarized in Section 6.4, where the prediction error of ^{99}Mo number density is 0.07% and 0.2% for the target assembly and collection system, respectively [Choi 2015b].

2.4.3.2 Operation scheme of ^{99}Mo supply system

The target pins are continuously irradiated for [REDACTED]. The system will shut down when the MURR is shut down for 16 hours. The ^{99}Mo production process includes several steps until the final product (^{99}Mo) is delivered to the end-user in an appropriate physical form. The best estimate of process efficiency (or yield) and process time of each step are summarized in Table 2-2 and Table 2-3, respectively, for the cooling after irradiation, voloxidation for extraction, purification, etc.

5a, d,
e, f

Volatilization process for separating of ^{99}Mo from the irradiated uranium is a known process, which converts irradiated uranium pellet into powdered U_3O_8 [Motojima 1977]. The oxidation process completely changes the physical form from pellets to powder. The crystal structure also changes, which promotes the release of fission products kept within the crystal of uranium dioxide. To improve the efficiency of ^{99}Mo extraction, a process gas ([REDACTED]) is used, which produces [REDACTED]. Earlier experiments by Rosenbaum et al. [Rosenbaum 1978] have shown the Molybdenum release rate of 99% by weight without using [REDACTED] gas, when the molybdenum content in the pellet is greater than ~300 part per million (ppm). Considering that the process efficiency also depends on the process condition such as temperature and pressure, the collection efficiency of [REDACTED] is used in this analysis.

5a, d,
e, f

Table 2-2. Nominal process yield of ^{99}Mo production

Process	Efficiency
Collection cell process	[REDACTED]
Extraction cell process	[REDACTED]
Nordion purification process	[REDACTED]
Nordion packaging	[REDACTED]
Overall efficiency	[REDACTED]

5a, d,
e, f

Table 2-3. Nominal process time of ^{99}Mo production

Process	Time (hours)
Cooling after shutdown	[REDACTED]
Transportation to collection cell and process	[REDACTED]
Extraction and shipping preparation	[REDACTED]
Shipping to Nordion	[REDACTED]
Nordion purification process	[REDACTED]
Nordion packaging and shipping to customer	[REDACTED]
Six-day delay to customer	[REDACTED]
Overall reduction factor due to process time	[REDACTED]

5a, d,
e, f

3 DETERMINATION OF TARGET LOADING PATTERN

A single target assembly consists of 11 target rods, which are similar to LWR fuel rods except that the diameter and height of the target rod are much smaller than those of the conventional LWR fuel rod. In order to facilitate target assembly loading/unloading and mechanically stabilize the target rods during irradiation, the thermal/mechanical design implemented several supporting and cooling fixtures around the target rods as shown in Figure 3-1. From the neutronics design view point, the whole target assembly structure can be divided into:

- 1) Target rods including UO₂ pellets, cladding, top and bottom end-plugs, and a spacer spring.
- 2) A cassette that forms a flow channel for target rods, along with top and bottom locking fixture.
- 3) Aluminum container that provides a coolant flow path.
- 4) Stainless steel lower water plenum under the target assembly.
- 5) [REDACTED]

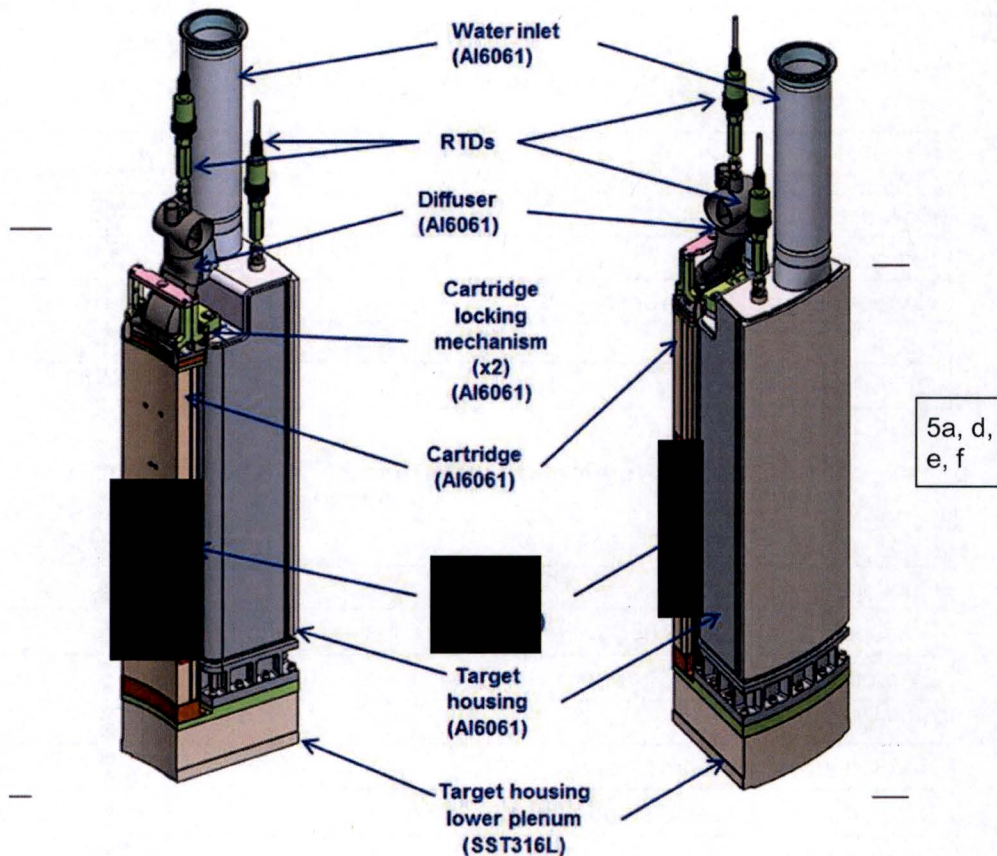


Figure 3-1. Target assembly schematic

Current target assembly design has been established through a series of scoping calculations, which include ^{99}Mo production capability, power distribution and temperature distribution [Choi 2015a]. The design parameters considered during the scoping studies are:

- Target pellet diameter and cladding thickness to estimate the target rod temperature distribution.
- Solid and annular pellet geometry to control peak pellet temperature.
- Active target rod height to increase the ^{99}Mo production rate.
- Variable rod pitches to improve neutron utilization.
- Number of target rods and loading position in the reflector region.
- Reflector material around the target assembly such as graphite, beryllium, and water.
- Axial reflector material of the target rod such as uranium, beryllium and graphite.
- Structural materials such as stainless steel and aluminum to enhance a higher mechanical strength as well as neutron economy.

3.1 Target Rod Model Description

Preliminary investigations of the thermal, mechanical, neutronic performance and manufacturing of the target rod recommended that:

- Use a single enrichment and the same dimensions for all target pellets.
- Solid pellets are preferred. The pellet diameter and pellet-cladding gap are kept small with a thin cladding to accommodate high power density.
- Minimize the use of metal around the target rods to promote thermal neutron population. Aluminum is used as the structural material.
- Use water instead of graphite or beryllium as the moderator.
- Remove top and bottom reflector but keep the spacer spring to minimize the solid waste from the ^{99}Mo collection process.

3.1.1 Target assembly dimensions

Target assembly physical dimensions and materials are summarized in Table 3-1, Table 3-2 and Table 3-3 for the pellet, target rod and target assembly, respectively. The target pellet has dishes and chamfers to reduce the mechanical interaction between the pellet and cladding. Because the pellet is modeled as a solid cylinder in the physics analysis, effective isotopic number densities are used for the pellet composition. It should also be noted that the target rod full height is slightly different from actual height (67.32 cm) in the numerical model.

Table 3-1. Pellet parameters (cold dimensions)

Pellet material	UO ₂
Pellet density (%)	95
Pellet ²³⁵ U enrichment range (wt%)	19.75
Pellet diameter (cm)	0.5
Pellet height (cm)	0.6
Dish height (cm)	0.012
Shoulder width (cm)	0.031
Chamfer height (cm)	0.008
Chamfer width	0.024
Pellet surface roughness	2.0×10 ⁻⁶

Table 3-2. Target rod parameters (cold dimensions)

Target rod full height (cm)	67.22
Target rod active height (cm)	60
Cladding material	Zircaloy-4 (Zirc-4)
Cladding thickness (cm)	0.05
Cladding surface roughness	5.0×10 ⁻⁷
Gap fill material	Helium
Gap width (cm)	0.005
End-plug material	Zirc-4

Table 3-3. Target assembly parameters

Target rod	Number of rods	11
Coolant channel	Number of coolant holes	11 (connected)
	Coolant hole pitch (cm)	1.12
	Coolant hole diameter, maximum (cm)	1.28
	Coolant material	water
	Coolant density (g/cm ³)	0.99339
	Coolant flow rate (m/s)	> 5
	Cassette material	Aluminum 6061-T6
	Cassette thickness, minimum (cm)	0.3
Supporting fixture	Structural material	Aluminum 6061-T6
	Top flange upper section (gram)	141.6
	Top flange middle section (gram)	143.4
	Top flange lower section (gram)	75.2
	Cassette base plate (gram)	416.0

3.1.2 Material compositions

Table 3-4 and Table 3-5 summarize material compositions of uranium and structural materials (Zircaloy-4, Aluminum 6061-T6 and stainless steel 316L) used for physics modeling. The uranium data is from Y-12 standard specification of LEU [Parker 2015]. In the physics analysis, impurities are not included to conservatively estimate the target power. The Zircaloy-4 specifications are provided by a manufacturer [ATI 2016]. The aluminum and stainless steel data are from the American Society of Mechanical Engineers (ASME) specifications [ASME 2011].

Table 3-4. Chemical specification of uranium metal

Element	Units	LEU
Uranium purity	weight %	≥ 99.90
U-232	µg/gU	≤ 0.002
U-234	weight %	≤ 0.260
U-235	weight %	19.75 ± 0.20
U-236	µg/gU	≤ 4,600
Total impurities	µg/gU	≤ 1,000
Equivalent boron content (EBC)	ppm	≤ 3.0

Table 3-5. Chemical composition (wt%) of materials for physics model

	Zircaloy-4	Aluminum	Stainless Steel
Material type	R60804	A96061	316L
Density (g/cm ³)	6.56	2.7	8.03
Aluminum		96.68	
Carbon			0.03
Chromium	0.1	0.195	17.0
Copper		0.275	
Iron	0.21	0.7	66.395
Magnesium		1.0	
Manganese		0.15	2.0
Molybdenum			2.5
Nickel			12.0
Oxygen	0.125		
Phosphorus			0.045
Silicon		0.6	1.0
Sulfur			0.03
Tin	1.45		
Titanium		0.15	
Zinc		0.25	
Zirconium	98.115		
Total	100	100	100

3.1.3 Target assembly MCNP6 model

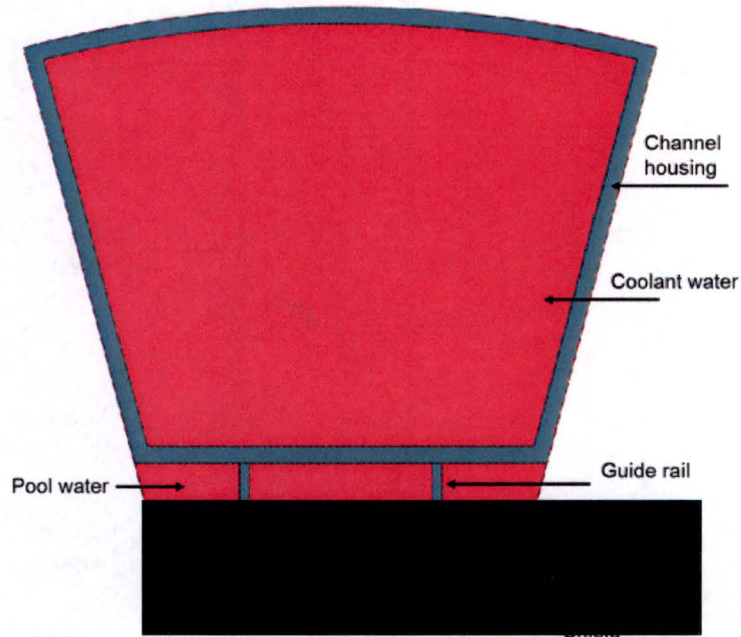
The MCNP6 model of the reference 11-rod target assembly is shown in Figure 3-2 at axial mid-plane [REDACTED]. The horizontal view includes 11 target rods, coolant channel, cartridge, aluminum housing and pool water. The vertical configuration of the target assembly and housing is shown in Figure 3-4. The vertical view doesn't show all the target rods, but it shows overall flow path through the aluminum housing and stainless steel low plenum. Figure 3-5 and Figure 3-6 show the horizontal and vertical views of target rod, respectively. The target pellet, cladding, pellet-cladding gap and upper plenum are explicitly modeled. The target rod numbering is shown in Figure 3-7, where target assemblies 1 and 2 reside in the MURR reflector 5A and 5B positions, respectively.

5a, d,
e, f

The target assemblies have been embedded in the MURR core model as follows:

- 1000 cells are used to define target pellets. Two pellets are defined as a single cell. The fuel gap, dish and chamfer voids are smeared into pellet.

- 100 surfaces are used to define the pellet, cladding, coolant and other structure.
- 10 materials are used for target pellets. 10 materials are used to define other structure.



• Figure 3-2. MCNP6 model of the reference target assembly at axial mid-plane



5a, d,
e, f

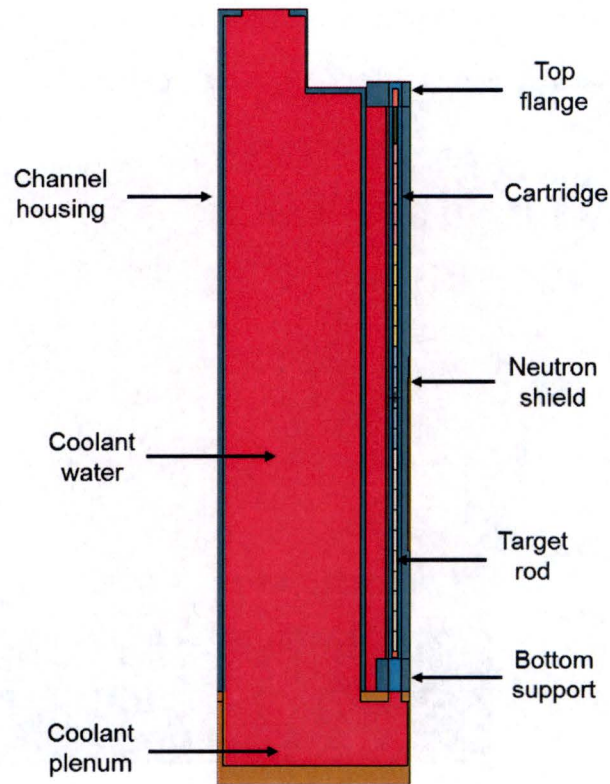


Figure 3-4. Vertical view of the target assembly

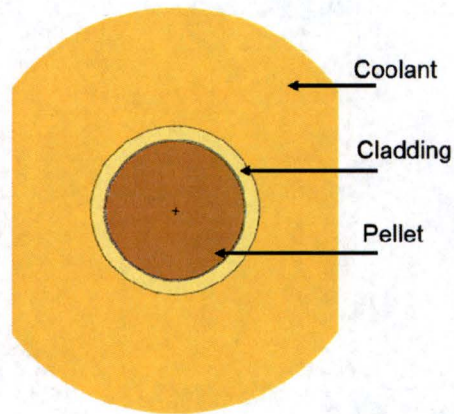


Figure 3-5. Horizontal view of the target rod model

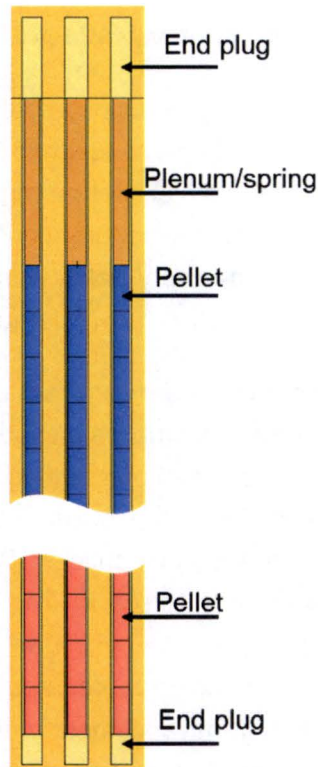
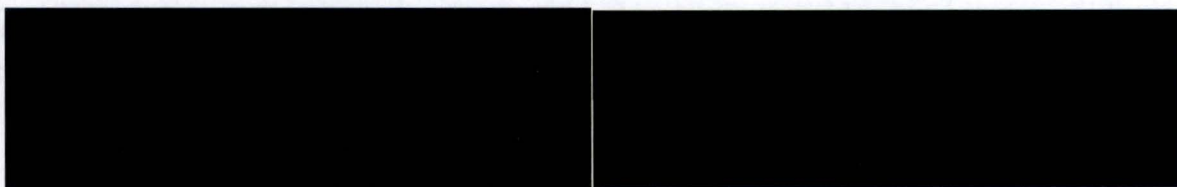


Figure 3-6. Vertical view of the target rod model



5a, d,
e, f

Figure 3-7. Target rod numbers and positions

3.2 Target Assembly Loading Pattern

The target assemblies are planned to be installed in reflector 5A and 5B positions as shown in Figure 2-6. Depending on MURR operating condition, especially the CB insertion depth, the flux level in the reflector region changes. In order to comply with the neutron flux variations and to maintain the cooling capability of the target assembly, the power density of the target assembly should be carefully determined by examining appropriate target rod positions (distance) from the



core. The target power is typically peaked at the axial middle zone. In order to reduce the axial power peaking and to increase the overall target power, a neutron shield is attached to the cartridge.

3.2.1 Selection of bounding values for control blade position

The MURR core has a one-week operation cycle. During each cycle, the CB travels in and out of core to compensate for excess reactivity of the fresh fuel and reactivity loss due to depletion. The actual CB insertion depth depends on the driver fuel burnup, CB absorber material depletion, reflector material degradation and any reactivity perturbations. Typically, the CB travels over 10 cm during first two days after startup, and then very slowly withdraws as fission products saturate. The driver fuel also has two distinct states: clean fuel and equilibrium xenon.

The critical CB positions of the equilibrium core are summarized in Table 3-6 for the core with and without target assemblies. When the target assemblies are loaded, CBs are inserted more deeply into the core. The estimated additional CB insertion depth is 2 to 10 cm depending on the core states. When these offset values are applied to the lowest and highest CB position during 2014-2015 operation, the estimated lowest and highest critical CB position with a 2-target assembly loading are 33.7 and 51.9 cm, respectively (given in Table 3-7). The CB offset values of <core_min> and <core_avg> were applied to BOC and Day-2 cases, respectively, while that of <core_max> was used for EOC CB position. Here, <core_max> doesn't necessarily mean the EOC state, but it at least considers burnup advancement of the core. In the actual simulation of the core with target assemblies, the lowest CB position was further extended to 44, 40, 30 and 30 cm for the maximum, average, minimum and extreme burnup core, respectively.

Table 3-6. Critical control blade position

	Extreme burnup core <core_ref>	Minimum burnup core <core_min>	Average burnup core <core_avg>	Maximum burnup core <core_max>
Xenon state	clean	clean	equilibrium	equilibrium
Regulating rod (cm)	25.4	25.4	38.1	38.1
Critical CB position without target assembly	41.67	35.09	59.87	65.0
Critical CB position with 2 fresh target assemblies	38.75	32.75	52.89	55.28
CB offset (cm)	2.92	2.34	6.98	9.72

Table 3-7. Expected control blade travelling range for target-loaded core

	Recorded critical CB position without target loading	Expected critical CB range with target loading

	Lowest	Highest	Lowest	Highest
BOC	36.6	42.6	33.7	39.6
Day-2	49.1	58.8	42.1	51.8
EOC	53.6	61.6	43.9	51.9

3.2.2 Selection of target rod position

The performance of the target assembly (i.e., ⁹⁹Mo production) depends on the target power which is determined by the target uranium enrichment and neutron flux level (or position) in the reflector. Table 3-8 shows a comparison of target performance for two different rod positions: rod number 6 center position at 1.5 and 2.1 cm from Be reflector water gap. The simulations have been conducted with lowest CB position for 4 core burnup states to consider power peaking in the low half of the core. The ⁹⁹Mo production was estimated in terms of 6-day Curies per week for 2 target assemblies which are irradiated for 1 week. It should be noted that the ⁹⁹Mo production is only for sensitivity purposes, because the production rate is seriously over-estimated here due to CB age and mechanical tilts.

The recommended upper limit of the peak linear power is [REDACTED] from the thermal-hydraulic design. Considering uncertainties associated with neutronics design (see Section 4.6), it has been recommended to keep the peak linear power at [REDACTED]. For the 4 core burnup states with the lowest CB position, the lowest peak linear power of target rods at [REDACTED] is [REDACTED], while the highest peak linear power of target rods at [REDACTED] cm is [REDACTED] kW/m. Therefore, an intermediate distance has been chosen as the reference position for the target assembly loading, i.e., [REDACTED] from the Be reflector water gap ([REDACTED] from the core center).

5a, d,
e, f

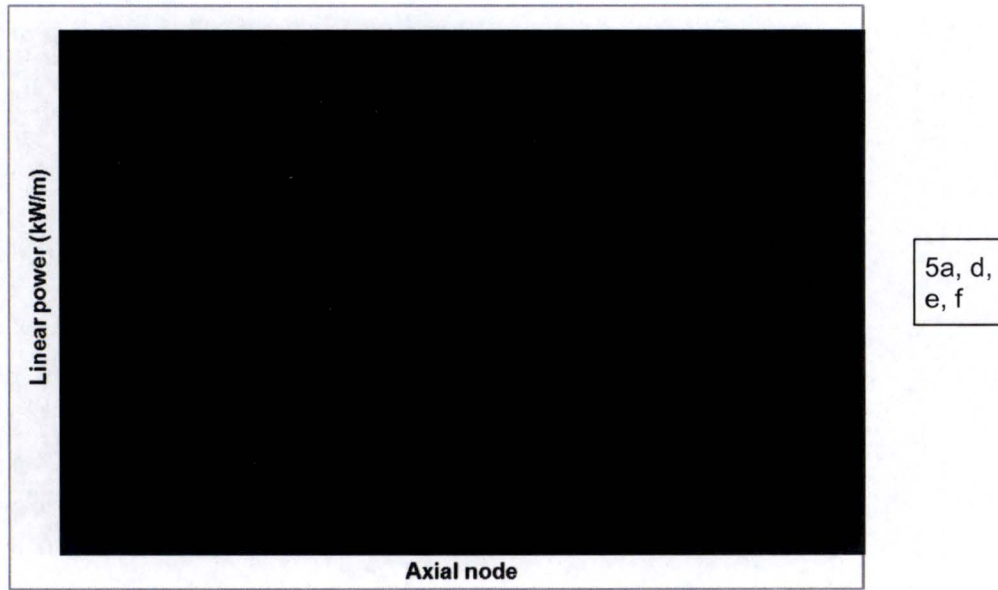


Figure 3-8. Axial power distribution of the peak power rod for the maximum burnup core

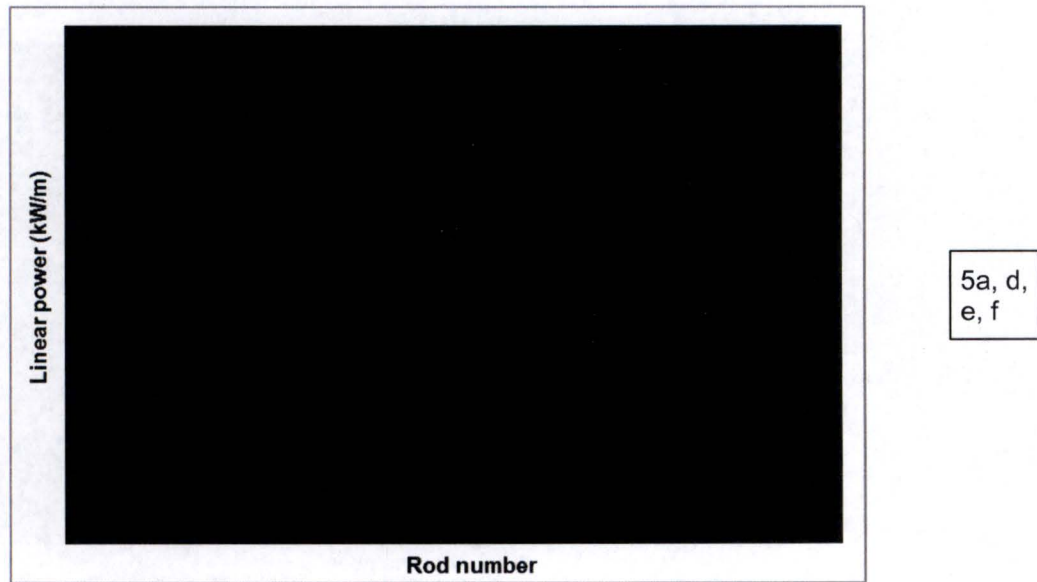


Figure 3-9. Azimuthal power distribution of the peak power node for the maximum burnup core



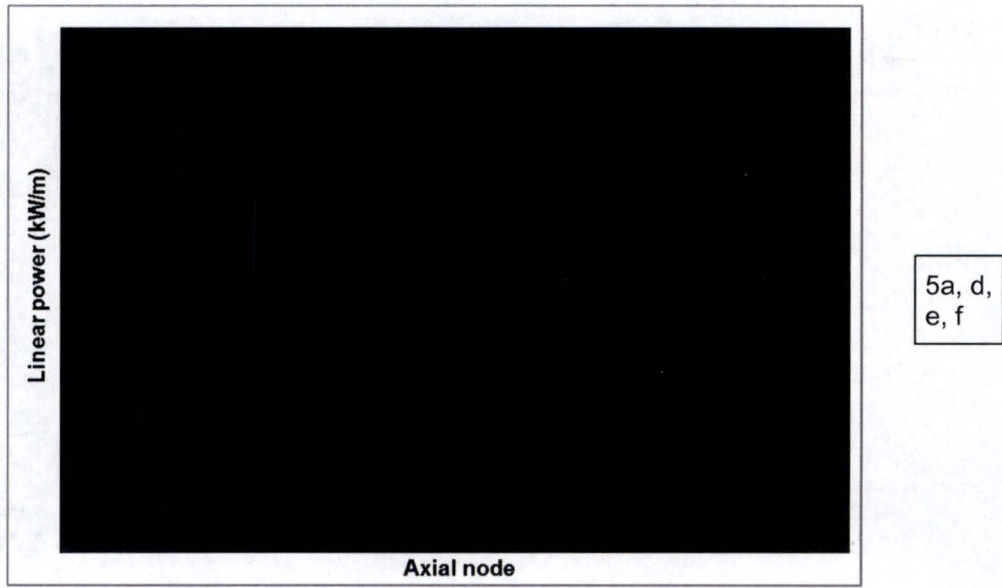


Figure 3-10. Axial power distribution of the peak power rod for the extreme burnup core

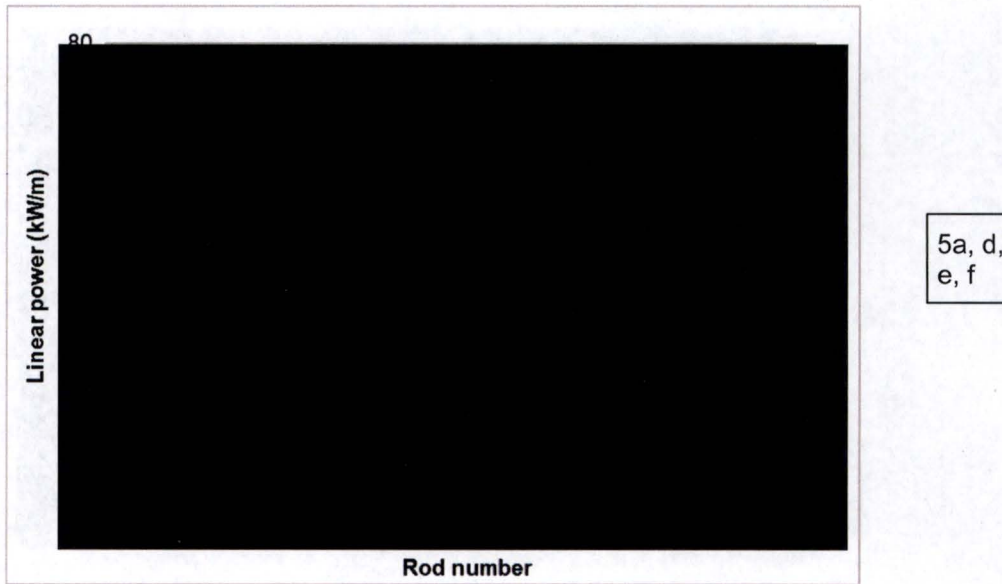
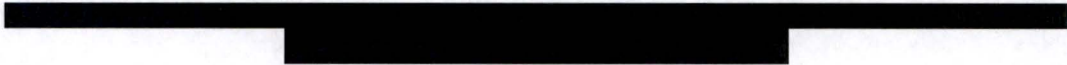


Figure 3-11. Azimuthal power distribution of the peak power node for the extreme burnup core



3.3 Target Assembly at Reference Position

The key performance parameters of the target assembly are summarized in Table 3-9 for target assembly loading at the reference position (i.e., [REDACTED] from the core center). The weekly ⁹⁹Mo production is given for two loading patterns: base and staggered. In case of the base loading, two fresh target assemblies (22 rod total) [REDACTED]. For the staggered loading, one target assembly (11 rod total) [REDACTED].

5a, d, e, f

Table 3-9. Reference target rod loading with critical CB position

Core burnup state	Target power (kW)	Peak linear power (kW/m)	Mo-99 production (6-day Ci/week)	
			Base loading	Staggered loading
Maximum with equilibrium xenon	[REDACTED]	[REDACTED]	[REDACTED]	[REDACTED]
Average with equilibrium xenon	[REDACTED]	[REDACTED]	[REDACTED]	[REDACTED]
Minimum without xenon	[REDACTED]	[REDACTED]	[REDACTED]	[REDACTED]
Extreme without xenon	[REDACTED]	[REDACTED]	[REDACTED]	[REDACTED]

5a, d, e

4 PHYSICS PERFORMANCE OF TARGET ASSEMBLY

Definitions of Target Assembly Loading Pattern and Operation

The reference target assembly consists of 11 target rods, aluminum cartridge and stainless steel shield. In addition to the base and staggered loading mentioned in Sec. 3.3, the target assembly can also be partially loaded to comply with the demand. The target assembly loading patterns and corresponding operating scenarios are summarized as follows:

- Base loading [REDACTED].
- Staggered loading [REDACTED].
- Partial loading uses a reduced number of target rods (i.e., < 11 UO₂ filled rods per assembly) and the operation scheme is the same as that of the base loading. Target rods [REDACTED].

5a, d, e

are symmetrically loaded in from the center rod position, i.e., rod position 6 and 17 (see Fig. 3-7).

Target Power and ⁹⁹Mo Production

The ⁹⁹Mo production is calculated from the target power. For all the physics simulations, the target power is calculated as follows:

- The target pellet is fresh UO₂ without impurities except for the staggered loading which has one irradiated target assembly. The initial composition of the irradiated target assembly doesn't include impurities either.
- The target assembly power is obtained by normalizing MURR core power to 10 MW thermal. Specifically, F7 (fission energy deposition) tally of the MCNP6 is used to edit the MURR core and target assembly power.
- The ⁹⁹Mo production calculation assumes that the neutron flux is constant throughout the irradiation. This will result in an over-prediction of ⁹⁹Mo production. The ⁹⁹Mo production is estimated for the average burnup core which is the most probable core during normal operation. Unlike core performance analysis, the ⁹⁹Mo production calculations are conducted with aged Be reflector and no CB age or mechanical tilt.

For the staggered loading, though the target power is calculated based

5a, d,
e

Evaluation of Target Assembly Performance and Core Characteristics

The performance of the target assembly and the associated MURR core characteristics have been evaluated for the key physics parameters as follows:

- criticality of the stand-alone target assembly;
- core coupling impact between the target assembly and MURR core (reactivity and power);
- core coefficients of reactivity and reactivity device worth;
- neutron flux and power of the target assembly for different operation schemes;
- effect of control blade movement on the target assembly performance;
- uncertainties due to numerical simulation and manufacturing;
- target material depletion and ⁹⁹Mo production.

4.1 Target Assembly Criticality

Conservative calculations of k_{eff} for two target assemblies were performed using the MURR core model by replacing the MURR driver fuel and cladding with water and assuming the control blades and regulating rod are completely withdrawn from the core. The calculated value of k_{eff} for the target assemblies located in reflector 5A and 5B is 0.65868 ± 0.00014 and 0.65870 ± 0.00018 , respectively. When both 5A and 5B are loaded, the k_{eff} is 0.65875 ± 0.00018 , indicating that the target assemblies will be subcritical with a large margin for uncertainty. The uncertainties are given in 95% confidence level, i.e., 2 standard deviations (2σ).

4.2 Impact of Target Assembly Loading on MURR Core

Loading two target assemblies in the MURR reflector region causes perturbations in neutronics and thermal performance of the MURR core as follows:

- The MURR core excess reactivity will increase, which will be compensated by the reactivity control devices
- The neutron flux and power of the adjacent F5 fuel elements will increase even though the total MURR driver fuel power is maintained at 10 MW.
- The thermal power generated by the target assemblies won't affect the MURR core cooling capability. The heat flow from the target assembly to the MURR pool will be negligible (i.e., ≤ 20 kW).

4.2.1 Reactivity insertion due to target assembly loading

The reactivity insertion due to target assembly loading is summarized in Table 4-1. The reactivity worth was calculated by replacing the water in the target assembly cartridge with fresh, cold target rods. Under the hot operating condition, the reactivity insertion due to a single assembly loading is less than 0.31% $\Delta k/k$. The maximum reactivity insertion due to hot target rod is the same as that of the cold target rod for all core burnup states.

Table 4-1. K_{eff} and reactivity insertion values for single target assembly

Core burnup state	5A/5B fully loaded	5A/5B with assembly housing	Target in 5A		Target in 5B	
			k_{eff}	$\Delta k/k$ (%)	k_{eff}	$\Delta k/k$ (%)
Maximum with equilibrium xenon	0.99995	0.99368	0.99658	0.29	0.99660	0.29
Average with equilibrium xenon	0.99999	0.99392	0.99673	0.28	0.99677	0.29
Minimum without xenon	0.99995	0.99385	0.99662	0.28	0.99690	0.31
Extreme without xenon	1.00002	0.99382	0.99667	0.29	0.99685	0.31

4.2.2 MURR core power peaking due to target assembly loading

The target assembly loading in the MURR reflector has a relatively small impact on power peaking of the MURR core driver fuel element. Table 4-2 compares the distribution of MURR fuel element power with and without target assembly loading. For most of core states, the fuel element F5 (closest to the target assembly, see Figure 2-6 for fuel element identification) peaking factor is the highest because the fuel burnup is the lowest and the fuel is located close to the target assembly.

Table 4-2. MURR core power peaking due to target assembly loading

Core burnup state	Number of target rods	Inner-most fuel plate		Outer-most fuel plate	
		Axial node*	Peaking factor	Axial node	Peaking factor
Maximum with equilibrium xenon	0	13 (F5)	2.541	13 (F1)	2.064
	22	11 (F5)	2.637	11 (F5)	2.218
Average with equilibrium xenon	0	12 (F5)	2.426	12 (F1)	1.999
	22	11 (F5)	2.511	11 (F5)	2.155
Minimum without xenon	0	8 (F5)	2.968	9 (F6)	2.444
	22	9 (F5)	3.031	9 (F6)	2.565
Extreme without xenon	0	10 (F5)	2.905	9 (F1)	2.200
	22	10 (F5)	2.976	8 (F5)	2.397

*Axial nodes 1 and 24 correspond to the bottom and top of MURR drive fuel plate, equally spaced.

For the F5 fuel element, the peaking factor of the inner plate is always higher than that of the outer plate. When two target assemblies are loaded, the increase of peaking factor is less than

4% for the inner plate, while the maximum increase of peaking factor is ~11% for the outer plate. However, the absolute value of the outer plate peaking factor is always less than that of the inner plate peaking factor. More detailed distributions of peaking factors for F5 element are given in Table 4-3, where the peaking factors are defined as follows:

- Element peaking = Fuel element power / (total core power/8)
- Radial peaking = Fuel plate average power density / Fuel element average power density
- Axial peaking = Axial node power density / Fuel plate average power density
- Total peaking = Element peaking × Radial peaking × Axial peaking

Table 4-3. MURR fuel element F5 power peaking factors

Element	Extreme burnup core			Minimum burnup core			Average burnup core			Maximum burnup core		
	Radial	Axial	Total									
	1.189			1.177			1.105			1.129		
1	1.859	1.346	2.975	1.867	1.379	3.030	1.798	1.264	2.511	1.837	1.271	2.636
2	1.508	1.356	2.431	1.516	1.374	2.452	1.473	1.269	2.066	1.486	1.269	2.129
3	1.301	1.343	2.077	1.308	1.375	2.117	1.270	1.275	1.789	1.276	1.266	1.824
4	1.163	1.351	1.868	1.169	1.384	1.904	1.139	1.275	1.605	1.135	1.271	1.629
5	1.068	1.341	1.703	1.072	1.371	1.730	1.044	1.281	1.478	1.041	1.272	1.495
6	1.000	1.360	1.617	1.007	1.383	1.639	0.979	1.274	1.378	0.974	1.269	1.395
7	0.950	1.345	1.519	0.959	1.384	1.562	0.930	1.270	1.305	0.925	1.267	1.323
8	0.915	1.348	1.467	0.921	1.380	1.496	0.895	1.268	1.254	0.890	1.265	1.271
9	0.887	1.344	1.417	0.892	1.381	1.450	0.868	1.262	1.210	0.862	1.271	1.237
10	0.867	1.349	1.391	0.871	1.387	1.422	0.850	1.264	1.187	0.844	1.265	1.205
11	0.851	1.348	1.364	0.857	1.389	1.401	0.834	1.266	1.167	0.832	1.264	1.187
12	0.838	1.344	1.339	0.845	1.391	1.383	0.825	1.268	1.156	0.822	1.264	1.173
13	0.831	1.348	1.332	0.839	1.385	1.368	0.818	1.273	1.151	0.815	1.262	1.161
14	0.827	1.358	1.335	0.832	1.389	1.360	0.818	1.275	1.152	0.812	1.257	1.152
15	0.827	1.345	1.323	0.830	1.388	1.356	0.818	1.276	1.153	0.813	1.259	1.156
16	0.830	1.348	1.330	0.833	1.406	1.379	0.823	1.281	1.165	0.819	1.269	1.173
17	0.837	1.359	1.352	0.840	1.414	1.398	0.833	1.278	1.176	0.830	1.266	1.186
18	0.851	1.357	1.373	0.852	1.417	1.421	0.851	1.285	1.208	0.847	1.274	1.218
19	0.876	1.365	1.422	0.872	1.423	1.460	0.879	1.277	1.240	0.876	1.275	1.261
20	0.909	1.374	1.485	0.907	1.435	1.532	0.922	1.288	1.312	0.919	1.283	1.331
21	0.963	1.377	1.577	0.955	1.454	1.634	0.985	1.304	1.419	0.981	1.296	1.435
22	1.044	1.396	1.733	1.035	1.475	1.797	1.079	1.309	1.561	1.078	1.298	1.580
23	1.174	1.413	1.972	1.159	1.501	2.048	1.224	1.315	1.779	1.231	1.304	1.812
24	1.396	1.444	2.397	1.371	1.532	2.472	1.472	1.325	2.155	1.491	1.317	2.217

4.2.3 Core reactivity characteristics

4.2.3.1 Coefficient of reactivity

Though the MURR core power distribution, or power peaking factor, is altered when two target assemblies are loaded, the core reactivity characteristics won't change due to target assembly loading. The reactivity coefficients of the core with two fresh target assemblies were calculated for the fuel temperature coefficient, coolant temperature coefficient and void reactivity as summarized in Table 4-4.

The MURR fuel temperature coefficient was calculated by increasing the fuel temperature by 906.4°C, i.e., from 20.44°C to 926.84°C. The variation of fuel temperature coefficients is consistent with core burnup state and kept negative. Due to the limitation in cross section data, however, the temperature dependence of lumped fission products (all fission products except for ^{135}I , ^{135}Xe , ^{149}Pm , ^{149}Sm) was not considered.

The coolant temperature coefficient was calculated by changing the coolant temperature from 20.44°C to 76.84°C, where the coolant density changes from 0.99815 to 0.97378 g/cm³. The principal cross section data used for the calculations are basically the same for both the lower and higher coolant temperature conditions, but the $S(\alpha, \beta)$ thermal scattering was correctly treated. The coolant void reactivity of the core was calculated by removing 99.9% of coolant from the core.

The statistical uncertainty (2σ) of the reactivity coefficient is $\sim 2.6 \times 10^{-4}$ when the error propagation rule is used. However, the perturbations of the fuel temperature and coolant density were large enough to obtain consistent results. The least negative values are -1.03×10^{-6} and -1.69×10^{-4} $\Delta k/k/^\circ\text{C}$ for the fuel and coolant temperature coefficient, respectively.

Table 4-4. Reactivity coefficients of core with two fresh target assemblies

Core burnup state	Fuel temperature coefficient ($\Delta k/k/^\circ\text{C}$)	Coolant temperature coefficient ($\Delta k/k/^\circ\text{C}$)	Coolant void reactivity ($\Delta k/k/\%\text{voiding}$)
Maximum with equilibrium xenon	-1.20×10^{-6}	-1.69×10^{-4}	-3.40×10^{-3}
Average with equilibrium xenon	-1.16×10^{-6}	-1.73×10^{-4}	-3.40×10^{-3}
Minimum without xenon	-1.27×10^{-6}	-1.85×10^{-4}	-3.40×10^{-3}
Extreme without xenon	-1.03×10^{-6}	-1.79×10^{-4}	-3.40×10^{-3}

4.2.3.2 Regulating rod worth

The impact of target assembly loading on the existing reactivity devices (CB and regulating rod) were estimated for their reactivity worth and subcriticality margin as summarized in Table 4-5. Reactivity worth of regulating rod was calculated from fully-in and fully-out conditions while the CB is kept at its critical position. For the selected core states, the lowest worth of the regulating rod is $3.41 \times 10^{-3} \Delta k/k$.

4.2.3.3 Control blade subcriticality margin

The CB subcriticality margin was at first calculated for the average burnup core. Among four CB's (A, B, C and D), the subcriticality margin of C is the largest even though it is almost the same as that of B. The subcriticality margin increases as the core burnup increases due to effective neutron flux changes. The lowest subcriticality margin with most reactivity CB (A) and regulating rod fully withdrawn is $0.055 \Delta k/k$ for the minimum burnup core.

Table 4-5. Reactivity device worth with two fresh target assemblies

Core burnup state	Subcriticality margin of control blade ($\Delta k/k$)	Regulating rod worth ($\Delta k/k$)
Maximum with equilibrium xenon	0.109	3.55×10^{-3}
Average with equilibrium xenon	0.106	3.41×10^{-3}
Minimum without xenon	0.055	3.69×10^{-3}
Extreme without xenon	0.076	4.02×10^{-3}

4.2.3.4 Core excess reactivity

The excess reactivity of the core with two fresh target assemblies was calculated for the minimum burnup core which has the largest excess reactivity. All CB's and regulating rod are fully withdrawn from the core. The excess reactivity of the cold core (all in room temperature) is $0.072 \Delta k/k$, while that of the hot operating core is $0.067 \Delta k/k$.

4.2.4 Kinetic parameters

The kinetic property of the core is dominated by the driver fuels, which is slightly perturbed by the presence of two target assemblies in the reflector region. The effective (or adjoint weighted) neutron generation time (Λ_{eff}) and effective delayed neutron fraction (β_{eff}) can be readily obtained from the MCNP6 calculation [Kiedrowski 2010]. The results are summarized in Table 4-6 for different burnup states of the core with and without target assemblies. The neutron generation time tends to increase when the two target assemblies are loaded, but the difference is very small. The effective delayed neutron fractions of the core with and without target assemblies

coincide within the uncertainty range ($\pm 2\sigma$). From the viewpoint of point kinetics, the target assembly loading won't deteriorate the slope of power increase (or inverse reactivity period) during the reactivity-induced transient.

Table 4-6. Kinetic parameters of the core with and without target assemblies

Target loading	Core burnup state	Λ_{eff} (μsec)	STD (1σ)	β_{eff}	STD (1σ)
No target	Maximum	62.3	0.273	0.00723	0.00015
	Average	60.6	0.278	0.00731	0.00015
	Minimum	53.7	0.244	0.00749	0.00016
	Extreme	57.0	0.248	0.00732	0.00015
Two target assemblies	Maximum	62.7	0.237	0.00730	0.00013
	Average	61.5	0.235	0.00745	0.00014
	Minimum	54.7	0.215	0.00766	0.00014
	Extreme	58.4	0.220	0.00769	0.00014

4.3 Target Assembly Flux and Power Distribution

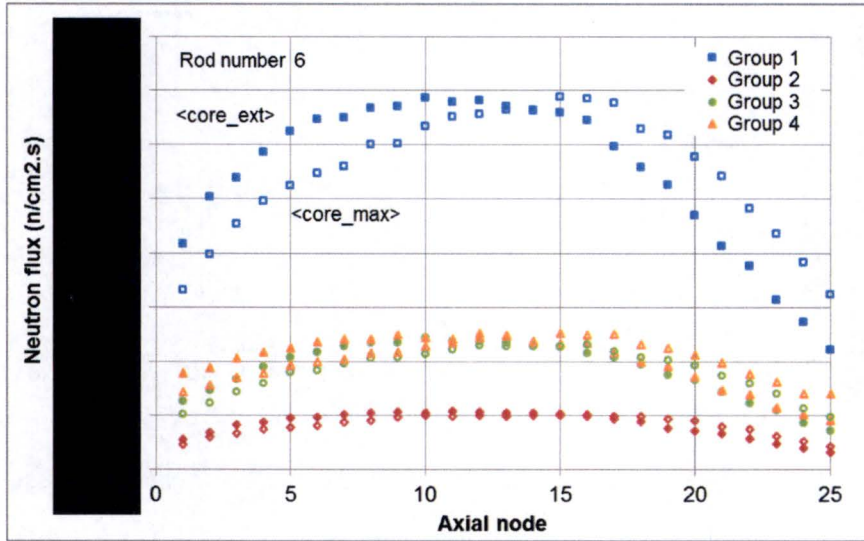
4.3.1 Base target assembly loading

The neutron flux in the target assembly is driven by incoming neutrons from the core even though the target assembly produces neutrons from fission reactions. Figures 4-1 and 4-2 show 4-group axial neutron flux distributions of the target rods 6 and 17 (see Fig. 3-7 for rod numbering) when two fresh target assemblies are loaded. The upper energy boundaries of the 4-group are 20 MeV (Group 1), 0.1 MeV (Group 2), 5.53 keV (Group 3), and 0.625 eV (Group 4). The solid and dotted lines indicate the MURR core states <core_ext> and <core_max>, respectively. The axial nodes 1 and 25 correspond to the bottom and top, respectively. It is obvious that the neutron flux drops at the bottom and top section of the target rod. The neutron flux is suppressed even more in the top section due to the control blades, which is relaxed to a certain extent when the control blades are pulled out in the maximum burnup core. The thermal neutron flux is effectively flattened in the vertical middle section, from node 5 to 20, owing to the neutron shield.

Figure 4-3 shows neutron flux in the azimuthal direction, from rod 1 to 11 (position 5A) and from rod 12 to 22 (position 5B), at axial middle plane. The neutron population is suppressed at the assembly edge region due to elongated neutron absorber on the cartridge edge. For the average

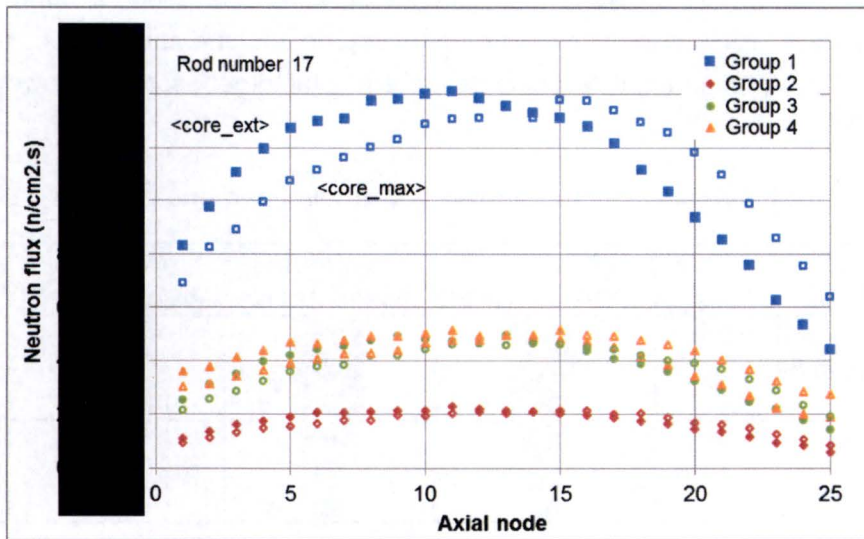
burnup core, the peak neutron fluxes of the target pellet are [REDACTED] for group 1, 2, 3 and 4, respectively.

5a, d,
e, f



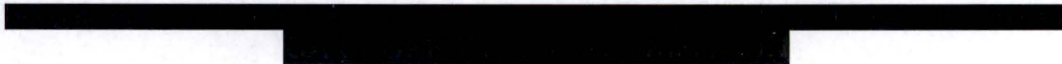
5a, d,
e, f

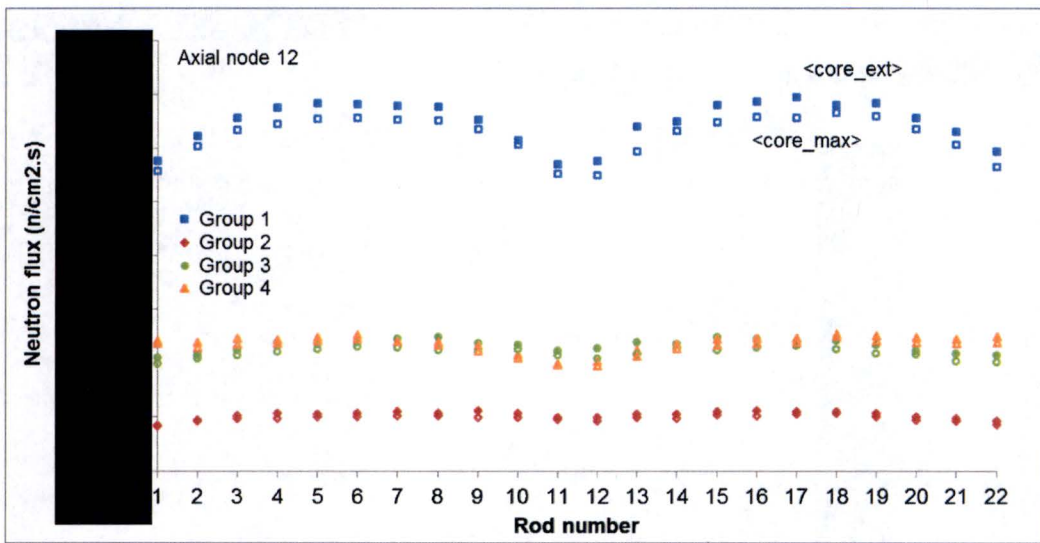
Figure 4-1. Target rod 6 axial neutron flux distribution in position 5A for the base loading



5a, d,
e, f

Figure 4-2. Target rod 17 axial neutron flux distribution in position 5B for the base loading





5a, d,
e, f

Figure 4-3. Target assembly azimuthal neutron flux distribution for the base loading

Calculated target assembly power and pellet linear power are given in Table 4-7. Figures 4-4 and Figure 4-5 show the pellet linear power envelope of the extreme and maximum burnup core, respectively. The target axial power profile is bottom-peaked for the extreme burnup core and changes to middle-peaked shape for the maximum burnup core as the regulating rod and control blades are withdrawn from the core. The distribution of pellet linear power is shown in Figure 4-6 for the four different MURR core states. For the most probable operating core condition, i.e., the average burnup core, the peak pellet linear power and total target assembly power are [REDACTED] and [REDACTED], respectively.

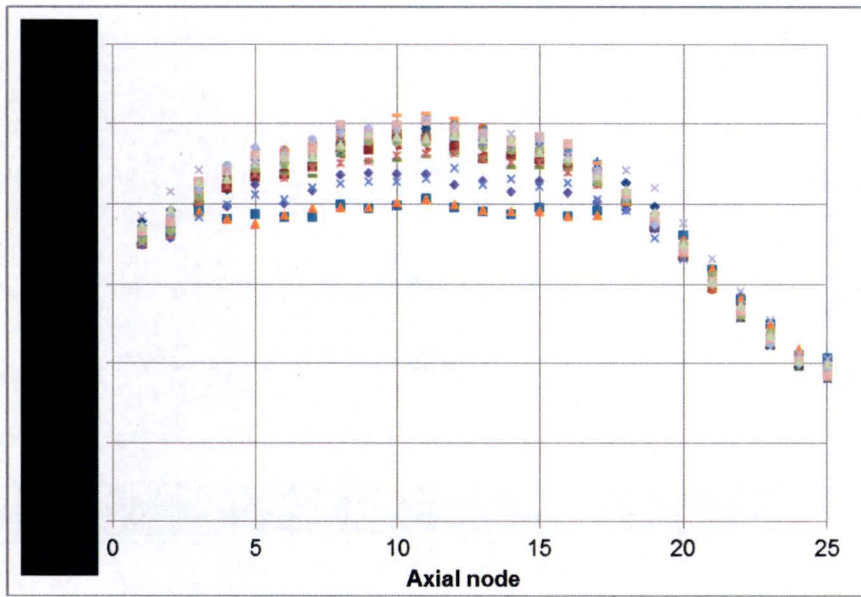
5a, d,
e, f

Table 4-7. Calculated target power level and linear power

	Extreme burnup core	Minimum burnup core	Average burnup core	Maximum burnup core
Assembly power (kW) Assembly in 5A Assembly in 5B	[REDACTED]	[REDACTED]	[REDACTED]	[REDACTED]
Peak linear power (kW/m) Rod number Axial node*	[REDACTED]	[REDACTED]	[REDACTED]	[REDACTED]

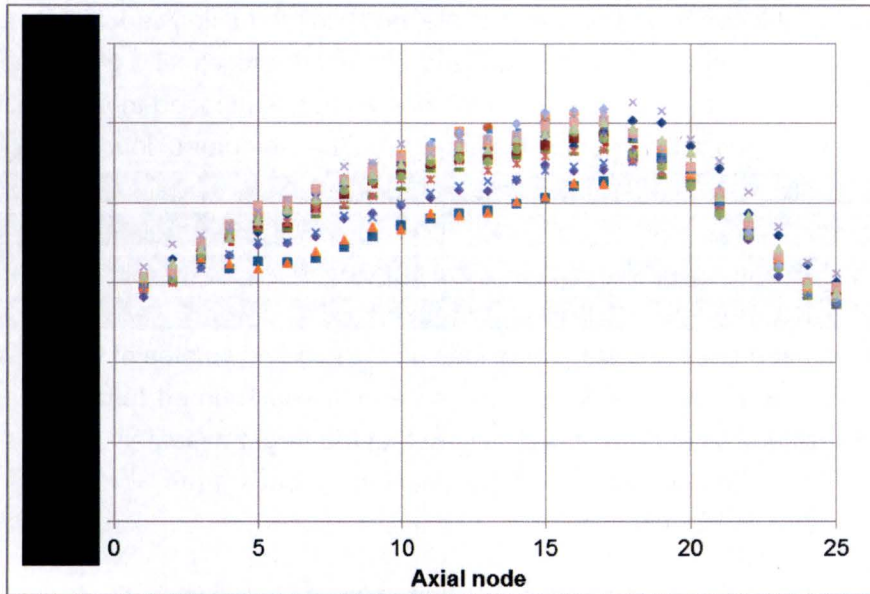
5a, d,
e, f

*Axial nodes 1 and 25 correspond to bottom and top node, respectively. All nodes are equally spaced.



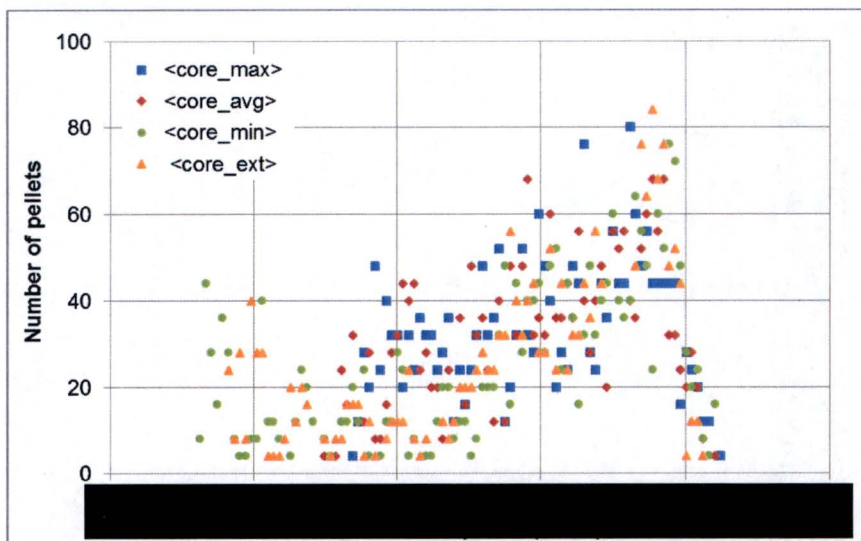
5a, d,
e, f

Figure 4-4. Power envelope of the base loading for the extreme burnup core



5a, d,
e, f

Figure 4-5. Power envelope of the base loading for the maximum burnup core



5a, d,
e, f

Figure 4-6. Target assembly pellet linear power distribution for the base loading

4.3.2 Staggered target assembly loading

Prior to the commercial operation of target assemblies (full loading), a prototype operation of target assembly will be conducted to demonstrate the ⁹⁹Mo production capability and performance of the target rod. The prototype target rod and assembly are exactly the same as those for commercial operation. However, the prototype operation is supposed to adopt different loading patterns such as staggered or partial loading. For the staggered loading, [REDACTED]

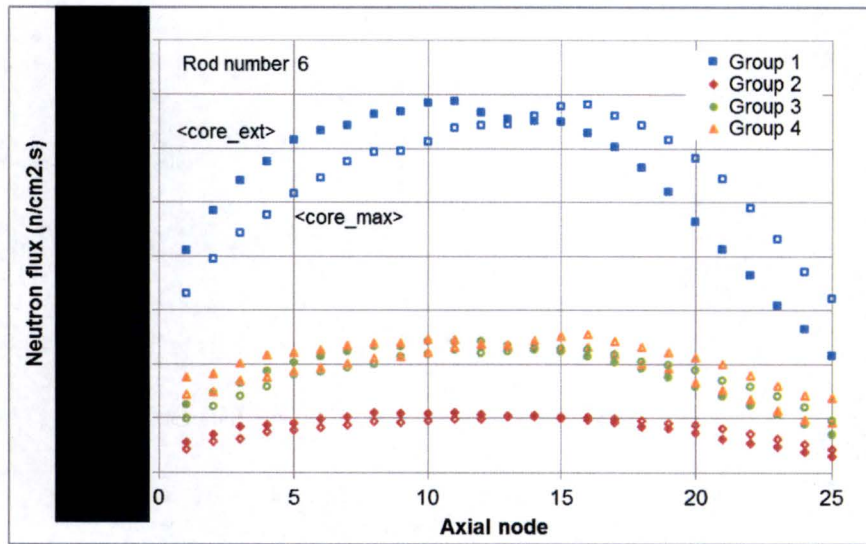
[REDACTED]
[REDACTED]
[REDACTED]
[REDACTED]

5a, d,
e, f

The difference between the base and staggered loading is the burnup states of target assemblies: the fresh target assembly is in one reflector position and 1-week-burned target assembly is in the other reflector position. Therefore, it is expected that the target assembly power and the impact on MURR drive fuel with the staggered target assembly loading are always less severe when compared with the base loading case.

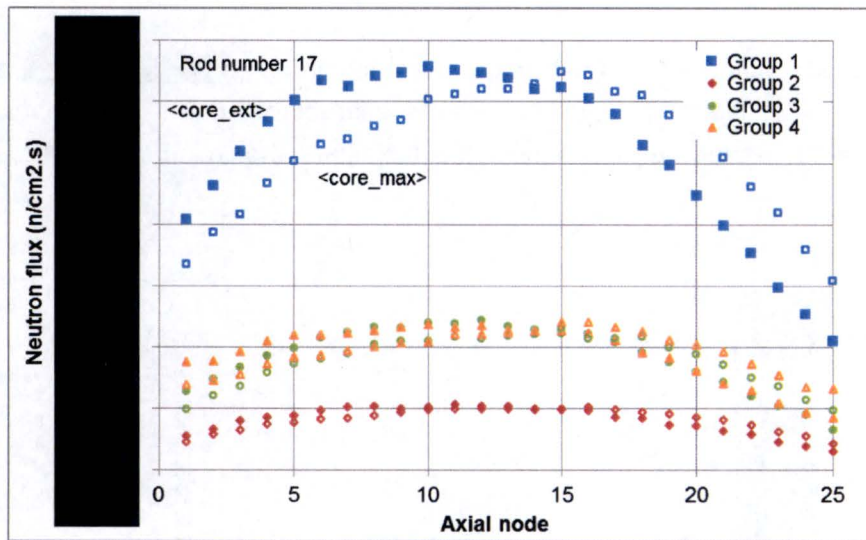
Figure 4-7 and Figure 4-8 show 4-group axial neutron flux distributions of the target rods 6 and 17, respectively, when a fresh target assembly is loaded in position 5A of the extreme and maximum burnup core. The axial flux shape of the target assembly is almost the same as that of the base loading. Figure 4-9 shows the azimuthal flux variation on the axial middle plane, which shows a slight decrease of neutron flux level in reflector 5B.

[REDACTED]



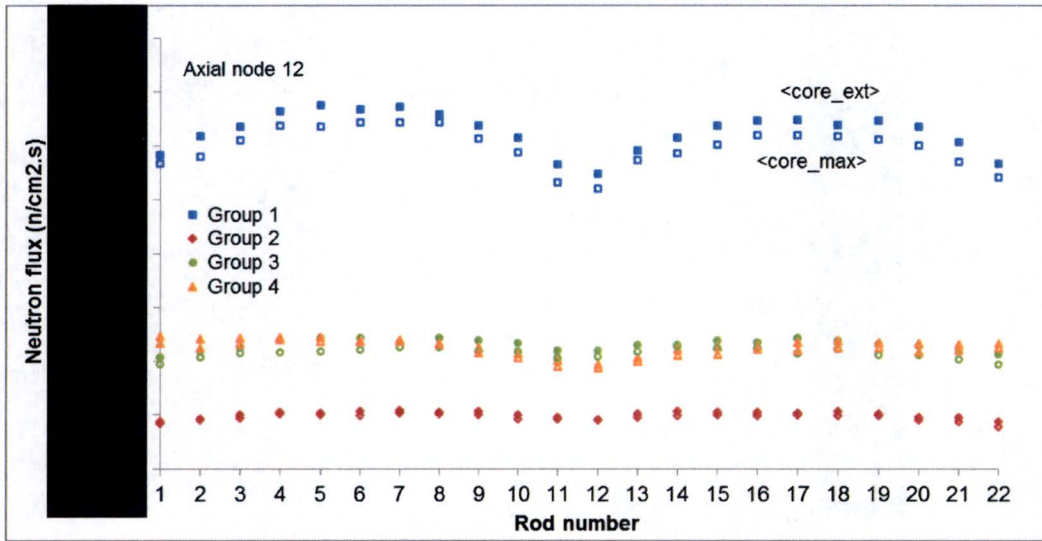
5a, d,
e, f

Figure 4-7. Target rod 6 axial neutron flux for the staggered loading with fresh assembly in 5A



5a, d,
e, f

Figure 4-8. Target rod 17 axial neutron flux for the staggered loading with fresh assembly in 5A

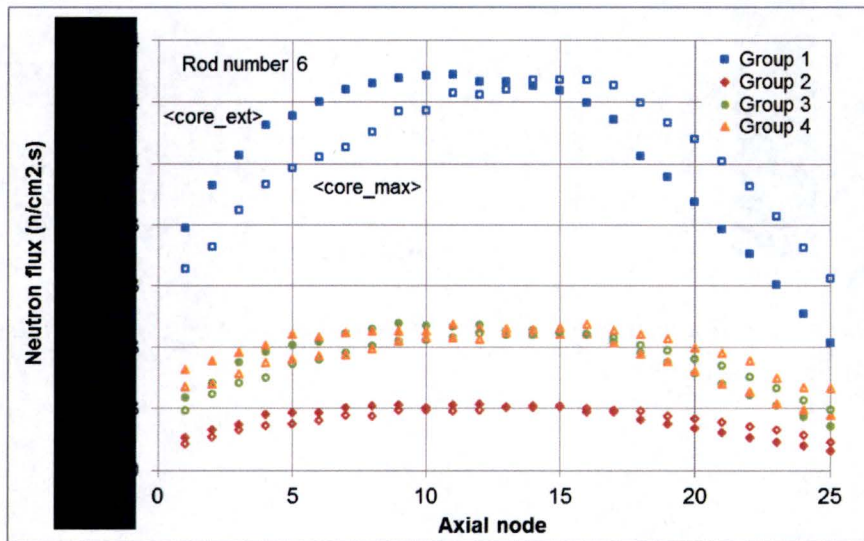


5a, d,
e, f

Figure 4-9. Target assembly azimuthal neutron flux for the staggered loading with fresh assembly in 5A

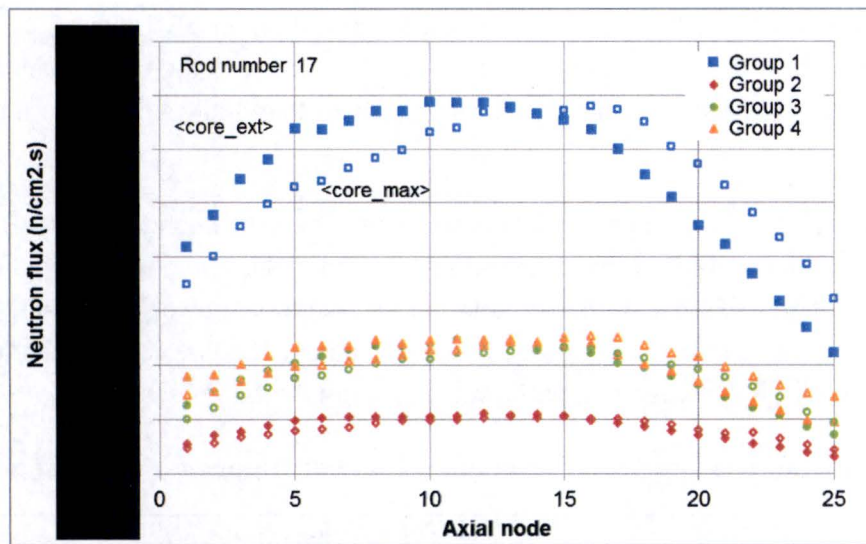
For the staggered loading with a fresh target assembly in 5B (a [redacted] assembly is in 5A), the 4-group axial neutron flux distributions of the target rods 6 and 17 are shown in Figure 4-10 and Figure 4-11, respectively. The azimuthal fluxes are shown in Figure 4-12.

5a, d,
e, f



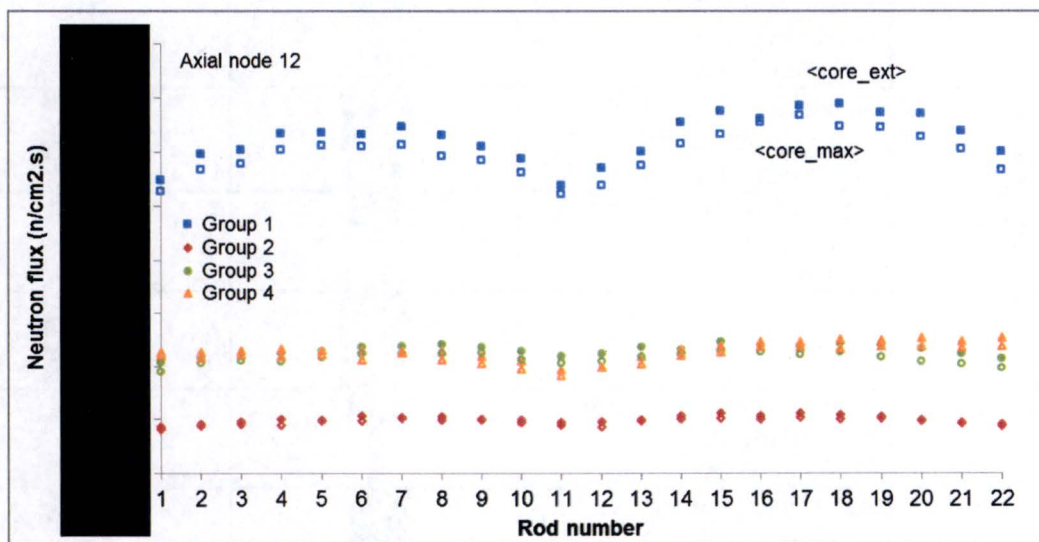
5a, d,
e, f

Figure 4-10. Target rod 6 axial neutron flux for the staggered loading with fresh assembly in 5B



5a, d,
e, f

Figure 4-11. Target rod 17 axial neutron flux for the staggered loading with fresh assembly in 5B



5a, d,
e, f

Figure 4-12. Target assembly azimuthal neutron flux for the staggered loading with fresh assembly in 5B

Target assembly power and rod linear power of the staggered target assembly loading are summarized in Table 4-8 when the fresh assembly is in reflector 5A. The linear power envelopes of the staggered loading are shown in Figure 4-13 and Figure 4-14 for the extreme and maximum burnup core, respectively. The distribution of pellet linear power is shown in Figure 4-15. The axial power profile of the staggered loading is the same as that of the base loading, but the overall linear power is slightly reduced in the burned assembly. For the most probable reactor condition,



i.e., average burnup core, the power of the target assembly in 5B is lower by 11 kW when compared with that of the target assembly in 5A, which is due to the target fuel depletion. The total target assembly power (5A and 5B) is slightly lower than that of the base target assembly loading by [REDACTED].

5a, d,
e, f

The pellet linear power envelopes of the staggered loading with fresh target in 5B are shown in Figures 4-16 and Figure 4-17 for the extreme and maximum burnup core, respectively, and their distribution is plotted in Figure 4-18. The total target assembly power of the staggered loading with fresh target assembly in 5A and 5B are almost the same. The power from the target assembly in 5B is higher by [REDACTED] when compared with that from the target assembly in 5A.

5a, d,
e, f

Table 4-8. Calculated target power level and pellet linear power of the staggered loading

Core burnup state	Target power	Staggered loading (fresh target in 5A)	Staggered loading (fresh target in 5B)
Maximum with equilibrium xenon	Assembly power (kW) Assembly in 5A Assembly in 5B	[REDACTED]	[REDACTED]
	Peak linear power (kW/m) Rod number Axial node	[REDACTED]	[REDACTED]
Average with equilibrium xenon	Assembly power (kW) Assembly in 5A Assembly in 5B	[REDACTED]	[REDACTED]
	Peak linear power (kW/m) Rod number Axial node	[REDACTED]	[REDACTED]
Minimum without xenon	Assembly power (kW) Assembly in 5A Assembly in 5B	[REDACTED]	[REDACTED]
	Peak linear power (kW/m) Rod number Axial node	[REDACTED]	[REDACTED]
Extreme without xenon	Assembly power (kW) Assembly in 5A Assembly in 5B	[REDACTED]	[REDACTED]
	Peak linear power (kW/m) Rod number Axial node	[REDACTED]	[REDACTED]

5a, d,
e, f



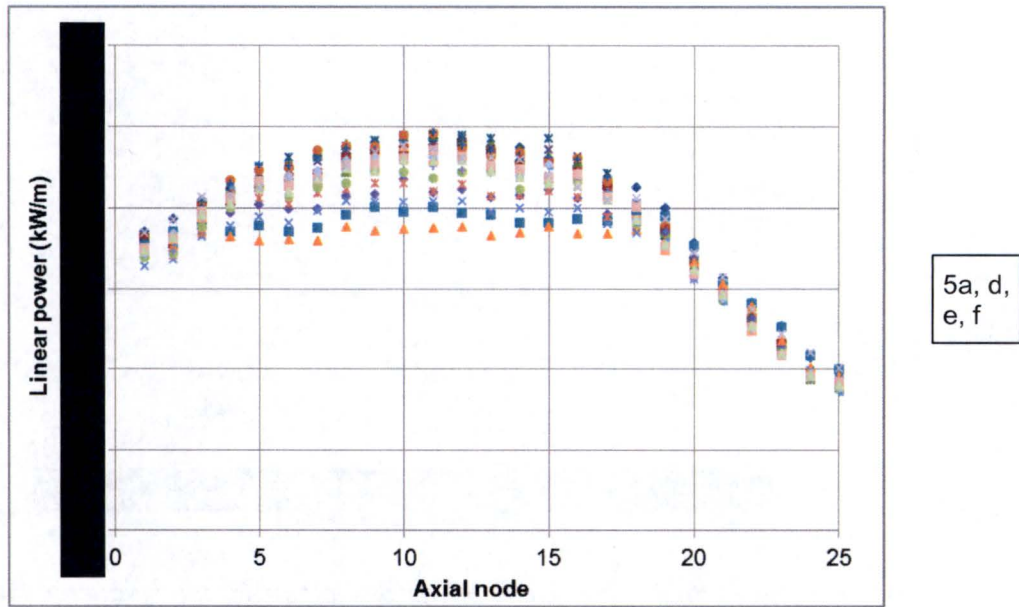


Figure 4-13. Power envelope of the staggered loading for the extreme burnup core (fresh target in 5A)

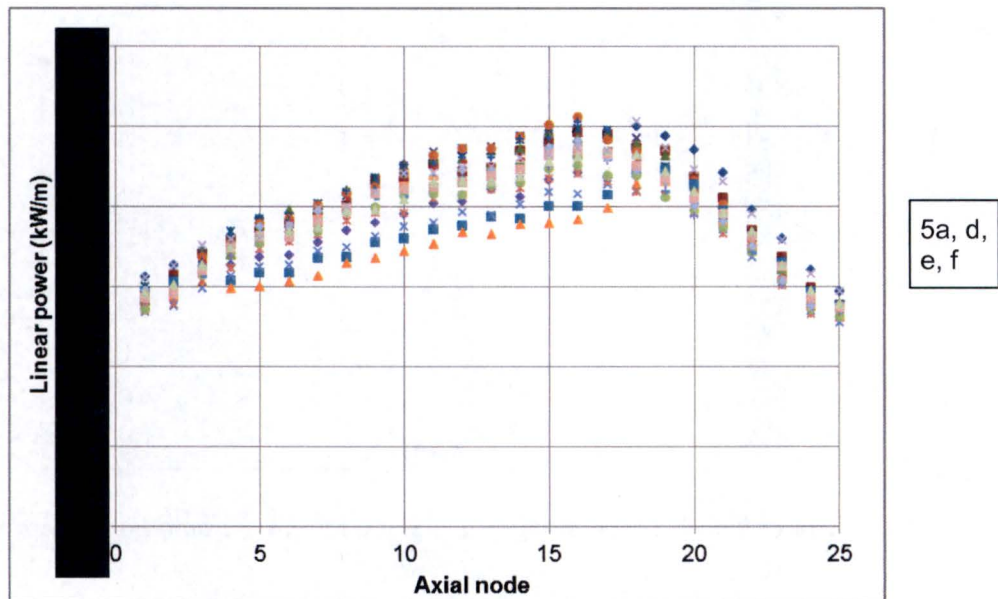
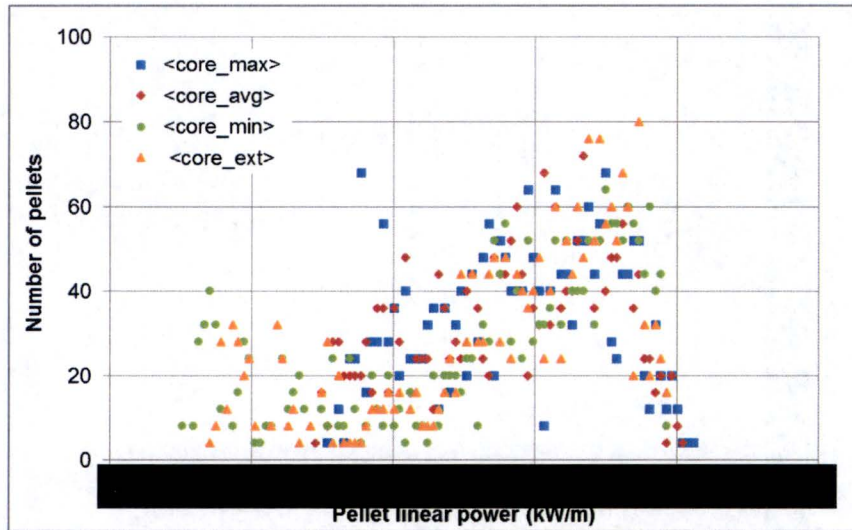
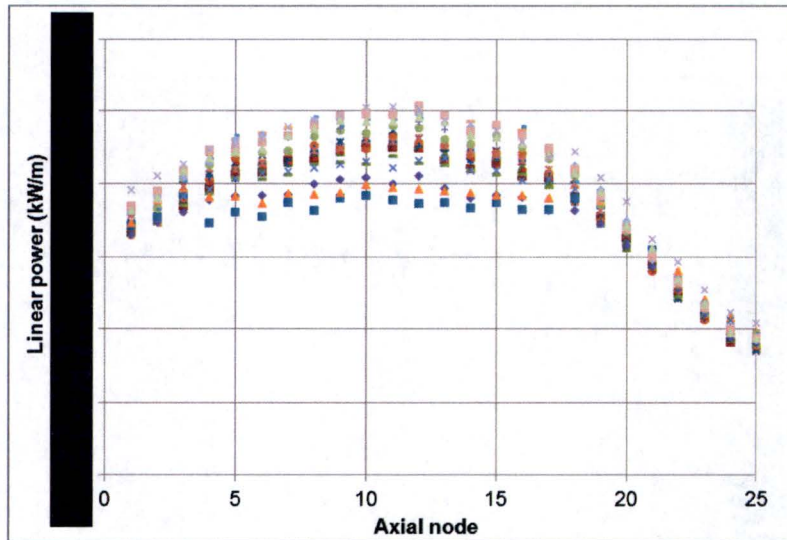


Figure 4-14. Power envelope of the staggered loading for the maximum burnup core (fresh target in 5A)



5a, d,
e, f

Figure 4-15. Target assembly pellet linear power distribution for the staggered loading (fresh target in 5A)



5a, d,
e, f

Figure 4-16. Power envelope of the staggered loading for the extreme burnup core (fresh target in 5B)

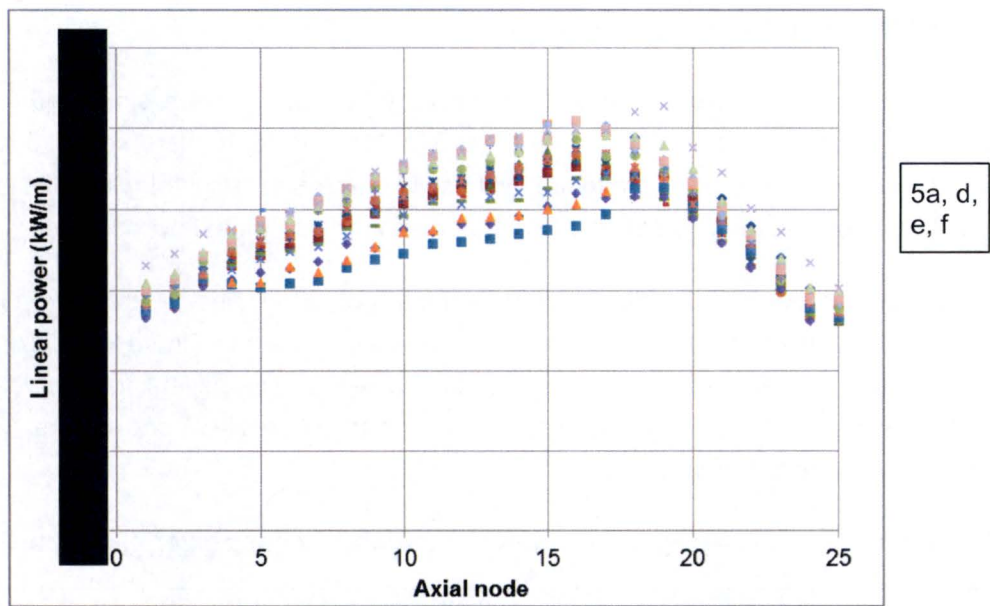


Figure 4-17. Power envelope of the staggered loading for the maximum burnup core (fresh target in 5B)

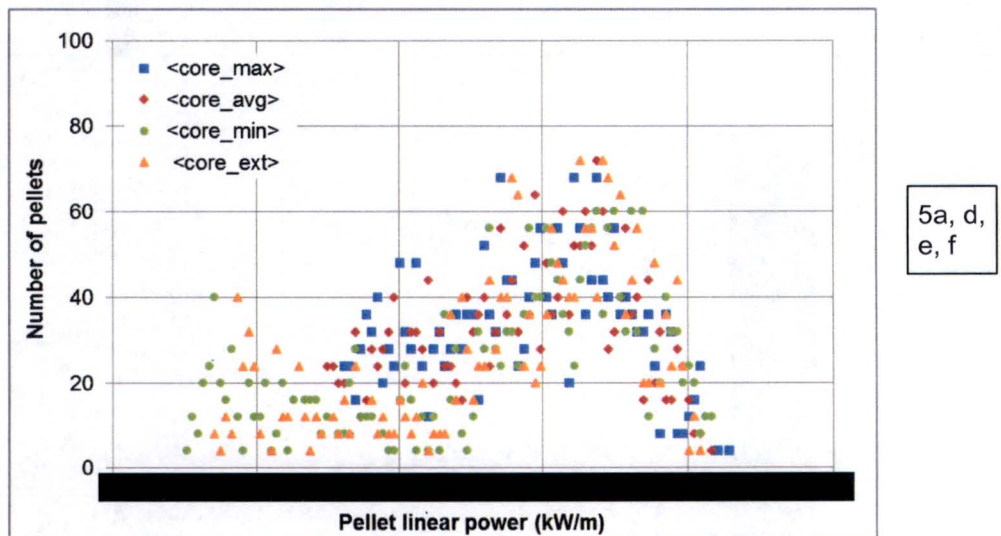


Figure 4-18. Target assembly pellet linear power distribution for the staggered loading (fresh target in 5B)

4.3.3 Partial Target Assembly Loading

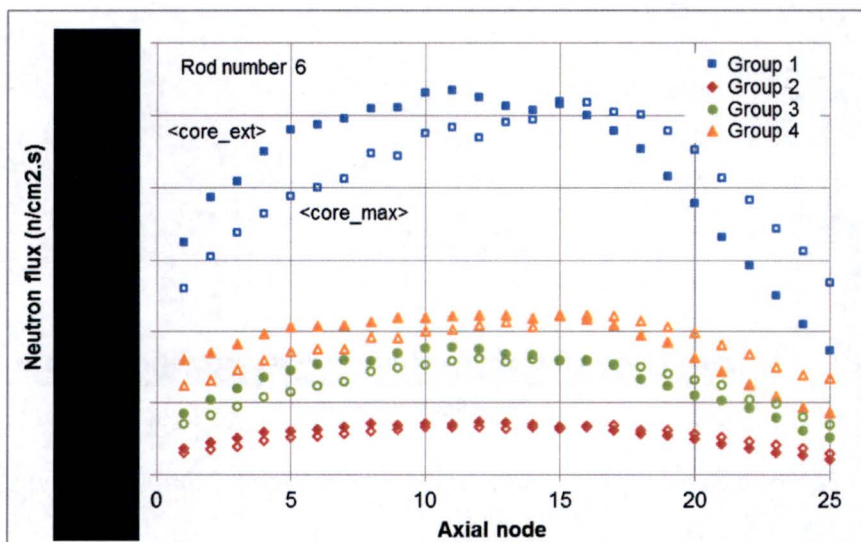
The neutron flux and power distribution of the target assembly were simulated for the case of 3-rod loading per assembly. The rod positions 5 to 7 and 16 to 18 were selected to maintain the symmetry. Other rod positions are loaded with solid stainless steel 316L rods (filler rods) to avoid unnecessary neutron thermalization while maintaining the nominal flow condition.

The 4-group axial neutron flux distributions of the target rods 6 and 17 are shown in Figure 4-19 and Figure 4-20, respectively. The azimuthal fluxes are shown in Figure 4-21. Target assembly power and pellet linear power are summarized in Table 4-9. The pellet linear power envelopes of the extreme and maximum burnup core are shown in Figure 4-22 and Figure 4-23, and their distribution is plotted in Figures 4-24.

Table 4-9. Calculated target power level and pellet linear power of the partial loading

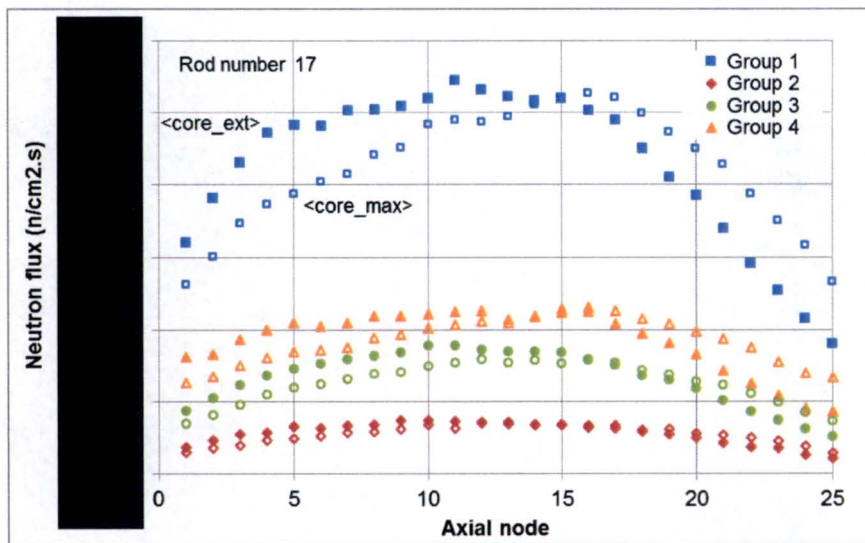
	Extreme burnup core	Minimum burnup core	Average burnup core	Maximum burnup core
Assembly power (kW)				
Assembly in 5A				
Assembly in 5B				
Peak linear power (kW/m)				
Rod number				
Axial node				

5a, d, e, f



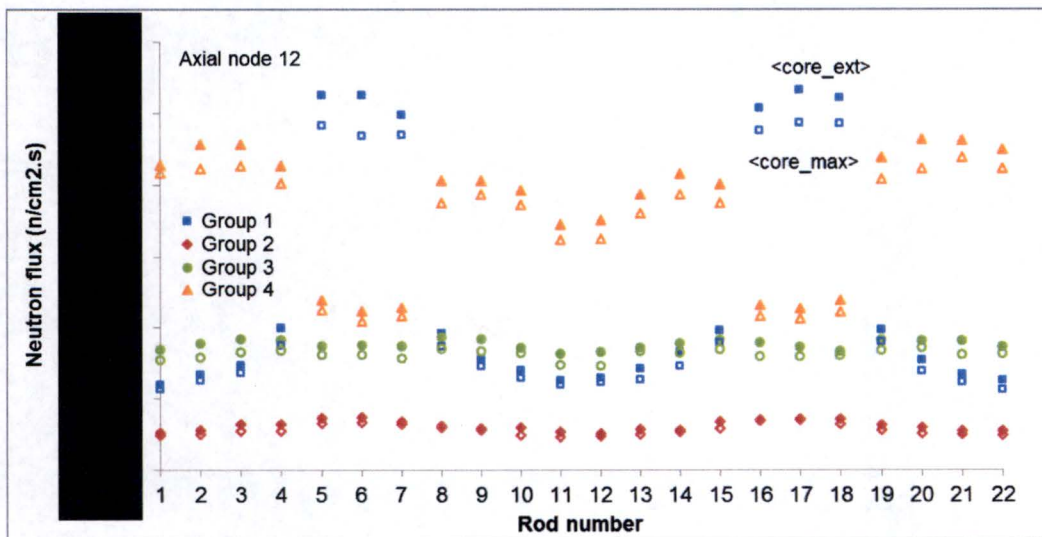
5a, d, e, f

Figure 4-19. Target rod 6 axial neutron flux for the partial loading



5a, d,
e, f

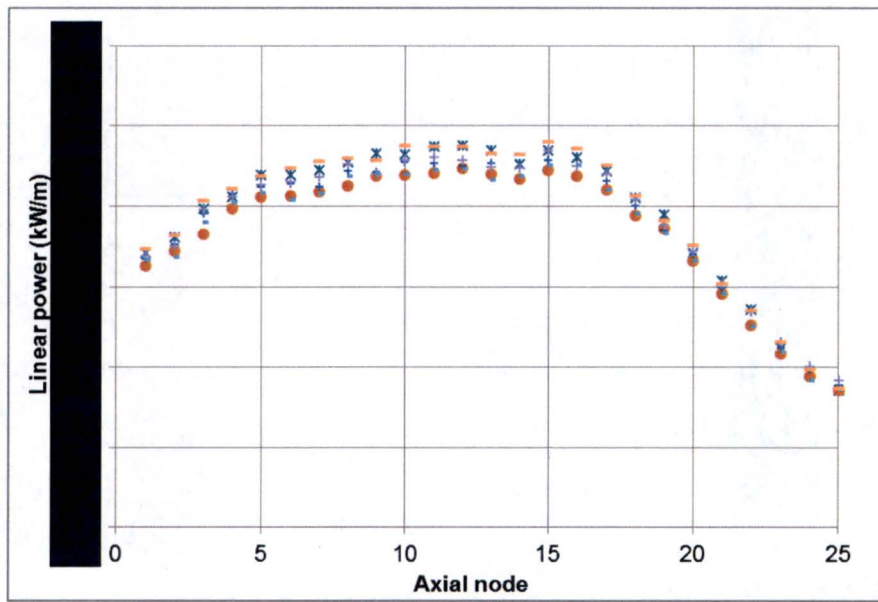
Figure 4-20. Target rod 17 axial neutron flux for the partial loading



5a, d,
e, f

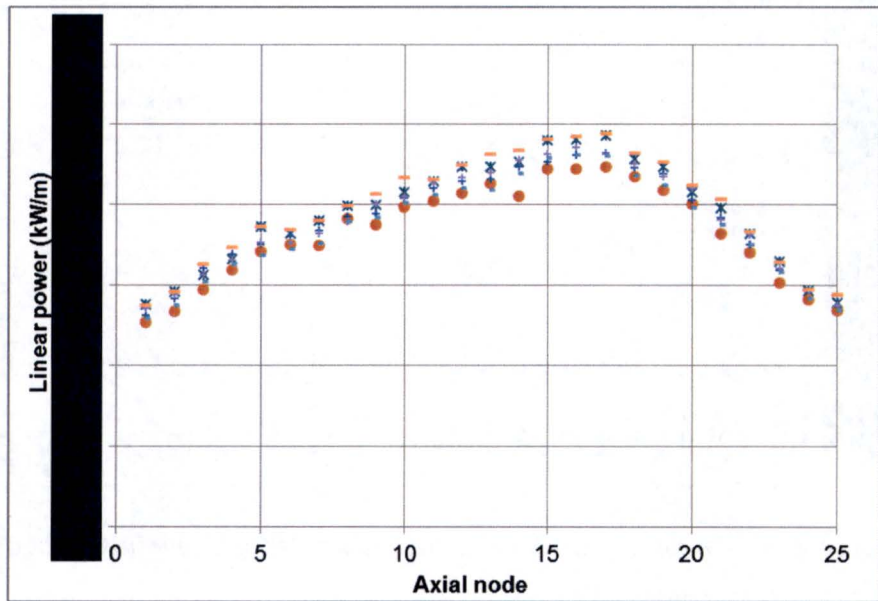
Figure 4-21. Target assembly azimuthal neutron flux for the partial loading





5a, d,
e, f

Figure 4-22. Power envelope of the partial loading for the extreme burnup core



5a, d,
e, f

Figure 4-23. Power envelope of the partial loading for the maximum burnup core

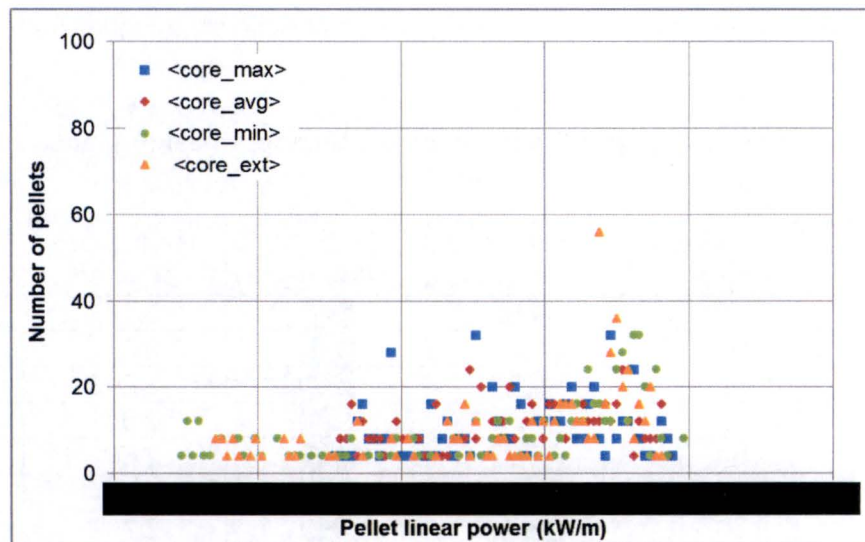
5a, d,
e, f

Figure 4-24. Target assembly pellet linear power distribution for the partial loading

4.4 Sensitivity to Control Blade Position for Base Target Assembly Loading

The peak linear power of the target rod is dominated by the CB insertion depth. The sensitivity of peak linear power to the CB position was calculated for the maximum, average, minimum and extreme core burnup states. The CB position represents the core response to all kinds of reactivity perturbations to the core such as the fuel depletion and material aging. In order to determine limiting cases for the thermal-hydraulic and cooling system design, the effects of CB position on the peak linear power and total target assembly power have been estimated for both the non-critical and critical cores.

4.4.1 Sensitivity of non-critical core cases

The sensitivity calculations have been conducted for a wide range of CB position beyond the estimated minimum and maximum critical CB position for the base target assembly loading pattern (described in Section 3.2.1). In this simulation, the regulating rod was fixed to its typical position: 25.4 cm for the extreme and minimum burnup core and 38.1 cm for the average and maximum burnup core. It should be noted that the CB movement is synchronized with the regulating rod in real operation. Therefore, the actual operating range of CB will be smaller than the values used for simulations.

The results are summarized in Table 4-10 for the total target power, peak target linear power (LP) and driver fuel peaking factors. The total target power is relatively low for the BOC condition which is a relatively short term period. For the equilibrium core (average and maximum burnup cores), the target power stays within [REDACTED]. The peak linear power of the target rod is kept between [REDACTED] for the simulated equilibrium core states and CB position. The variations of total [REDACTED]

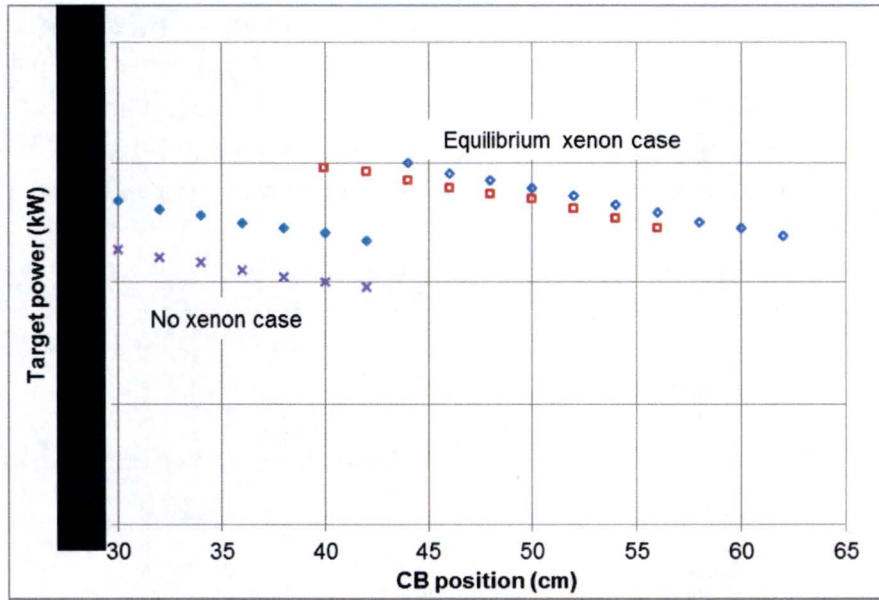
5a, d,
e, f

target power and peak linear power versus CB position are shown in Figure 4-25 and Figure 4-26, respectively.

Table 4-10. Sensitivities of target assembly power and core peaking factors for the base loading

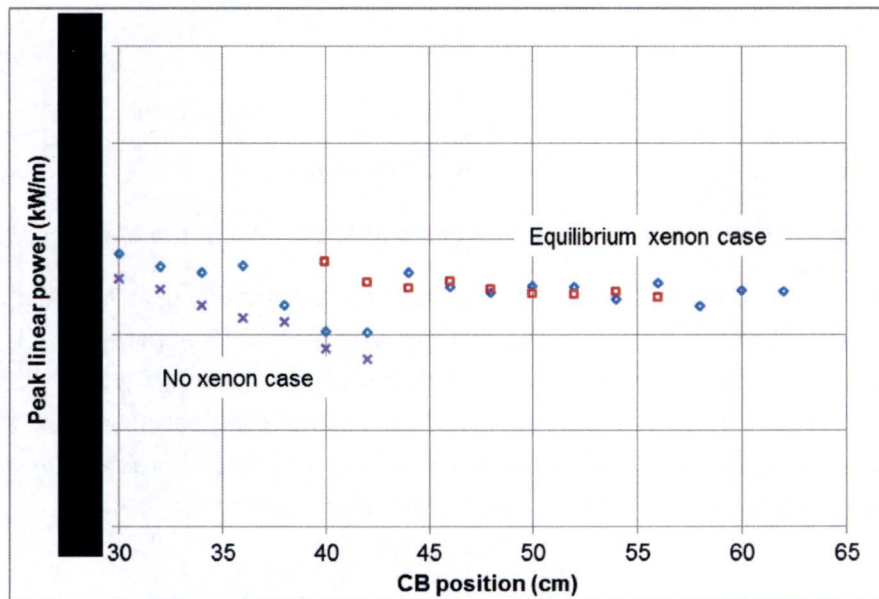
Core state	CB position (cm)	Target power (kW)	Peak LP (kW/m)	Inner plate peaking	Outer plate peaking
Maximum burnup with equilibrium xenon	62			2.573	2.147
	60			2.577	2.173
	58			2.605	2.192
	56			2.622	2.208
	54			2.662	2.239
	52			2.674	2.273
	50			2.709	2.302
	48			2.755	2.348
	46			2.792	2.385
	44			2.861	2.441
Average burnup with equilibrium xenon	56			2.488	2.109
	54			2.505	2.131
	52			2.529	2.163
	50			2.575	2.192
	48			2.609	2.240
	46			2.648	2.263
	44			2.684	2.310
	42			2.757	2.374
Minimum burnup without xenon	42			2.790	2.386
	40			2.857	2.419
	38			2.898	2.453
	36			2.944	2.489
	34			3.046	2.546
	32			3.055	2.576
	30			3.120	2.609
Extreme burnup without xenon	42			2.906	2.301
	40			2.930	2.351
	38			2.991	2.403
	36			3.053	2.475
	34			3.130	2.539
	32			3.182	2.594
	30			3.231	2.636

5a, d,
e, f



5a, d,
e, f

Figure 4-25. Variation of target power vs. control blade position



5a, d,
e, f

Figure 4-26. Variation of peak linear power vs. control blade position

The MURR fuel element power peaking occurs in the fuel element F5. The fuel element peaking is higher for the BOC state when the CB and regulating rod are deep into the core. The calculated maximum peaking factor is 3.231 for the inner plate. For the outer plate that faces the target assembly, the maximum peaking factor is 2.636, which is lower than that of the inner plate for all core state and CB positions. The variations of fuel element peaking factor versus CB position is shown in Figure 4-27.

The maximum linear power found from the sensitivity calculation is [REDACTED] for the extreme burnup core with CB positioned at 30 cm and regulating rod positioned at 25.4 cm, which is recommended for the thermal-hydraulic, critical heat flux (CHF) margin analysis. The maximum target assembly power is [REDACTED] for the maximum burnup core with CB at 44 cm and regulating rod at 38.1 cm, which is recommended for the target assembly cooling analysis.

5a, d,
e, f

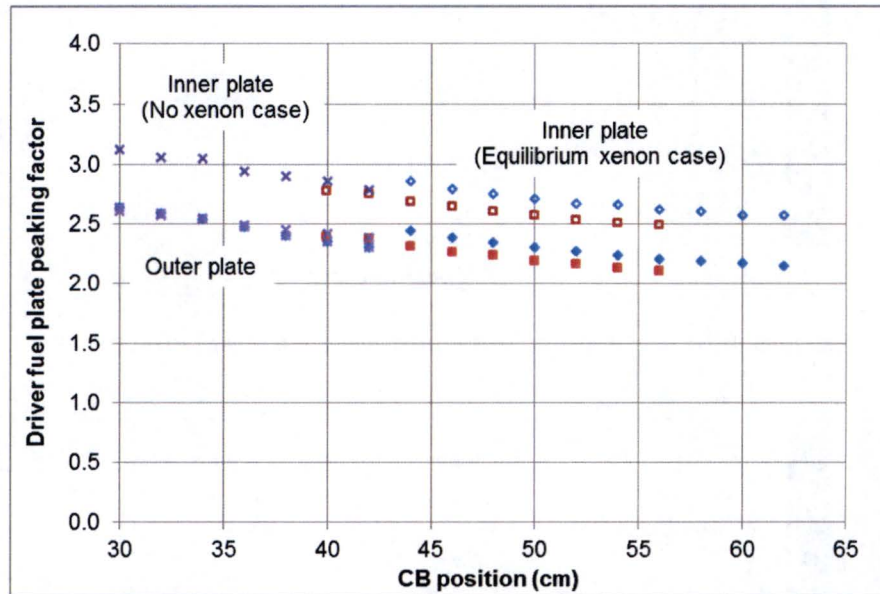


Figure 4-27. Variation of driver fuel peaking factor vs. control blade position

The sensitivities of non-critical core to the CB position have also been calculated for the staggered and partial target assembly loading cases. Tables 4-11 and 4-12 summarize the performance parameters of the staggered loading with a fresh target assembly in 5A and 5B, respectively. Table 4-13 summarizes the partial loading core with 3 target rods per assembly. It can be seen that the total target assembly power and peak linear power of these cores are always lower than those of the base loading case when the CB is at its estimated lowest position.

Table 4-11. Sensitivities of target assembly power and core peaking factors for the staggered loading (5A)

Core state	CB position (cm)	Target power (kW)	Peak LP (kW/m)	Inner plate peaking	Outer plate peaking
Maximum burnup with equilibrium xenon	62	█	█	2.571	2.140
	60	█	█	2.588	2.159
	58	█	█	2.603	2.184
	56	█	█	2.643	2.198
	54	█	█	2.668	2.227
	52	█	█	2.678	2.265
	50	█	█	2.723	2.306
	48	█	█	2.777	2.322
	46	█	█	2.811	2.376
	44	█	█	2.863	2.410
Average burnup with equilibrium xenon	56	█	█	2.490	2.098
	54	█	█	2.502	2.128
	52	█	█	2.535	2.148
	50	█	█	2.582	2.187
	48	█	█	2.612	2.223
	46	█	█	2.664	2.264
	44	█	█	2.690	2.306
	42	█	█	2.769	2.342
	40	█	█	2.810	2.382
Minimum burnup without xenon	42	█	█	2.789	2.373
	40	█	█	2.825	2.416
	38	█	█	2.906	2.453
	36	█	█	2.959	2.492
	34	█	█	3.009	2.529
	32	█	█	3.072	2.551
	30	█	█	3.120	2.601
Extreme burnup without xenon	42	█	█	2.901	2.282
	40	█	█	2.952	2.351
	38	█	█	3.014	2.396
	36	█	█	3.047	2.456
	34	█	█	3.129	2.522
	32	█	█	3.193	2.577
	30	█	█	3.238	2.637

5a, d,
e, f

Table 4-12. Sensitivities of target assembly power and core peaking factors of the staggered loading (5B)

Core state	CB position (cm)	Target power (kW)	Peak LP (kW/m)	Inner plate peaking	Outer plate peaking
Maximum burnup with equilibrium xenon	62	████	████	2.555	2.144
	60	████	████	2.568	2.163
	58	████	████	2.602	2.180
	56	████	████	2.611	2.209
	54	████	████	2.663	2.239
	52	████	████	2.677	2.267
	50	████	████	2.719	2.294
	48	████	████	2.761	2.332
	46	████	████	2.802	2.364
Average burnup with equilibrium xenon	44	████	████	2.853	2.417
	56	████	████	2.477	2.109
	54	████	████	2.497	2.136
	52	████	████	2.541	2.163
	50	████	████	2.582	2.190
	48	████	████	2.603	2.232
	46	████	████	2.673	2.266
	44	████	████	2.701	2.295
	42	████	████	2.750	2.357
Minimum burnup without xenon	40	████	████	2.780	2.396
	42	████	████	2.789	2.384
	40	████	████	2.844	2.419
	38	████	████	2.911	2.457
	36	████	████	2.939	2.490
	34	████	████	3.023	2.544
	32	████	████	3.066	2.578
Extreme burnup without xenon	30	████	████	3.123	2.614
	42	████	████	2.895	2.284
	40	████	████	2.935	2.340
	38	████	████	3.005	2.402
	36	████	████	3.076	2.476
	34	████	████	3.122	2.519
	32	████	████	3.165	2.583
30	████	████	3.244	2.630	

5a, d,
e, f

Table 4-13. Sensitivities of target assembly power and core peaking factors for the partial loading

Core state	CB position (cm)	Target power (kW)	Peak LP (kW/m)	Inner plate peaking	Outer plate peaking
Maximum burnup with equilibrium xenon	62	████	████	2.555	2.070
	60	████	████	2.566	2.073
	58	████	████	2.583	2.100
	56	████	████	2.619	2.117
	54	████	████	2.646	2.141
	52	████	████	2.662	2.177
	50	████	████	2.702	2.193
	48	████	████	2.739	2.236
	46	████	████	2.792	2.284
	44	████	████	2.852	2.338
Average burnup with equilibrium xenon	56	████	████	2.472	2.029
	54	████	████	2.509	2.038
	52	████	████	2.525	2.080
	50	████	████	2.552	2.093
	48	████	████	2.606	2.138
	46	████	████	2.620	2.177
	44	████	████	2.683	2.205
	42	████	████	2.731	2.255
	40	████	████	2.772	2.295
Minimum burnup without xenon	42	████	████	2.778	2.327
	40	████	████	2.830	2.363
	38	████	████	2.891	2.407
	36	████	████	2.933	2.442
	34	████	████	3.000	2.468
	32	████	████	3.040	2.511
	30	████	████	3.125	2.542
Extreme burnup without xenon	42	████	████	2.897	2.200
	40	████	████	2.927	2.266
	38	████	████	3.005	2.332
	36	████	████	3.046	2.379
	34	████	████	3.119	2.454
	32	████	████	3.158	2.501
	30	████	████	3.222	2.550

5a, d,
e, f

4.4.2 Sensitivity of critical core cases

During normal operation, the reactor is critical all the time. However, it is difficult to model a critical core without knowing the status of driver fuel burnup, CB depletion, Be reflector age, etc. Therefore, a simplified model is proposed in this analysis to simulate critical cores with different CB positions: the CB age has been changed from 0-year to 8-year. Table 4-14 shows the CB age matrix used for the critical core calculations. The critical core was searched for k_{eff} value of 1 ± 0.00006 .

For all the critical core cases of the base target assembly loading shown in Table 4-15, the calculated total target power and the maximum linear power are less than those of non-critical core cases. For the extreme burnup core, the peak linear power is 54.2 and 51.3 kW/m for the non-critical and critical core, respectively, when the average CB age is the same (4-year) for both cases. The peak linear power is the highest for the CB average age of 4-years which has the largest age tilt in the CB age model (Table 4-14). If the CB age is 8-years, the peak linear power drops to 50.3 kW/m even though the critical CB position is deep into the core, i.e., 32.28 cm, because the CB age tilt is assumed to be zero. Therefore it is crucial to use the appropriate CB age model when estimating target assembly power to avoid unnecessary over-design of the target assembly.

The investigation of MURR operation history of the CB age has shown that the average CB age during the operation period of April 2006 and October 2016 is 3.65-year. During this period, the maximum CB age tilt between AD and BC is 6.3-years, while the maximum tilt of any CB pair is 9.2-years. The analysis also has shown that the CB age tilt is the highest when the CB average age is 4- to 5-years and the tilt is small when the CB average age is very low (~1-year) or high (~7-years) as shown in Figure 4-28. In summary, the average CB age used for the simulation is close to the actual operating data. The CB age tilt used for the simulation is higher than the operation data, but could be conservatively used. The non-critical core analysis that uses the CB age tilt of 8-years will be the conservative estimation of the target power.

Table 4-14. Control blade age model for critical core conditions

CB	Control blade age (year)				
	0	4	8	8	8
A	0	0	0	4	8
B	0	4	8	8	8
C	0	4	8	8	8
D	0	0	0	4	8
Average	0	2	4	6	8

Table 4-15. Sensitivity of target assembly power and peaking factors for the critical core of the base loading

Core state	CB age (year)	CB position (cm)	k_{eff}	Target power (kW)	Peak LP (kW/m)	Inner plate peaking	Outer plate peaking
Maximum burnup with equilibrium xenon	0	58.86	1.00000	█	█	2.622	2.208
	2	57.61	1.00002	█	█	2.617	2.213
	4*	55.28	0.99995	█	█	2.637	2.218
	6	52.41	1.00002	█	█	2.642	2.220
	8	47.71	1.00005	█	█	2.678	2.227
Average burnup with equilibrium xenon	0	56.74	0.99998	█	█	2.537	2.134
	2	55.25	0.99994	█	█	2.535	2.147
	4*	52.89	0.99999	█	█	2.511	2.155
	6	50.08	1.00000	█	█	2.530	2.155
	8	45.40	0.99995	█	█	2.534	2.154
Minimum burnup without xenon	0	38.06	1.00004	█	█	3.039	2.511
	2	36.12	1.00005	█	█	3.032	2.523
	4*	32.75	0.99995	█	█	3.031	2.565
	6	30.36	1.00003	█	█	3.027	2.536
	8	26.69	1.00005	█	█	3.065	2.497
Extreme burnup without xenon	0	43.65	1.00003	█	█	3.004	2.366
	2	41.88	1.00001	█	█	2.984	2.389
	4*	38.75	1.00002	█	█	2.976	2.397
	6	36.26	1.00005	█	█	2.991	2.400
	8	32.28	0.99995	█	█	3.008	2.376

5a, d,
e, f

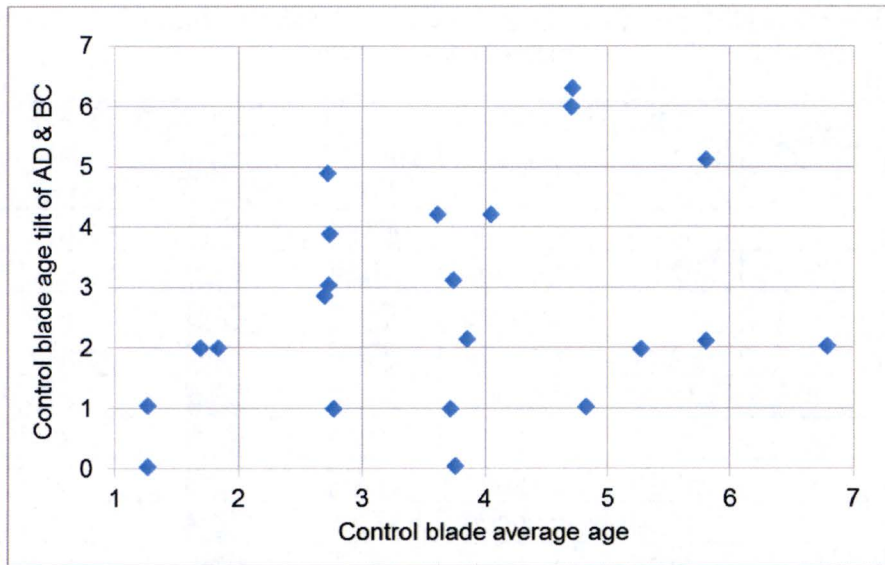


Figure 4-28. MURR control blade age tilt vs age distribution

4.4.3 Limiting core configuration

The critical core calculations have shown that the non-critical core calculations conservatively estimate the target power and the maximum linear power. However, it should also be noted that the critical core simulation here is limited by the range of CB age and, therefore, the variation of CB position is smaller when compared with the expected CB traveling range (see Section 3.2.1). This means that consideration of CB age is not sufficient to realistically model the critical core. It is also true that in the actual core the CB position could be even higher or lower than those used for the critical core calculations due to Be reflector aging and other reactivity perturbations. And it is also logical to assume that the target power and its axial shape are dominated by the CB position. Therefore, the limiting core configuration has been selected from the non-critical core cases as follows:

- For the total target power, the maximum burnup core with the equilibrium xenon and CB at 44 cm is used. The corresponding total target power is [REDACTED]
- For the peak linear power, the extreme burnup core without xenon and CB at 30 cm is used. The corresponding peak linear power is [REDACTED].

5a, d,
e, f

The power peaking factor of the driver fuel and linear power of the target rod are given in Appendices A and B, respectively, for the limiting core configurations.

4.4.4 Sensitivity to regulating rod position

The effect of regulating rod position was assessed for critical cores. Three regulating rod positions, i.e., lowest (25.4 cm), highest (38.1 cm) and middle (31.75 cm), were considered while the CBs were at their critical positions. The results in Table 4-16 show that the target peak linear power and total assembly power are [REDACTED] and [REDACTED], respectively, which are less than those of the limiting core cases. The maximum inner and outer plate peaking factors of the diver fuel are 3.043 and 2.576, respectively, for the minimum burnup core. The effect of regulating rod position is relatively small when compared with that of the CB.

5a, d,
e, f

Table 4-16. Effect of regulating rod position on target power and peak linear power

Core state	Regulating rod (cm)	Target power (kW)	Peak LP (kW/m)	Inner plate peaking	Outer plate peaking
Maximum burnup with equilibrium xenon	38.1	[REDACTED]	[REDACTED]	2.637	2.218
	31.75	[REDACTED]	[REDACTED]	2.641	2.147
	25.4	[REDACTED]	[REDACTED]	2.638	2.046
Average burnup with equilibrium xenon	38.1	[REDACTED]	[REDACTED]	2.511	2.155
	31.75	[REDACTED]	[REDACTED]	2.542	2.093
	25.4	[REDACTED]	[REDACTED]	2.528	1.973
Minimum burnup without xenon	38.1	[REDACTED]	[REDACTED]	3.037	2.576
	31.75	[REDACTED]	[REDACTED]	3.043	2.563
	25.4	[REDACTED]	[REDACTED]	3.031	2.565
Extreme burnup without xenon	38.1	[REDACTED]	[REDACTED]	2.988	2.531
	31.75	[REDACTED]	[REDACTED]	2.999	2.507
	25.4	[REDACTED]	[REDACTED]	2.976	2.397

5a, d,
e, f

4.5 Uncertainty Analysis

The physics analysis has an inherent uncertainty due to the solution method of the MCNP6 code. The standard deviation (1σ) of the pellet power is [REDACTED] for almost all the pellet numerical nodes when 100 million particles are used for the calculation. For the total target power, the standard deviation (1σ) is as small as [REDACTED]. Other uncertainties considered are impurities of target uranium, pellet density, fissile content and target rod position due to manufacturing tolerance. Table 4-17 shows impurities of the target uranium, cladding, cartridge and neutron shield. For the aluminum (cartridge) and stainless steel (neutron shield), the impurity was assumed to be 10 part per million (ppm) natural boron.

5a, d,
e, f

Table 4-17. Material impurities for uncertainty analysis

	Uranium (wt%)	Zircaloy-4 (wt%)	Aluminum (ppm)	Stainless steel (ppm)
²³² U	2×10^{-7}			
²³⁴ U	0.26			
²³⁶ U	0.46			
Boron	3 ppm	0.00005	10	10

4.5.1 Sensitivity calculations

The uncertainties of the total target power and peak linear power were estimated for the limiting core configurations of all four core burnup states. In order to estimate the sensitivity of the core and target performance parameters, the uncertainties of design parameters were defined as follows:

- For the statistical uncertainty of the solution method, $\pm 2\sigma$ value is used to estimate the eigenvalue, total target power and peak linear power with a 95% confidence level.
- The impurities always reduce the target power and are regarded as a bias. The uncertainty is estimated as 95% of performance parameter change due to the maximum impurity level of the target uranium, assuming a flat distribution of impurity between its minimum and maximum values.
- The manufacturing tolerances of the pellet density and fissile content are [REDACTED] and [REDACTED], respectively. The target performance is relatively insensitive to the variation of these parameters. For conservatism, the tolerance value is taken as the uncertainty. In the simulation, only a positive value is used as a bias to estimate the power increases. 5a, b, e, f
- The uncertainty of the target rod position is [REDACTED] which is 2/3 of the manufacturing/installation tolerance [REDACTED], i.e., approximately a 2σ value when a triangular distribution is assumed between the minimum and maximum values with the mode (average) at 0. The [REDACTED] means that the rod is closer to the core by [REDACTED]. Though the target rod could be either closer to or farther from the core, [REDACTED] is used as a bias to estimate the power increase of the target. 5a, b, e, f

The estimated uncertainties (positive components) of the core eigenvalue, target total power and peak linear power due to the statistical and manufacturing uncertainties are summarized in Table 4-18, Table 4-19 and Table 4-20, respectively. The impact of the pellet fabrication density and fissile content uncertainty on the core eigenvalue and target peak linear power is very small, which makes it difficult to obtain consistent results by direct perturbation calculations. Therefore, these

uncertainties were increased by a factor of 5 in the direct perturbation calculation, and the results were linearly interpolated.

The uncertainty (positive variation) of the eigenvalue due to manufacturing tolerance (pellet density and fissile content) is estimated to be less than 11 pcm. The impact of rod position uncertainty is the largest among five uncertainties for all core states. For the target total power, the statistical uncertainty is very small, while the target rod position uncertainty dominates the total uncertainty. The estimated uncertainty due to manufacturing tolerance is [redacted] and [redacted] for the pellet density and enrichment, respectively, while the uncertainty due to target rod position is [redacted] for the maximum burnup core. For the peak linear power, the statistical uncertainty prevails over the uncertainties due to the pellet density and enrichment, but it is comparable to the uncertainty due to target rod position.

5a, b, e, f

Table 4-18. Uncertainty of core eigenvalue due to simulation and manufacturing

Core burnup state	Statistical uncertainty (pcm)	Impurity (pcm)	Fabrication density (pcm)	Enrichment (pcm)	Rod position (pcm)
Maximum with equilibrium xenon	■	■	■	■	■
Average with equilibrium xenon	■	■	■	■	■
Minimum without xenon	■	■	■	■	■
Extreme without xenon	■	■	■	■	■

5a, b, e, f

Table 4-19. Uncertainty of target power due to simulation and manufacturing

Core burnup state	Statistical uncertainty (%)	Impurity (%)	Fabrication density (%)	Enrichment (%)	Rod position (%)
Maximum with equilibrium xenon	■	■	■	■	■
Average with equilibrium xenon	■	■	■	■	■
Minimum without xenon	■	■	■	■	■
Extreme without xenon	■	■	■	■	■

5a, b, e, f



Table 4-20. Uncertainty of peak linear power due to simulation and manufacturing

	Statistical uncertainty (%)	Impurity (%)	Fabrication density (%)	Enrichment (%)	Rod position (%)
Maximum with equilibrium xenon	████	████	████	████	████
Average with equilibrium xenon	████	████	████	████	████
Minimum without xenon	████	████	████	████	████
Extreme without xenon	████	████	████	████	████

5a, b, e, f

4.5.2 Total uncertainties of the limiting core performance parameters

The total uncertainties of the key performance parameters (eigenvalue, total target power, and peak linear power) were estimated in two ways as summarized in Table 4-21:

- A simple arithmetic summation of individual uncertainties. Note that the uncertainty due to impurity is always negative, but is not included in the summation for conservatism.
- A root-mean-square (RMS) of individual uncertainties. The total uncertainty is obtained as a product of statistical uncertainty and RMS of fabrication density, enrichment, and target rod position uncertainties. For example, the upper bound of the power (P) is estimated as $P = P_0(1 + \sigma_s) \left(1 + \sqrt{\sigma_d^2 + \sigma_e^2 + \sigma_p^2} \right)$, where P_0 is the power without uncertainty, subscripts s, d, e, and p refer to the uncertainties due to statistical, density, enrichment, and position, respectively. The uncertainty due to impurity is neglected for conservatism.

The simple arithmetic summation means that individual constituent uncertainties occur simultaneously, which is a very low probability case and could be too conservative. It was decided to use the RMS model to estimate the total uncertainty. For the limiting core configurations, the total uncertainties were finally applied to the design values of the target performance parameters:

- For the eigenvalue, the estimated uncertainty is ██████.
- For the total target power, the estimated uncertainty is ██████ for the maximum burnup core. The estimated upper bound of the total target power is then ██████.

5a, b, e, f



- For the peak linear power, the estimated uncertainty is [REDACTED] for the extreme burnup core. The estimated upper bound of the peak linear power is then [REDACTED].

5a, b, e, f

Table 4-21. Total uncertainty of the performance parameter

Core burnup state	Eigenvalue (pcm)		Target total power (%)		Peak linear power (%)	
	Arithmetic	RMS	Arithmetic	RMS	Arithmetic	RMS
Maximum	[REDACTED]	[REDACTED]	[REDACTED]	[REDACTED]	[REDACTED]	[REDACTED]
Average	[REDACTED]	[REDACTED]	[REDACTED]	[REDACTED]	[REDACTED]	[REDACTED]
Minimum	[REDACTED]	[REDACTED]	[REDACTED]	[REDACTED]	[REDACTED]	[REDACTED]
Extreme	[REDACTED]	[REDACTED]	[REDACTED]	[REDACTED]	[REDACTED]	[REDACTED]

5a, b, e, f

4.6 Target Material Depletion

As the fissile material burns in the target assembly, the target assembly power steadily decreases as the target assemblies are being irradiated, under the condition that the incoming neutron flux level is constant. Table 4-22 lists the isotopic mass of two target assemblies irradiated for two weeks for the average burnup core, which is the most probably core state. The ⁹⁹Mo production calculations have been conducted under following core conditions:

- Mid-life (~ 4-year) Be reflector composition is used.
- The average CB age (4-year) is used for all CB's. There is no CB mechanical tilt.
- The average burnup core fuel composition is used for driver fuel elements. The CB's are at their critical position.

The ⁹⁹Mo buildup is shown in Figure 4-29 for different loading and operational schemes. For the base operation scheme, the calculated ⁹⁹Mo weekly production is [REDACTED], when 2 fresh target assemblies are irradiated for [REDACTED] and discharged. In order to satisfy the requirement of 3,000 6-day Curies per week, one or both reflector shall be loaded [REDACTED].

5a, b, e, f

For the staggered operation, the weekly ⁹⁹Mo production is [REDACTED], when 2 target assemblies are irradiated for [REDACTED]. For the partial loading with 3 rods per assembly, the calculated weekly production [REDACTED]. Based on these results, the ⁹⁹Mo production per target rod is obtained as [REDACTED] per week for the base, staggered and partial loading pattern, respectively. For the partial loading, the production rate from 1-, 5-, 7- and 9-rod per assembly is [REDACTED] respectively,

5a, b, e, f

for two-target assembly loading. It should be noted again that these products rates were estimated under the assumption of constant neutron flux in the target which will result in an overestimation of the production rate.

As the fissile uranium depletes, the target assembly power linearly decreases as shown in Figure 4-30. At the end of [redacted] irradiation, the target assembly power drops to [redacted] for the base loading pattern, which corresponds to a [redacted] reduction when compared to the initial power of [redacted]. The average target pellet burnup is [redacted].

5a, b, e, f

Table 4-22. Target material composition and burnup for the average burnup core

Calendar day	Operation	Burnup (MWd/tHM)	²³⁵ U (gram)	²³⁸ U (gram)	²³⁹ Pu (gram)	⁹⁹ Mo (mg)
[redacted]	[redacted]	[redacted]	[redacted]	[redacted]	[redacted]	[redacted]
[redacted]	[redacted]	[redacted]	[redacted]	[redacted]	[redacted]	[redacted]
[redacted]	[redacted]	[redacted]	[redacted]	[redacted]	[redacted]	[redacted]
[redacted]	[redacted]	[redacted]	[redacted]	[redacted]	[redacted]	[redacted]

5a, b, e, f

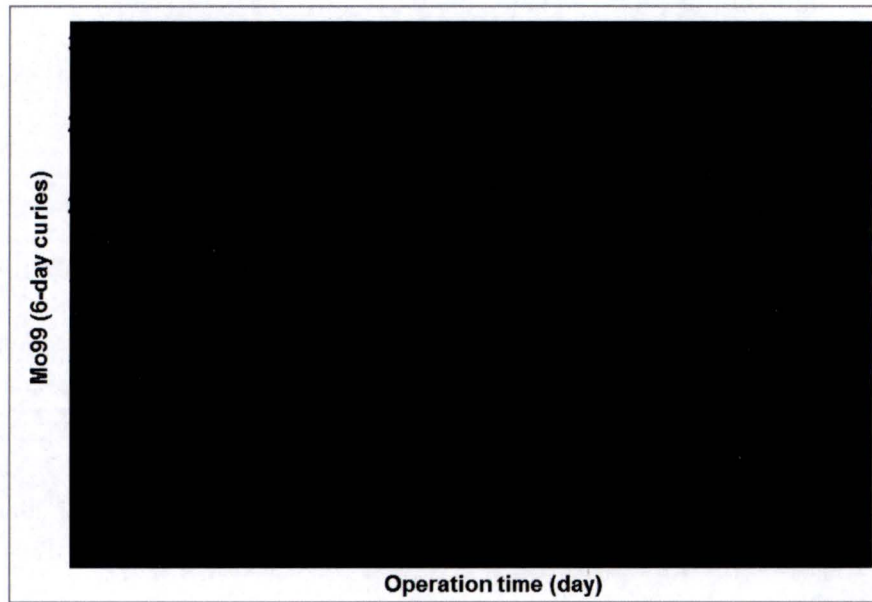


Figure 4-29. Estimation of weekly ⁹⁹Mo production for different loading patterns



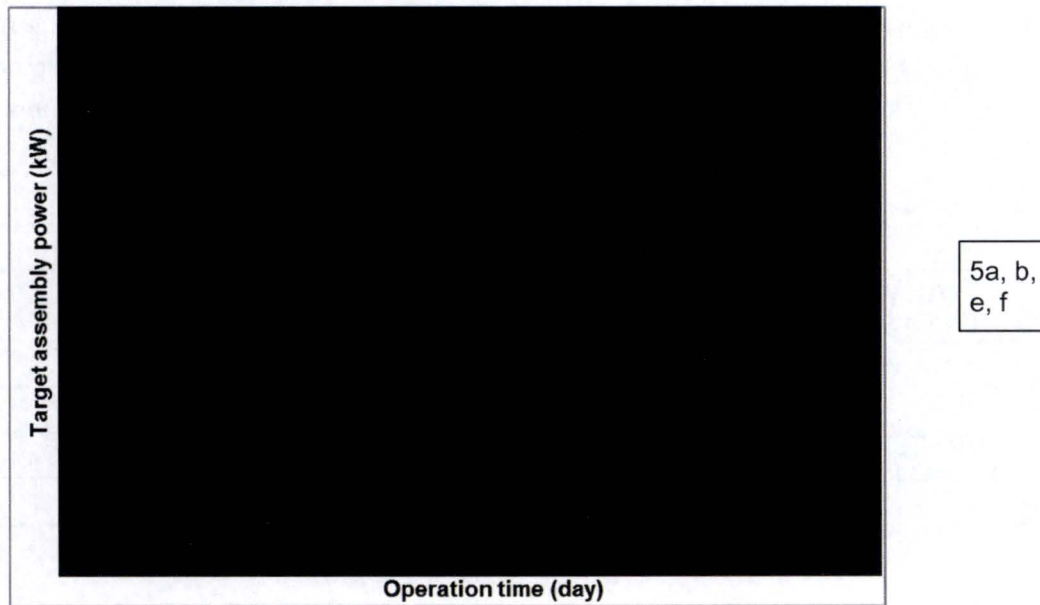


Figure 4-30. Estimation of the target assembly power during 2-week operation

4.7 Structural Component Heating

4.7.1 Steady-state structural component heating

The structural component heating was estimated by MCNP6 code using the kinetic energy deposited by the fission fragments, prompt neutrons and the delayed neutrons. In addition to the neutron data used for neutron flux calculation, the heating calculation uses photon-atomic data (mcplib04) [White 2003], photon-nuclear data (endf7u) [White 2000], electron data (el03) [Briesmeister 2000], and delayed neutron/gamma data (cinder.dat, delay_library.dat, cindergl.dat, delay_library_v2.dat) [Durkee 2012, Pelowitz 2013]. The MCNP6 adopts the CINDER'90 model to calculate delayed particle emissions from all of the radionuclides in the decay chain for a fission product. The photon emission time for delayed-neutron and delayed-photon emission was adjusted to 10^5 sec (the default value is 10^{10} sec), under which the statistical uncertainty (1σ) of the calculated heat deposit in the Be reflector is ~5%. The structural component heating is summarized in Table 4-23 for the maximum burnup core which has the highest radiation heating of the components. The Be reflector heating is higher for the maximum burnup core by 3.3% when compared with the minimum burnup core. For the maximum burnup core, The Be reflector heating is 216.2 kW and 205.7 kW with and without two target assemblies, respectively. The heat in the cartridge and neutron shield is 12.7 kW and 7.6 kW, respectively, when two target assemblies are loaded.

The spatial distribution of the Be reflector heating is given in Table 4-24 for 6 azimuthal sectors and 15 segments of sector 1 which faces target assemblies. The 15-segment of sector 1 consists

of 5 axial nodes and 3 radial nodes. Though the total Be reflector heating is the highest for the maximum burnup core, the local heating is the highest for the minimum burnup core, when the CB is at its estimated lowest position, due to skewed axial power shape as summarized in Table 4-25.

Table 4-23. Component radiation heating of the maximum burnup core

Target loading	Component	Neutron heating	Photon heating	Electron heating	Total (kW)
No target	Be reflector	41.6	81.9	82.2	205.7
Two target assemblies	Be reflector	42.9	86.2	87.1	216.2
	Al cartridge	0.27	6.2	6.2	12.7
	Steel shield	0.05	3.8	3.8	7.6

Table 4-24. Spatial distribution of Be reflector radiation heating for the maximum burnup core

Target loading	Sector	Heating (kW)	Axial layer of sector 1	Radial segmentation of Sector 1		
				Inner	Middle	Outer
No target	1	33.63	5	0.99	0.94	0.76
	2	34.60	4	3.12	2.71	2.26
	3	34.33	3	4.86	4.01	3.22
	4	34.84	2	3.17	2.64	2.12
	5	34.08	1	0.98	0.96	0.90
	6	34.11				
Two target assemblies	1	41.49	5	1.10	1.14	1.00
	2	35.98	4	3.58	3.27	3.17
	3	32.94	3	5.57	5.08	4.77
	4	34.02	2	3.31	3.21	2.99
	5	34.53	1	1.05	1.13	1.12
	6	37.10				

Table 4-25. Spatial distribution of Be reflector radiation heating for the minimum burnup core

Target loading	Sector	Heating (kW)	Axial layer of sector 1	Radial segmentation of Sector 1		
				Inner	Middle	Outer
No target	1	34.34	5	0.74	0.64	0.62
	2	34.43	4	2.45	2.22	1.94
	3	31.68	3	4.86	4.41	3.42
	4	32.24	2	3.77	3.23	2.53
	5	31.87	1	1.27	1.15	1.09
	6	34.31				
Two target assemblies	1	41.78	5	0.78	0.76	0.69
	2	36.00	4	2.64	2.56	2.34
	3	31.49	3	5.83	5.12	4.65
	4	31.90	2	4.18	3.94	3.86
	5	32.72	1	1.54	1.42	1.46
	6	37.04				

4.7.2 Post-shutdown structural component heating

The post-shutdown structural component heating was estimated by a combination of ORIGEN2 and MCNP6 calculations. This is necessary due to photo-neutron effects after shutdown, where photons from MURR driver fuel and SGE target rods react with the Be reflector, releasing neutrons which then cause fission in the SGE target rods, leading to heating in rods and assembly components.

ORIGEN2 cases modeled irradiation of the MURR driver fuel elements to their respective burnup values, followed by several decay steps. Results show that the initial 30 minutes into the decay has the largest reduction in photon source (gammas released per second). Details of the photon sources (18-group mean energy and probability distributions) were input to MCNP6 via the SDEF (source definition) card. Photonuclear physics was turned on by the MODE card. The same nuclear, photon-atomic, photon-nuclear, and electron data was utilized as the steady-state structural component heating calculations.

Tallied results indicate that the total heating is very small. One second into the decay, total heating is 0.469 W for the beryllium reflector, 0.016 W for the SGE target rods and 0.107 W for the SGE target assemblies. After 30-minutes into the decay, total heating reduces to 0.209 W for the beryllium reflector, 0.007 W for the SGE target rods and 0.048 W for the SGE target assemblies.

These results are considered credible upon closer evaluation. The total photon (p) flux in the beryllium reflector is 6.2×10^9 p/cm²-sec. Noting that the threshold for photonuclear reactions are for energies greater than 1.6 MeV, the photon flux in the beryllium reflector within the threshold is reduced to 2.9×10^8 p/cm²-sec. The total photonuclear cross section (from the '70u' library) is very small, averaging 4.3×10^{-4} barns. Using these numbers, the photonuclear reaction rate in the Be reflector is 1.53×10^4 reactions/cm³-sec, essentially the initial neutron density in the Be reflector. This low neutron density made it difficult to achieve great statistics, where the tallied target rod neutron flux is 5.2×10^6 n/cm²-sec with an error of 15%. These results confirm that post-shutdown photo-neutron effects have a negligible impact on heating in the Be reflector, SGE target rods and SGE assembly components.

5 VALIDATION OF METHODS USED IN PHYSICS DESIGN

It is essential that the computational tools and methods should predict the target assembly as well as the reactor core accurately so that the target assembly operates safely and economically as designed. The confidence in the nuclear design and analysis results can only be obtained by comparing calculated results with measurement data. The MCNP code has been benchmarked against various experimental results [Whalen 1992, Mosteller 2002, Mosteller 2010] and recognized as the most robust tool in criticality and radiation-shielding calculations. However, the code validation is an integral assessment of the solution method, geometry modeling, and nuclear data and, therefore, it is problem-specific. The best benchmark model of MCNP for the application to the target assembly design and analysis would be validating MURR core itself or MURR-like core by the MCNP code. Two benchmark models of MCNP and one verification test of the ⁹⁹Mo production model have been selected as follow:

- Section 5.1 presents MURR technical report on the validation of MCNP model for predicting critical control blade position. The model includes detailed fuel and core geometry as well as depletion of fuel and structural components such as control blades and beryllium reflector [Peters 2013].
- Section 5.2 presents the validation results of MURR control blade depletion model. The model includes detailed segmentation of the control blade based on their in-core service period and comparison to measured criticality [Peters 2012a].
- Section 5.3 presents a criticality benchmarking of ATR [Kim 2005], of which the fuel specifications are similar to those of MURR. The core is also cooled by light water and reflected by beryllium.
- Section 5.4 presents a verification test of the ⁹⁹Mo prediction model against the ORIGEN2.2 code for ⁹⁹Mo content in the target assembly and collection system [Choi 2015b].

5.1 Validation for Computational Methods and Calculations at MURR

MURR Core Description and MCNP Model

The MURR has a cylindrical core consisting of eight highly-enriched uranium (HEU) fuel elements surrounding a central flux trap. A primary beryllium reflector ring is located inside a secondary graphite reflector ring, which surrounds the core. The core is cooled and moderated by light water. Several irradiation locations are present in the flux trap region as well as the graphite reflector region of the core. Its excess reactivity is controlled by the movement of four axially-banked Boral® shim control rods (blades). The blades travel within an annular water gap between the outer surface of the outer pressure vessel and the inner surface of the beryllium reflector. Figure 5-1 shows the MCNP model of the MURR core configuration.

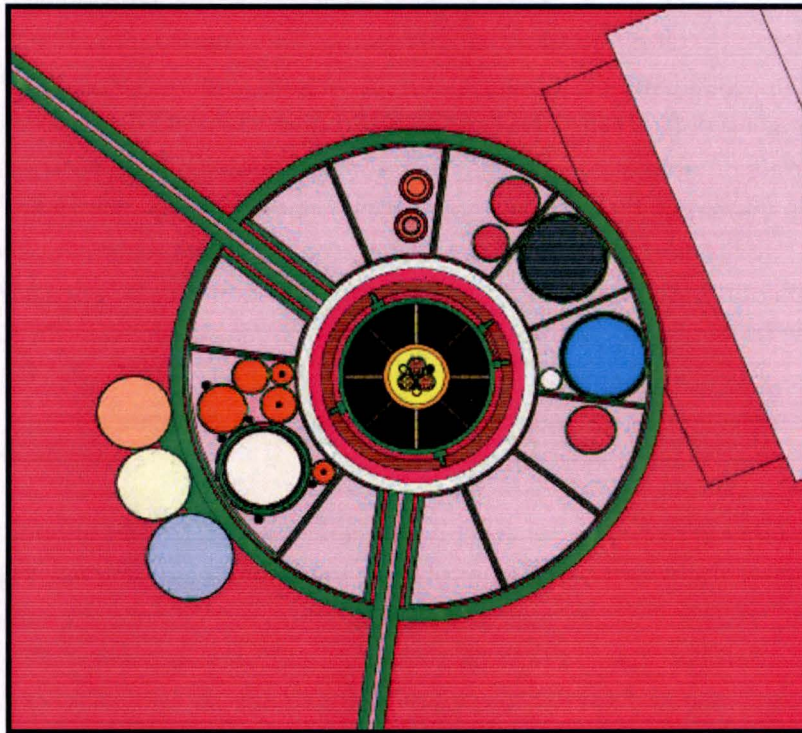


Figure 5-1. A detailed MCNP model of the MURR core

To properly model a MURR's "mixed-core" fuel configuration in MCNP, a separate fuel depletion study was done previously using MONTEBURNS-2.0 [Trellue 1999]. This study generated the fuel material definitions needed in MCNP, i.e., atom densities of various isotopes in the fuel matrix, for a range of xenon-free fuel elements from fresh (0 MW-days or no fuel depletion) to almost spent status (approximately 150 MW-days). For the ECP prediction calculation, fuel element

definitions can be individually selected from this fuel burn up database to make up the starting xenon-free core comprising of eight fuel elements.

In addition to having a mixed-core fuel configuration, MURR also employs a mixture of four independently depleted Boral® shim control blades (rods). Here, each blade has a different core runtime, and hence, different axial and radial boron depletion profile. In order to accurately predict the ECP, the depletion state of each in-core shim control blades have to be accurately defined in the MCNP core model. Similar to the fuel depletion simulations, a separate control blade depletion study [Peters 2012a] was also undertaken to generate control blade definitions for various stages of control blade burn up.

Other major factors that influence the ECP prediction, which were included in the MCNP model are the runtime depletion of the beryllium reflector and the status of the central flux trap region. Depletion studies of the beryllium reflector using MONTEBURNS were done to understand the changes in the core's reactivity as a function of runtime. This study produced a library of beryllium material definitions describing its burnup status at various runtimes from a fresh state up to 8 years; MURR usually replaces the beryllium reflector after every 8 years of runtime. As with the fuel and control rods databases, a particular beryllium material definition can be selected from the library to improve the accuracy of the full-core MCNP model. MURR utilizes the central flux trap, the peak thermal flux region of the core, extensively for irradiating various positive and negative reactivity-worth samples each week for research as well as commercial applications. The mixtures of samples irradiated in this region vary slightly from week to week. Reactor Safety Limits also limits the total reactivity worth of the flux trap. Therefore, in the MCNP model, various targets that go into the flux trap region as well as the graphite reflector of the core were modeled accurately in order to reduce the error in the ECP prediction.

Using the information previously discussed the final MCNP MURR model was created to accurately reflect the status of the fuel, control rod beryllium reflector and flux trap or a given core configuration. The MCNP5 KCODE option was used for all calculations. The parameters were set to run 20 million particles, (i.e., 20000 particles per 1000 active cycles). The (n,p) MODE of calculations was selected and the ENDF-BVII.0 neutron cross-section data set was used for both fast and (s, α) thermal scattering neutron interactions. Specifically, the (s, α) thermal scattering data for all moderator material was initially set at 300K.

Automated Critical Rod Height Search Routine

A critical rod height search routine was developed to predict the ECP for a given weekly xenon-free MURR core configuration. Given an initial guess of the critical rod height, the search routine utilizes a series of MCNP5 criticality (KCODE) calculations in order to calculate the critical control rod height. The routine first uses the initial critical rod height guess in a KCODE calculation to estimate the k_{eff} for the selected MURR core configuration. If the calculated $k_{\text{eff}} \neq 1.0000$ (within a

specified error range), the routine will automatically adjust the control rod height in a subsequent KCODE calculation. The process is repeated until the predicted k_{eff} is essentially equal to 1.0000. For this work, the accepted tolerance for the reactor considered being critical was set at $1.0000 \pm 0.03\%$.

Modified MONTEBURNS

To accurately predict the hot-startup ECPs, it is necessary to track the buildup of xenon in the core during start up and subsequent steady state operation as well as the buildup and decay of the poisons during shutdown and restart. MONTEBURNS 2.0 was selected to simulate the fission products poison transients (particularly Xe-135) and the ECP prediction of the MURR core.

MONTEBURNS utilizes the capabilities of ORIGEN 2.2 for isotope generation and depletion calculations and MCNP5 for continuous energy, flux and reaction rate as well as criticality calculations. However, the program is not designed as such to handle the transient period from reactor startup through critical, and into steady state operation without some modifications since the process involves the control rod motion as well. Although there are computer codes available that can track control rod movements, it was decided to modify and utilize the system of codes that are already adapted to MURR core modeling and predictions. Therefore, MURR Hot Startup ECP predictions were performed using a modified MONTEBURNS by incorporating the in-house developed critical rod search routine. The data-flow diagram for the modified version of MONTEBURNS used here is shown in Figure 5-2.

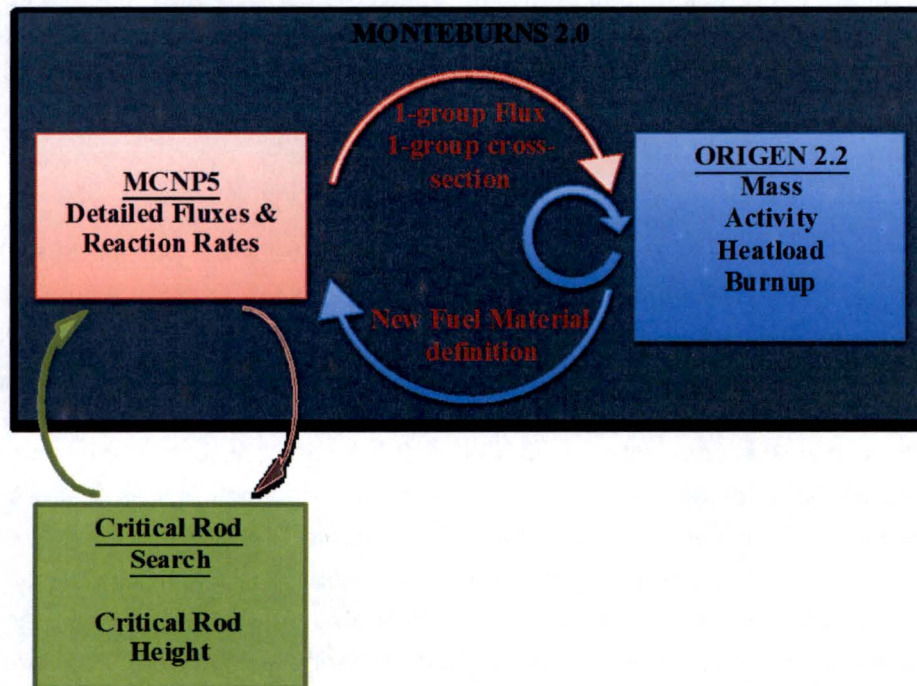


Figure 5-2. A depiction of the generalized information flow in the modified MONTEBURNS simulation for predicting hot startup ECPs

The normal flow of data in MONTEBURNS is a cyclic, stepwise process where every depletion or burn step involves both MCNP and ORIGEN calculations, and every decay step employs ORIGEN calculations only. In Figure 5-2, this is represented as the flow between the MCNP5 and ORIGEN2.2 within the MONTEBURNS block. In the modified MONTEBURNS simulations, the Critical Rod Search routine is placed external to this scheme and linked as shown in Figure 5-2. The Critical Rod Search routine ensures that the MCNP5 model that is used in the depletion calculation for a particular time-step in MONTEBURNS is that which represents the critical core state. This modified MONTEBURNS simulation methodology allows for the study of the MURR-core at any state-point; that is, whether at xenon-free initial critical state, or at the end-of-cycle equilibrium-xenon critical state or at other specified point in between. Moreover, when the fuel 'feed' option is employed in MONTEBURNS, various startup and shutdown scenarios of the MURR core can be simulated with high accuracy.

Benchmarking ECP Predictions from the Computational Methodology

In order for the shutdown scenarios to be accurately simulated, the results from the critical rod height search routine were first benchmarked separately. Here, initial ECP predictions using the critical rod search routine for various weekly startup cores were compared with the actual initial (start-up) critical data. Eight weeks of benchmarking were undertaken to ensure consistency in the routine's ability to predict the initial ECP accurately. Table 5-1 shows a span of data reported

over eight months. Startups at the MURR require an occasional "strainer" start up where initial critical data is taken without any flux-trap samples or irradiation tubes. Two strainer startups were reported in Table 5-1.

Table 5-1. A comparison of predicted initial critical rod height vs. actual at the MURR

Core Configuration Date	Actual Initial Critical Height (inches)	Predicted Initial Critical Height (inches)	Predicted Keffective	Flux Trap Configuration
Week 1/28/2013	16.79	16.67	0.99993	Strainer
Week 2/04/2013	16.52	16.27	0.99975	FT Samples
Week 4/29/2013	15.98	15.78	1.00017	FT Samples
Week 6/10/2013	15.44	15.42	0.99995	FT Samples
Week 8/05/2013	16.74	16.74	0.99985	Strainer
Week 8/12/2013	15.71	15.61	0.99985	FT samples
Week 8/19/2013	15.84	15.84	1.00016	FT samples
Week 8/26/2013	15.64	15.69	1.00029	FT samples

A negative bias of ~1.5% is seen in the predictions for the early benchmarks for the various core configurations. After some additional refinement of the MURR core MCNP model, which included the additional effects of MURR's aged beryllium reflector ring, and more appropriate (s,α) thermal scattering data for neutron in the primary coolant (i.e., data at 350K vs. 300K), the variations in the predictions were within ±0.8% of the actual critical rod heights. Figure 5-3 shows a plot of the predicted ECP percent deviation from actual critical. The improvements based on adding the beryllium age-effect and the higher-temperature (s,α) tables in the primary coolant/moderator to the MCNP models are both indicative of adding negative reactivity to the core, hence causing an increase in the control rod heights to values closer to the actual values.

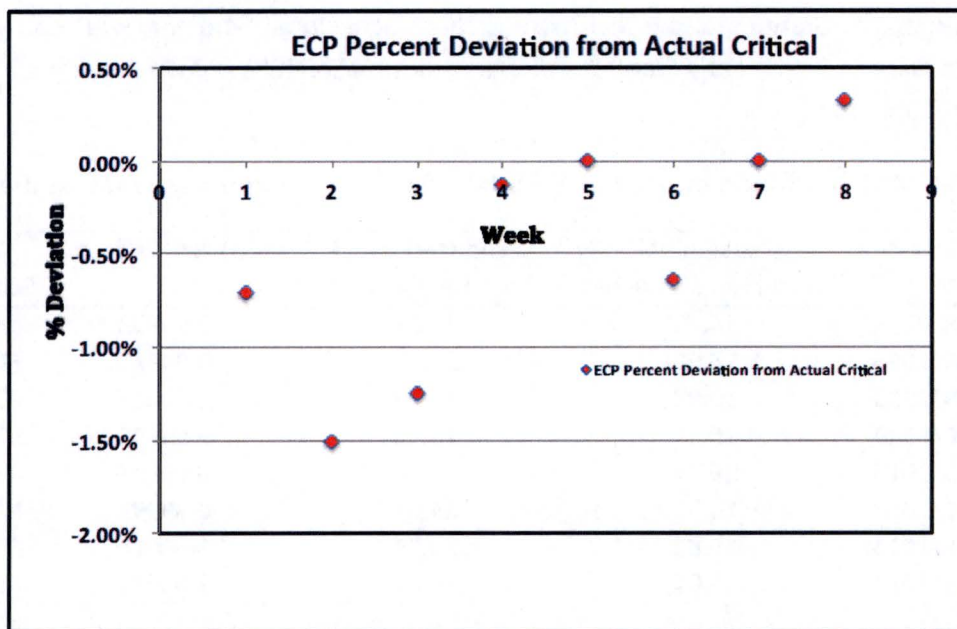


Figure 5-3. A plot of the predicted ECP vs. actual initial critical height

The first hot-startup benchmark was based on an unscheduled shutdown event occurred during normal operation initially starting with the week-4 cold clean core configuration having total megawatt-days of 600.9 and an average control rod runtime of 4 years. Here, the unscheduled shutdown occurred 11.5 hours after normal operation at 10 MW following the initial startup. The total down period of the reactor, which includes to where the reactor is critical at 50 kW, lasted for 1.5 hours. Here, the low-powered Hot-start criticality (i.e., reactor power less than 50 kW) was achieved in 19 minutes and to a power of 5 MW at 24 minutes after startup. Based on this information, the event was simulated in this work and the results are presented in Table 5-2. Another occurrence of an actual hot-startup attempt was simulated, where an unscheduled shutdown occurred 26.0 hours after operating at full power following the initial startup, using a core with total megawatt-days of 613.7 and an average control rod runtime of 3.625 years. The hot-startup was attempted after 2 hours of downtime. Failure for the reactor to restart indicated that the xenon-135 concentration could not be override by the withdrawal of the control rods even at maximum travel. The benchmark of this simulation is presented in Table 5-3.

Table 5-2. A Comparison of the predicted ECP vs recorded rod height data for an actual hot startup from an unscheduled-shutdown event

Time into normal operation from critical (Hours)	Actual Control Rod height inches	Predicted Control Rod Height inches	% Deviation
0	15.44	15.41	0.194%
5.75	17.16	17.19	-0.175%
11.5	19.25	19.15	0.519%
Time into Hot Startup operation from critical (Hours)			
0	22.95	22.73	0.959%
1.00	21.04	21.00	0.190%

The data presented in Table 5-2 shows very good agreement between the predicted control-rod heights and the actual recorded heights at startup, during normal operations and at shutdown, after 11.5 hours. The deviations between the predictions and actual control-rod heights are less than $\pm 1.0\%$. At MURR, almost all of the excess-reactivity loss during normal operation is due to xenon poisoning, therefore it is seen here that the transient xenon-135 quantity is predicted accurately at any given state point. Since Hot-startups rely on whether there is sufficient core excess-reactivity established to override the buildup of xenon-135 by continuous withdrawal of the rods, taking startup critical rod-height data during hot-startups is not as precise as a normal startup and is often not recorded. For this simulated unscheduled scenario, the predicted hot-startup ECP is quite close to the observed startup rod height of 22.95 inches. At one hour of operation after the hot-startup, the simulation predicts a lowering in the control rods. This response is expected, and is seen in the actual data since the xenon-135 burnout rate at this point is larger than its buildup rate from the decay of iodine-135, causing a decrease in the total xenon-135 concentration, therefore, adding positive reactivity to the core.

Table 5-3. A Comparison of the predicted ECP vs recorded rod height data for an actual failed hot startup from an unscheduled-shutdown event

Time into normal operation from critical (Hours)	Actual Control Rod height inches	Predicted Control Rod Height inches	% Deviation
First startup with loaded FT			
0	16.25	16.26	-0.062%
26.00	22.8	22.63	0.746%
Time into Hot Startup operation from critical (Hours)			
0.0833	no startup Maximum CR travel	26.00 Maximum CR travel	

For the next unplanned shutdown simulation, Table 5-3 shows the control rod height comparison between the simulation and the actual measurements for this hot-startup attempt. The deviations between the predicted critical rod heights and the actual recorded rod heights show good agreement i.e., within 1.0%. Like the actual hot-startup attempt, the simulation predicts no possibility for a hot-startup; here, the control rods are fully withdrawn (at 26.0 inches) with a predicted subcritical k_{eff} of 0.99568.

5.2 Validation of MURR Control Blade Depletion Model

The University of Missouri Research Reactor (MURR[®]) is a 10 MW research and training reactor that is owned and operated by the University of Missouri-Columbia. The reactor is designed as a compact-type, pressurized, cylindrical core consisting of eight fuel elements surrounding a central flux trap. The core is primarily moderated by light water and has a primary beryllium reflector inside a secondary graphite reflector ring. Controlling excess reactivity for reactor operation comes from the movement of four axially-banked BORAL[®] shim control blades. The blades travel within an annular water channel between the outer surface of the outer reactor pressure vessel and the inner wall of the beryllium reflector. Figure 5-4 below shows a horizontal cross-sectional view of the MURR core. The poison zone of each blade spans an arc of 72 degrees, has a length of 34 inches and a thickness of 0.1 inch. The travel distance for the active region of each blade is constrained to the length of the fuel meat at 26 inches. A fifth control blade, constructed of stainless steel and located in the same water channel, is used for only very minor adjustments to excess reactivity during steady-state full power operation.

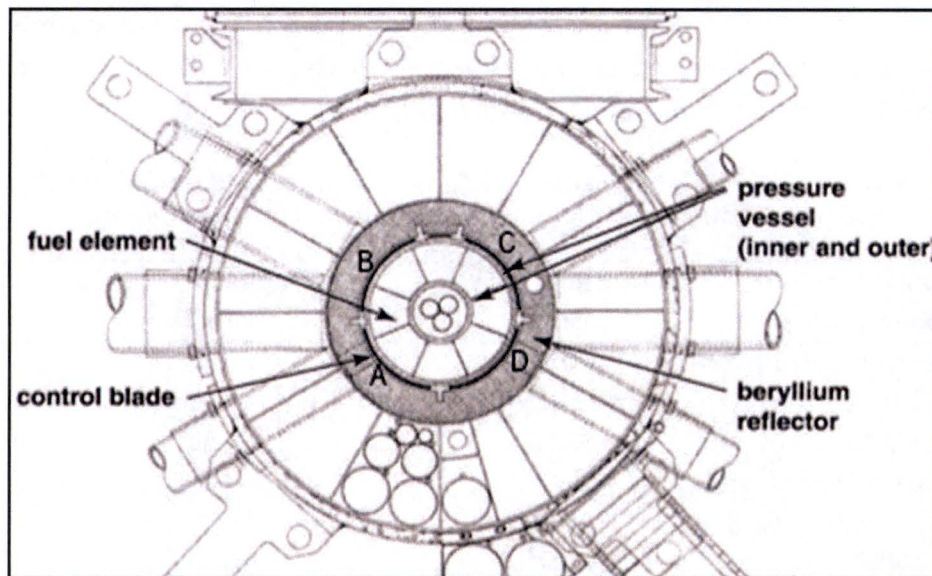


Figure 5-4. Cross sectional view of the MURR core

In collaboration with the Global Threat Reduction Initiative (GTRI) program at Argonne National Laboratory (ANL), MURR took part in a feasibility study [McKibben 2009] for the use of a low-enriched uranium (LEU) molybdenum alloy (U-10Mo) as a new monolithic fuel in the reactor core. The neutronic analyses performed for the feasibility study included a criticality study using LEU fuel, a fuel depletion analysis, as well as a power peaking analysis for an all-fresh core and for mixed cores consisting of fuel elements at various stages of burnup. In order to benchmark the feasibility neutronic analyses, which were performed using the 3-dimensional radiation transport code MCNP [LANL 2003] and ANL's transport and depletion modules DIF3D [Lawrence 1983] and REBUS [Olson 2001], several criticality analyses were performed for the current MURR highly-enriched uranium (HEU) core. Although the criticality benchmarks predicted k_{eff} values relatively close to the measured values, a deficiency was noted where all of the studies employed fresh (non-depleted) control blades. This tended to bias the predicted k_{eff} values.

The use of control blades in the MURR core is very complex since several "active" shim control blades are cycled in and out of the core multiple times during their useable lifetime and, at any given time, blades in each of the four possible control blade locations are at different stages of burnup. Currently, there are 19 active control blades in use at the MURR. These active control blades have an independent operational cycling scheme where each blade has about a two-year irradiation (or core residence) time in one of four positions – "A", "B", "C" or "D" – of the MURR core (see Figure 5-4) and a potential maximum lifespan of about 10 years – providing the blade is usable after each two-year irradiation cycle. Since a given replacement blade is selected with minimal consideration given to its burnup status, for a set of in-cycle blades, the "effective" lengths and atom density of boron-10 (^{10}B) in the poison zone for each blade may vary significantly. This disproportion in the effective lengths of the poison regions between the blades is expected to affect the power peaking factors on each fuel element differently. Although the MURR HEU fuel cycle and predictions of the LEU fuel cycle were studied in detail using the ANL-MURR MCNP models in the LEU feasibility study [McKibben 2009], until now no similar study for the control blades was available.

The importance of using a full depletion model of the control blades for the reactor safety analysis is clear. In this work, a methodology was developed to individually model the ^{10}B depletion history for each active control blade that went through the MURR control blade operational cycle. Verification of this methodology was done by benchmarking the calculated k_{eff} , using control blade depletion models against actual critical rod height measurements.

Computational MethodologyMCNP Model

Highly discretized control blade models representing each of four possible positions "A", "B", "C" and "D" of the MURR core configuration were incorporated into the ANL-MURR MCNP model. Each control blade model was divided into 292 independent zones (cells), which include:

- 4 azimuthal sections (over the entire length)
- 9 radial sections over each 1/4 inch sections of the first axial (bottom) inch for each azimuthal section
- 9 radial sections over each of the next three incremental one-inch sections for each azimuthal section
- 2 radial sections over each of the next five incremental six-inch sections for each azimuthal section

This discretization scheme was chosen to properly account for the ^{10}B atom density burnout profile in the most active regions of each control blade. Figure 5-5 shows the increased discretization towards the bottom tip of the control blade model. Because the bottom portion of any control blade is constrained to be within (or near) the length of the fuel meat zone whether at startup, at equilibrium xenon build-up, or at the almost fully withdrawn state, it is expected to have the fastest rate of ^{10}B depletion.

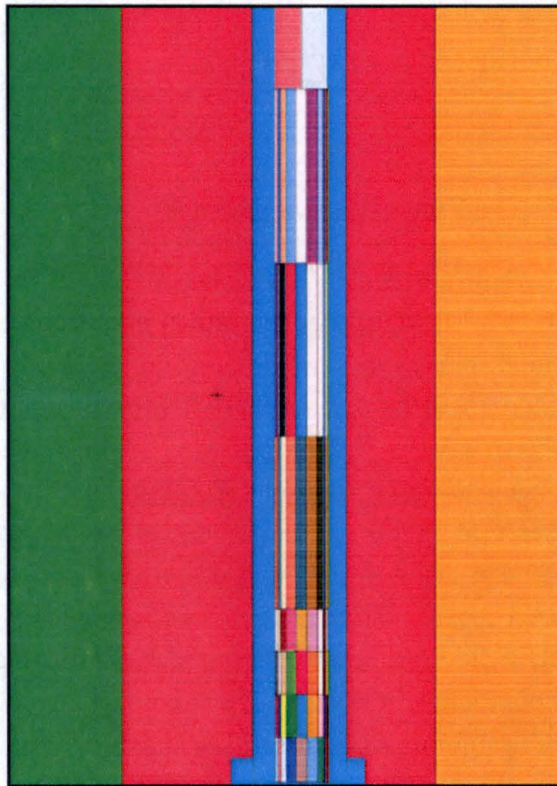


Figure 5-5. Axial and radial discretization in the bottom 4" of the MURR MCNP control blade model

Depletion Methodology

The ^{10}B depletion calculations were done using the actual run-time histories for each of the 19 active control blades, shuffling them through their life-cycle positions "A", "B", "C" or "D" as appropriate. Each control blade initially begins its potential ten-year cycle with the atom densities for fresh BORAL[®] in each depletion zone. To include control blade travel during the 150-hour weekly operating cycle, the fuel definitions for two state points of the typical HEU mixed core cycle were used for improved accuracy; i.e., fuel definitions for the control blade (CB) at 17 inches and CB at 23 inches. Here it was approximated that the reactor configuration at the first state point (i.e., CB height at 17 inches) accounts for the first 36 hours of the typical MURR one week-long operating cycle (where the xenon is building up in the core and the blades are moving out). The second state point (i.e., CB height at 23 inches) accounts for the remaining 114 hours of the weekly operating cycle (where equilibrium xenon levels are established and the shim control blades are mostly out of the peak flux region of the core).

The ^{10}B (n, α) reaction rates in each zone and for each state point were tallied in MCNP. Next, the reaction rates were used in a macro-modified EXCEL[®] worksheet where the actual ^{10}B atom density depletion in each zone was calculated. For the control blade burnup simulation, a time

step of six months was used and each control blade was irradiated for a minimum of two years before being set aside for decay and potential reuse.

Results

Effects of Core Configuration on Control Blades Depletion

To study the effects of different reactor configurations on the ^{10}B (n,α) reaction rate profiles in each control blade position, the ^{10}B (n,α) reaction rate in each zone of each blade position was tallied and compared for fresh blades in eight different reactor configurations. Various reactor configurations were simulated using the ANL-MURR MCNP models to reflect the major changes in the graphite reflector region over a 30-year period. The 1971 reflector was nearly a single sleeve of graphite surrounding the core while the 2008 graphite region possesses much less graphite due to the addition of numerous experimental irradiation channels. The material definitions for the fuel assemblies in the weekly start-up core were chosen from two burnup states; either all-fresh fuel or a typical cycle consisting of both fresh and partially depleted fuel assemblies derived from an ANL REBUS-DIF3D simulation of the MURR HEU fuel cycle. The control blade positions for each weekly operational cycle were either approximate critical blade height at startup or approximate height at equilibrium xenon levels. The different reactor configurations used are as follows:

- (a) all fresh fuel, 1971 graphite reflector; critical (CB at 17 inches)
- (b) all fresh fuel, 1971 graphite reflector; equilibrium Xe (CB at 23 inches)
- (c) all fresh fuel, 2008 graphite reflector; critical (CB at 17 inches)
- (d) all fresh fuel, 2008 graphite reflector; equilibrium Xe (CB at 23 inches)
- (e) mixed fuel, 1971 graphite reflector; critical (CB at 17 inches)
- (f) mixed fuel, 1971 graphite reflector; equilibrium Xe (CB at 23 inches)
- (g) mixed fuel, 2008 graphite reflector; critical (CB at 17 inches)
- (h) mixed fuel, 2008 graphite reflector; equilibrium Xe (CB at 23 inches)

Plots of the ^{10}B (n,α) reaction rates vs. the axial and radial dimensions for each control blade depletion zone were examined and showed that each reactor configuration has a unique impact on the ^{10}B (n,α) reaction rate profiles in each blade position. However, the effects were observed to be small and are therefore not very significant. The results also showed that each blade position has a unique profile and that the most active regions of the blade are within the bottom four inches of the blade. Figures 5-6 and 5-7 show examples of the combined axial and radial ^{10}B (n,α) reaction rate profiles over the blade's bottom four inches, for reactor configurations (e) and (g) –

MURR's current typical configuration. It also shows that the highest reaction rates occur at the surfaces of the control blade.

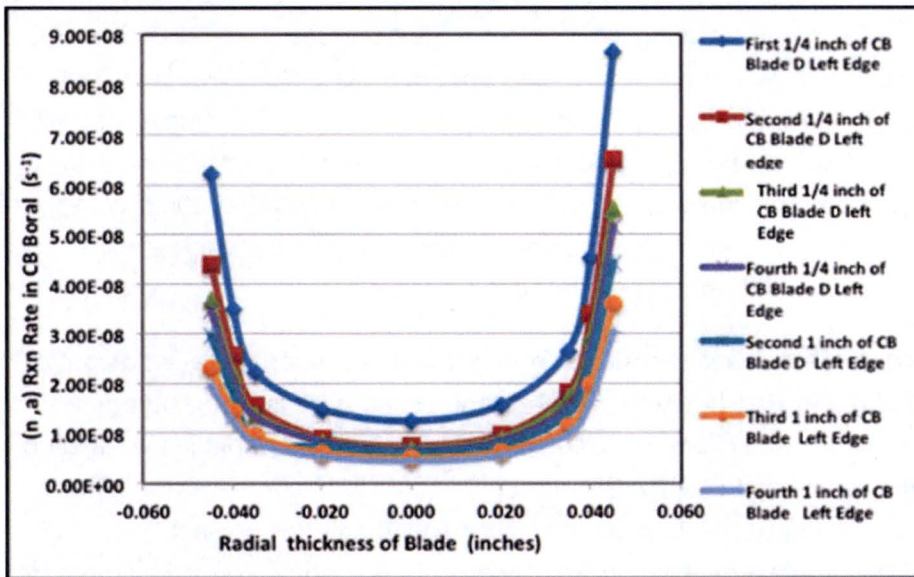


Figure 5-6. Control blade ^{10}B reaction rates for; mixed fuel core; 1971 graphite reflector; critical (CB at 17 inches)

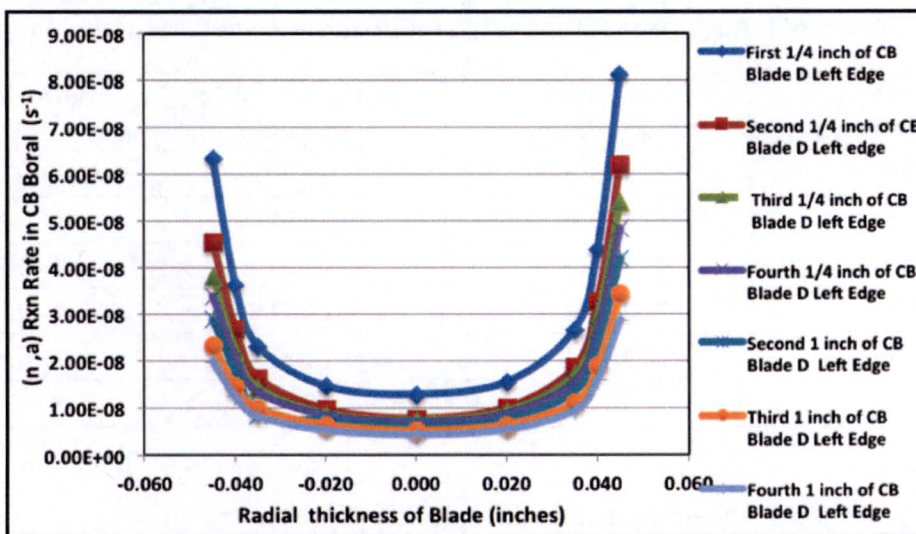


Figure 5-7. Control blade ^{10}B reaction rates for; mixed fuel core; 2008 graphite reflector; critical (CB at 17 inches)

Benchmarking: Comparison of Calculated k_{eff} Values

The data presented in Table 3.8 of Ref. [McKibben 2009] (LEU feasibility study) showed the deviation of calculated core k_{eff} values for the measured critical control blade positions for various blade histories. For that study, the partially burned fuel assemblies for each criticality measurement was modeled using fuel compositions generated by a REBUS-DIF3D simulation of a two-year HEU fuel cycle shuffling scheme done for MURR in previous work [McKibben 2009; Deen 2003]. The average burnup of the cores was 620 Megawatt-days and all of the control blades were modeled as fresh (non-depleted). The flux trap content was modeled as the typically loaded configuration and the graphite reflector was modeled as the "2008" configuration. Several cores from that previous study were selected and the core k_{eff} values were recalculated with depleted control blade models during the present study.

Table 5-4 shows the deviation in $\% \Delta k/k$ from critical state when there is no control blade burnup effect included (as in Ref. [McKibben 2009]) and when there is blade burnup effect included for each in-use control blade (from this work). When all-fresh control blades were used in the MCNP simulation (the column labeled "No CB Burnup" in Table 5-4), cores with the combination of blades that have the greatest total burnup, and correspondingly the lowest measured critical blade heights, had the greatest deviation from critical at measured critical rod heights. However, when the blades are modeled with the depleted blade compositions (the column labeled "With CB Burnup" in Table 5-4), the deviation from critical is always smaller and for the case with the maximum control blade history the deviation is reduced from 1.735% to 0.422%.

Table 5-4. Deviations for the estimated k_{eff} values from critical for the case with fresh control blades (from feasibility study) and with depleted blades

CB History (In-cycle Days)	CB Bank Height (inches)	No CB Burnup (% $\Delta k/k$)	With CB Burnup (% $\Delta k/k$)
287	17.63	-0.260	-0.232%
308	18.06	-0.144	-0.139%
1040	17.22	-1.301%	-0.730%
1192	16.72	-1.307%	-0.532%
1709	16.64	-1.743%	-0.390%
1835	16.00	-1.735%	-0.422%

Figure 5-8 shows plots of the deviation of the calculated k_{eff} values from critical at the measured critical control blade height when the blades are modeled as fresh as well as with their burnup history. As seen from the plot, the result of adding the depleted control blades to the existing HEU MURR core model shows a significant improvement; the average deviation from critical is -0.41% $\Delta k/k$ when the blade depletion is modeled, compared with -1.1% $\Delta k/k$ if the blades are modeled

as fresh. It can also be seen from the plot that for those cases with small total control blade burnup history, the two deviations are practically the same – indicating the effect is more pronounced for the cases involving control blades with large total burnup.

However, there is still a small negative bias in the predicted k_{eff} values even when the control blade depletion effect is incorporated in the present HEU MURR model. The bias is seen as the slight negative slope in the trend line fitting the solid red squares in Figure 5-8 and could be due to under-depletion of the ^{10}B in some of the larger axial zones above the blade tip where smaller divisions could have been more appropriate. Another contributor to this negative bias could be the MCNP MURR model itself or the bias in the partially burned fuel assemblies incorporated in the weekly start-up cores.

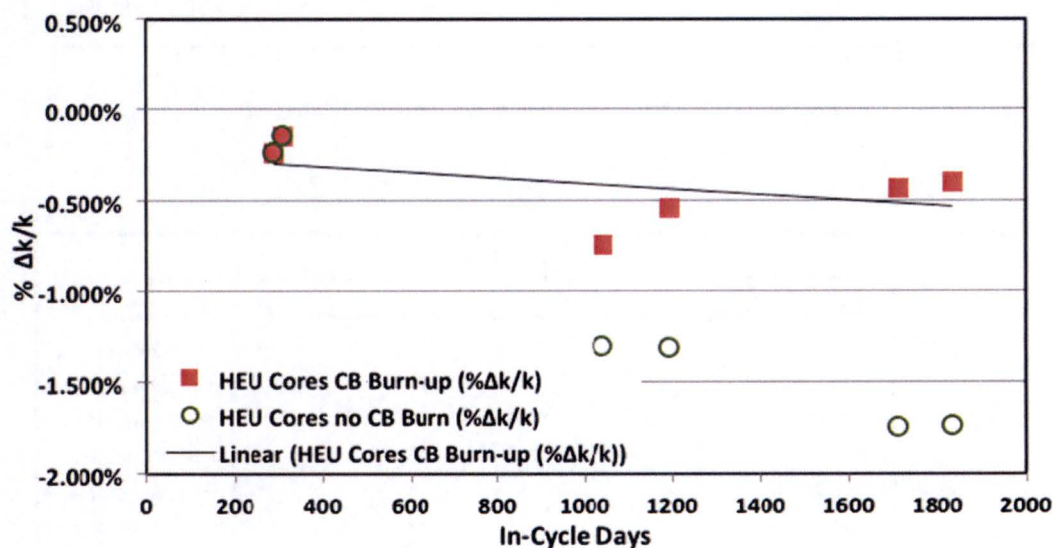


Figure 5-8. k_{eff} deviations from critical vs. control blade burnup history for fresh control blades and those blades with depletion history modeled

Blade Burnout Profiles

The ^{10}B depletion results for control blade number 5-08, which began operation in position “C” for its first cycle and remained in the same position for two more consecutive cycles, are shown in Figures 5-9, 5-10 and 5-11. In Figures 5-9 and 5-10, the azimuthally-averaged radial ^{10}B atom densities are shown for the bottom $\frac{1}{2}$ -inch of the control blade at each time step. This shows that the overall control blade ^{10}B depletions are predominantly a surface driven effect with an asymmetry in the depletion rate on the surface towards the beryllium reflector. This is due to an enhancement in the thermal neutron density on the beryllium side of the blade.

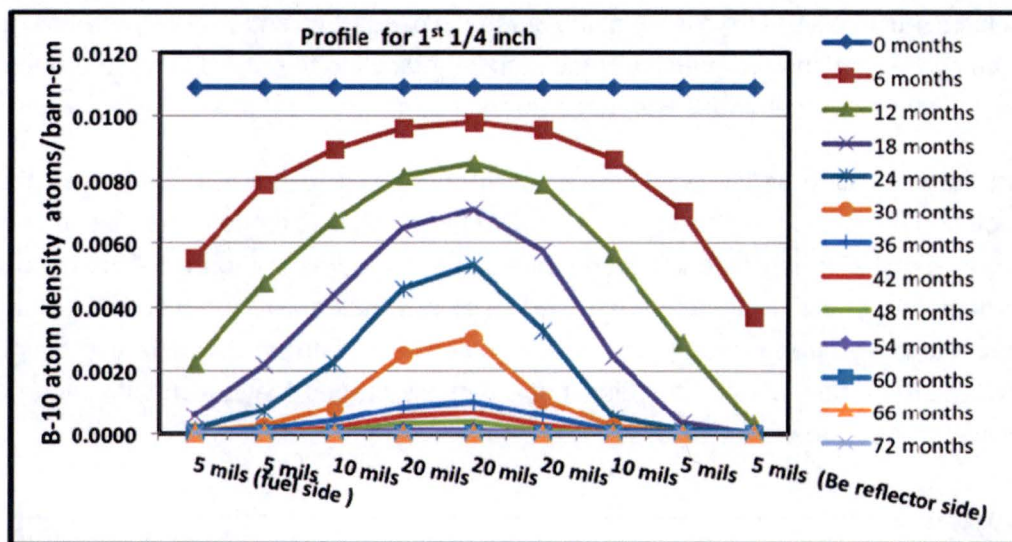


Figure 5-9. Bottom half-inch radial depletion profiles for control blade number 5-08

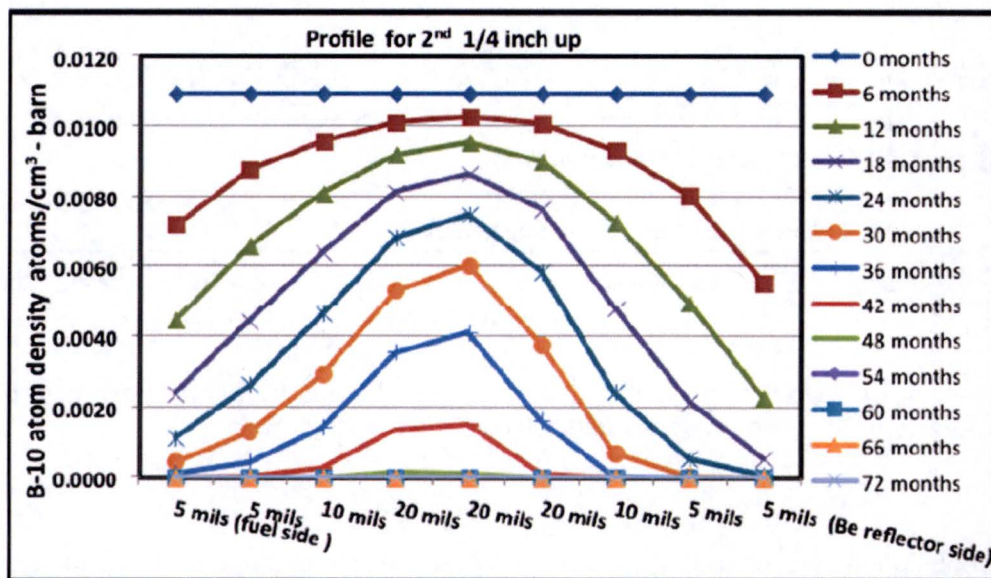


Figure 5-10. Bottom half-inch radial depletion profiles for control blade number 5-08

Figure 5-11 shows the axial profile of the ¹⁰B atom density averaged over radial and azimuthal zones for control blade number 5-08 at residence times of 0.5, 4.0 and 8.0 years. At 8 years, the ¹⁰B atom density is essentially zero in the bottom four inches of the blade.

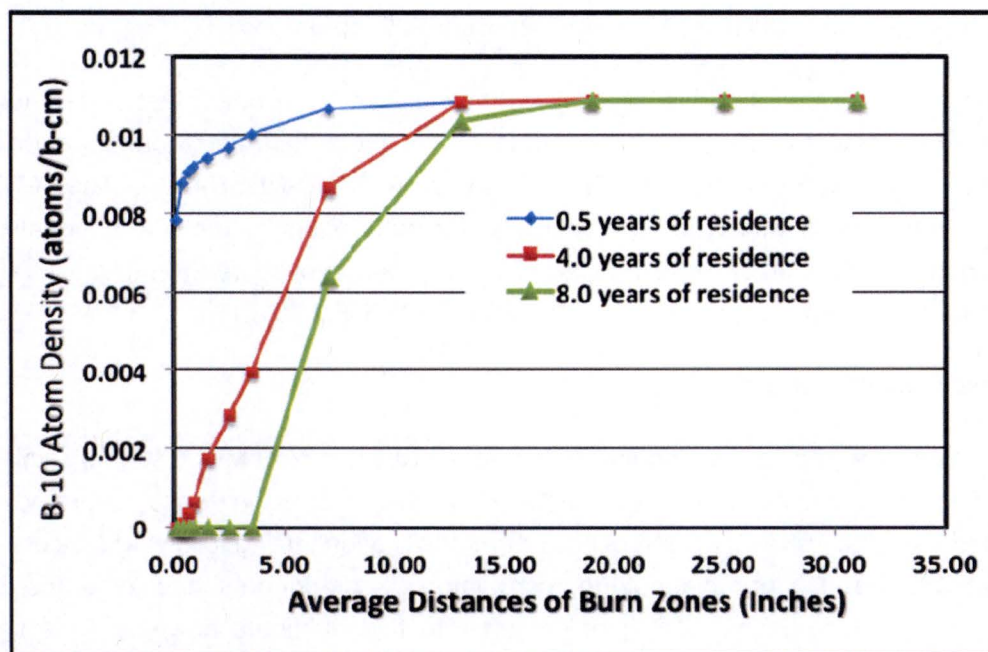


Figure 5-11. Axial ^{10}B atom density profiles for different residence times for control blade number 5-08

Conclusion

A comprehensive study was performed first to estimate the MURR control blade depletion profile and then to incorporate the depleted control blade models into the existing HEU MURR MCNP core model. Using a typical MURR core configuration in two fully modeled state-points, the full control blade depletion cycle was simulated, which yielded the full burnup history for 19 individual control blades. The initial part of the study focused on understanding the impact of different core configurations on the ^{10}B reaction rate profiles for each blade position. The effect of core configuration was found to have little impact on the B_{10} depletion. The overall ^{10}B depletion is predominantly a surface driven effect in the bottom four inches of the control blade with an asymmetry in the depletion rate on the surface towards the beryllium reflector. Combining the depleted blade models with that of partially burned fuel elements for weekly start-up cores significantly improved agreement of the calculated core k_{eff} compared to critical measurements. The deviation ($\% \Delta k/k$) of the calculated core k_{eff} values from critical was reduced from an average of -1.1%, when the blades are modeled as fresh, to -0.41% when the depleted blade model is included. There remains a small negative bias in the results, which can be attributed to either the need for finer discretization of the blade depletion model or a bias in the MURR MCNP model developed for the feasibility study.

5.3 Advanced Test Reactor Criticality Benchmark Problem

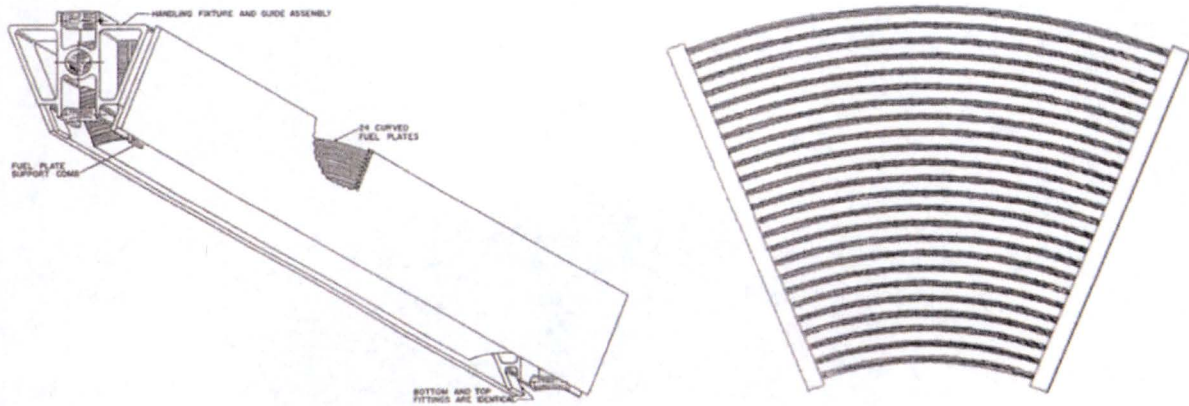
The ATR benchmark model is given in the International Handbook of Evaluated Reactor Physics Benchmark Experiment under the category of HEU fuel, metal fuel, and thermal neutron with an identification number HEU-MET-THERM-022 (or ATR-FUND-RESR-001). The ATR-FUND-RESR-001 was initially reviewed and approved for publication by the International Criticality Safety Benchmark Evaluation Project (ICSBEP) and was approved by the International Reactor Physics Experiment Evaluation Project (IRPhEP) in 2008 [NEA 2010].

Overview of Experiment

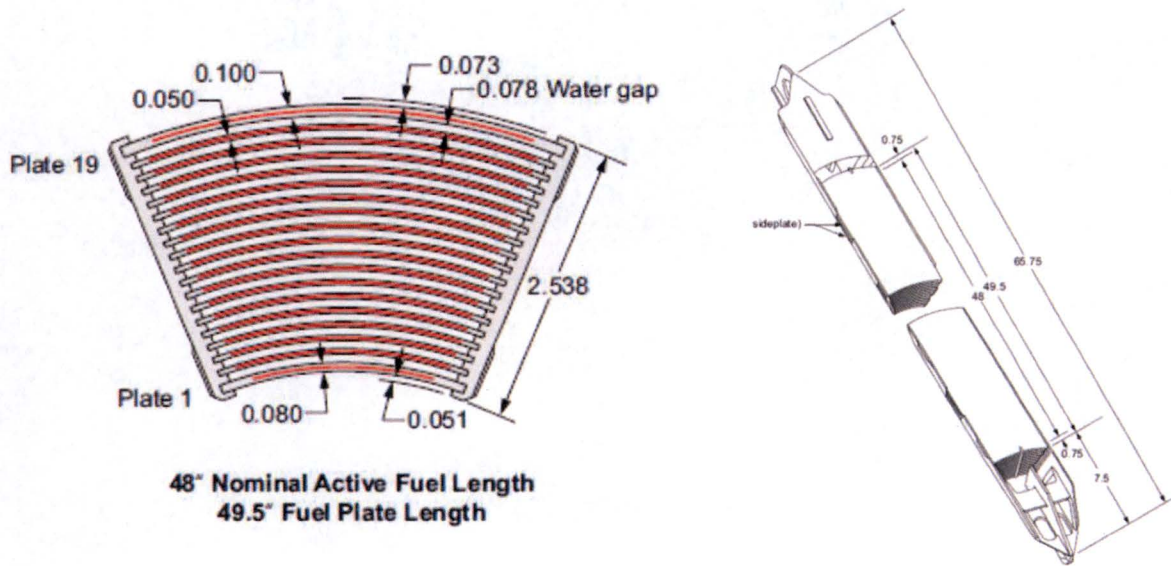
The ATR located at the Idaho National Laboratory (INL) is a 250-MW (thermal) high flux test reactor. The ATR critical experiment reported in this evaluation was performed in 1994 (designated as Cycle 103A-2) as part of nuclear requalification testing following the core internals change-out outage. During this outage, core internal components, including the beryllium reflector, were replaced. The ATR core contains 40 fuel elements arranged in a serpentine annulus between and around nine flux traps. The fuel element consists of 19 curved plates of different width, attached to side plates, forming a 45-degree sector of a circular annulus in cross section. The fuel meat consists of highly enriched (93 wt.%) uranium aluminide fuel powder dispersed in aluminum. The fuel plates are moderated by light water, and reflected by beryllium blocks. Table 5-5 compares key core characteristics of MURR [Foyto 2014] and ATR [Marshall 2013]: the fuel type, enrichment, coolant and reflector. The fuel element configuration of MURR and ATR are compared in Figure 5-12. The ATR core model is shown in Figure 5-13.

Table 5-5. Comparison of MURR and ATR core characteristics

	MURR	ATR
Thermal power (MW)	10	250
Fuel assemblies in core	8	40
Fuel type	U-Al _x plate, 24/assembly	U-Al plate, 19/assembly
Fuel material	HEU (93% ²³⁵ U)	HEU (93% ²³⁵ U)
Coolant	Light water	Light water
Pressure	68.4 psia	355 psig
Reflector	Beryllium, Graphite	Beryllium



(a) MURR fuel element



(b) ATR fuel element

Figure 5-12. Comparison of MURR and ATR fuel elements

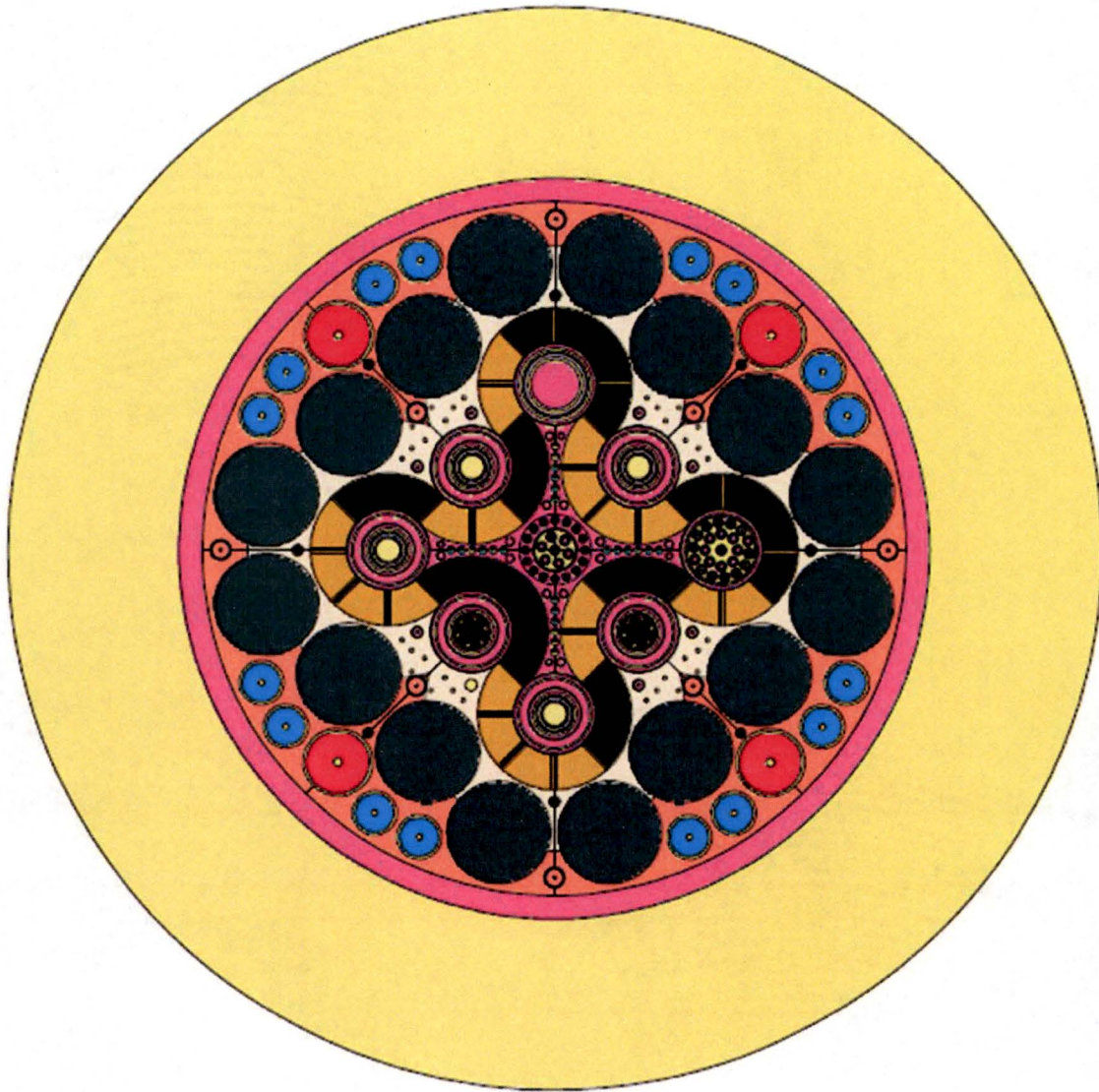


Figure 5-13. MCNP model of ATR core

Evaluation of Experimental Data

All the MCNP calculations used continuous-energy cross sections, employing 1250 generations of neutrons with 5,000 histories per generation. The first 50 generations were excluded from the statistics for each case, producing 6,000,000 active histories in each calculation. The statistical uncertainties associated with those Monte Carlo calculations are about ± 0.00035 for the perturbed and the reference cases. The study judged that the sensitivity effect is insignificant when the calculated value is within the Monte Carlo uncertainty (± 0.00035).

Results of Sample Calculations

The results in the International Handbook of Evaluated Reactor Physics Benchmark Experiment are presented in Table 5-6. The evaluated continuous energy ENDF/B-V cross-section data used in MCNP is for 27°C. Additional cross-section data sets have been implemented to provide a comparison. Cross section data for thermal scattering treatment in the JENDL-3.3 library were unavailable so thermal scattering cross sections from the ENDF/B-VII.1 library were used.

GA has conducted the criticality benchmark calculation of ATR using MCNP6 with ENDF/B-VII.1 cross section data. A total of 1,000,000 source particles were used: 100,000 particles per cycle and 1000 cycles. The calculation was performed on the Blue High Performance Computing (HPC) Cluster (named "Northshore") at GA. The results are included in Table 5-6 and compared to other published numbers. The calculated off-criticality is 0.181%Δk which is less than the averaged off-criticality of other five cases (i.e., 0.246%Δk).

Table 5-6. ATR criticality benchmark calculation

International Handbook of Evaluated Criticality Safety Benchmark Experiments					GA
MCNP5 (ENDF/B-V.0)	MCNP5 (ENDF/B-VI.8)	MCNP5 (ENF/B-VII.0)	MCNP5 (JEFF-3.1)	MCNP5 (JENDL-3.3)	MCNP6 (ENDF/B-VII.1)
0.9983	0.9937	1.0008	0.9983	1.0018	0.99819 ± 0.00026

5.4 Verification of Physics Method for Estimating ⁹⁹Mo Production

An analytic physics model was developed to estimate the ⁹⁹Mo production rate based on the Bateman equation considering ⁹⁹Mo production and extraction rates. The nuclear data and neutron flux used in the analytic model is obtained from the MCNP calculation so that these two calculations are consistent from each other. For the purpose of verifying formulations and calculations schemes, the analytic calculation was conducted for a single pellet of the target assembly and the results were compared to those of independent transmutation calculations by ORIGEN2.2 code. Note that the target assembly used for the verification test is an earlier version of target assembly which has 56 target rods. This model is used for the verification test because it has diverse neutron spectra such that there are pellets of which the neutron cross sections are the same as those of the ORIGEN2.2 single group library. The earlier model also adopts a more complicated process during the target irradiation when compared with the once-through operation scheme of the reference target assembly. The verification test model is as follows:

- The target assembly is continuously irradiated for ⁹⁹Mo production and ⁹⁹Mo is continuously extracted.

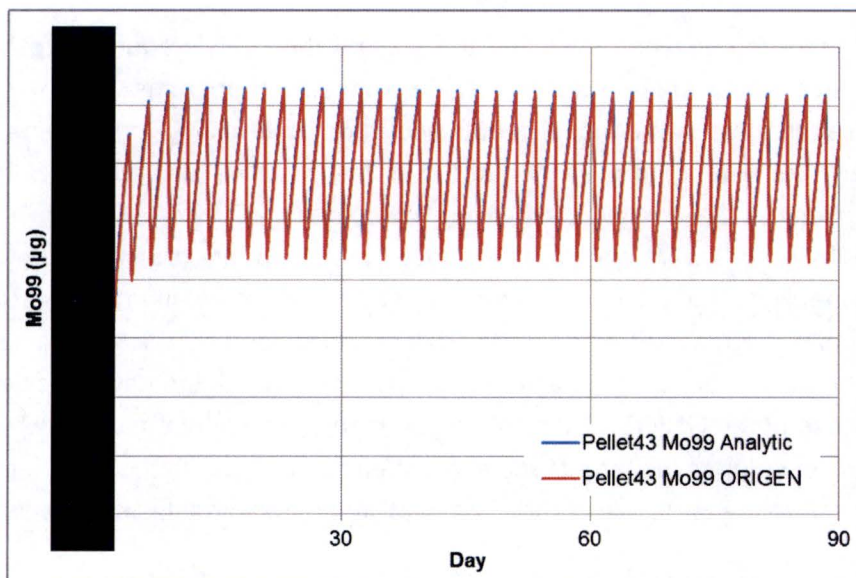
- The ⁹⁹Mo is extracted three times a week and collected in the hot cell. The extraction rate is 60% in 8 hours, i.e., 2.06×10^{-5} /sec. The collected ⁹⁹Mo is delivered every week.
- The operation continues for 1 year and the comparison is made at the end of 52nd week.

In the target assembly, each pellet has its own cross sections, while the ORIGEN2.2 uses one-group cross section libraries. For a fair comparison between the analytic model and ORIGEN2.2, a single pellet, of which the cross sections are the same as those of ORIGEN2.2, was searched. The selected pellet is pellet number 43 (from the bottom) of rod 33. The cross sections of the assembly and the selected pellet are compared with the ORIGEN2.2 library in Table 5-7.

The difference of ⁹⁹Mo content between the analytic model and ORIGEN2.2 calculation is 0.07% and 0.2% for the target pellet and collection system, respectively. The variation of ⁹⁹Mo is shown in Figure 5-14 and Figure 5-15 for the target pellet and collection system, respectively. It can be seen that the calculation results of both analytic and ORIGEN2.2 calculations are overlapping. This confirms that the physics model has been correctly formulated to predict ⁹⁹Mo content in the target assembly.

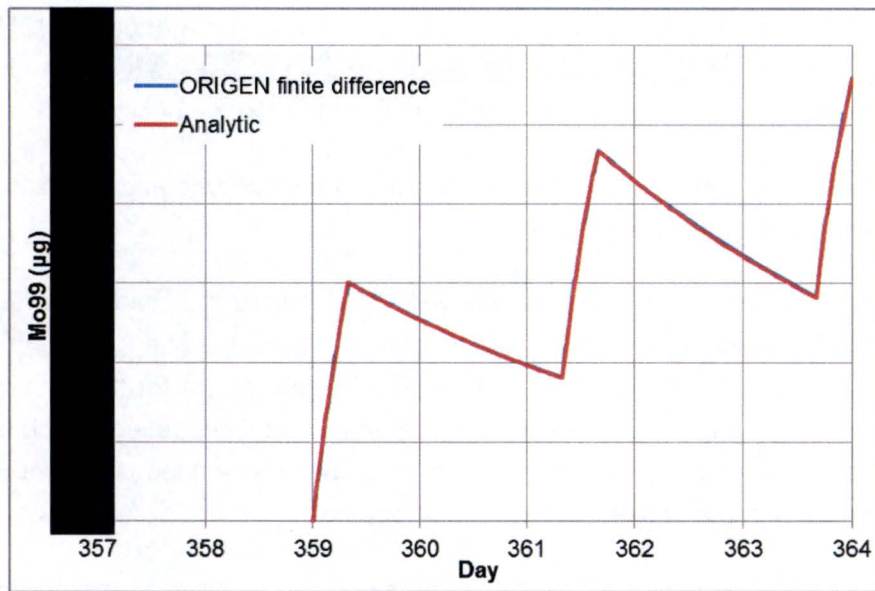
Table 5-7. Comparison of ²³⁵U cross sections

	Absorption (barn)	Fission (barn)
ORIGEN2.2	57.2	46.7
Rod33-Pellet43 (MCNP)	57.1	46.9
56-rod assembly-average (MCNP)	114.8	96.3



5a, b,
e, f

Figure 5-14. Comparison ⁹⁹Mo content in the pellet between analytic model and ORIGEN2.2



5a, b,
e, f

Figure 5-15. Comparison ⁹⁹Mo content in the collection system between analytic model and ORIGIN2.2

6 SUMMARY

The nuclear performance of the target assembly has been evaluated using a single target pellet enrichment of 19.75 wt% and 11-rod loading per assembly. The evaluation results of the reference target assembly model are as follows:

- The stand-alone 2 target assemblies together have a sufficiently low sub-criticality below 0.659.
- The MURR driver fuel element power peaking factor is less than 3.27 when two fresh target assemblies are loaded.
- The variation of target pellet linear power and total target assembly power due to CB movement is small. For the equilibrium core conditions [redacted] [redacted] respectively, when the control blades travel from position 46 cm to 62 cm.
- The variation of the eigenvalue due to pellet manufacturing tolerance does not exceed 11 pcm when the fabrication density changes by [redacted] or the enrichment changes by [redacted].

5a, b,
e, f

5a, b,
e, f

- The uncertainty due to mechanical tolerance of the target rod loading [REDACTED] of the extreme burnup core and total target power of the maximum burnup core, respectively.
- The peak linear power and total target power of the staggered and partial loading are less than those of the base loading.

5a, b,
e, f

Nuclear compatibility of the target assembly with MURR core has been assessed based on applicable MURR technical specifications. In general, because the power from the target assembly is relatively small (~5% of the nominal MURR core power for the full target assembly loading) and the target assemblies are loaded outside the beryllium reflector, the effect of target assembly on the core reactivity characteristics is small as summarized below for representative core burnup states with the base target assembly loading:

- The least negative core primary coolant temperature coefficient of reactivity is -1.69×10^{-4} ($\Delta k/k$)/ $^{\circ}\text{C}$, which is more negative than -1.08×10^{-4} ($\Delta k/k$)/ $^{\circ}\text{C}$ of Technical Specification 5.3.a. The primary coolant temperature range in this calculation was from 20.44°C to 76.84°C .
- The core primary coolant void coefficient of reactivity is -3.4×10^{-3} ($\Delta k/k$)/%void, which is more negative than -2.0×10^{-3} ($\Delta k/k$)/%void of Technical Specification 5.3.b. The primary coolant density in the calculation was changed from 100% nominal to 0.1%.
- The highest regulating rod reactivity worth is 4.02×10^{-3} $\Delta k/k$, which is less than 6.0×10^{-3} $\Delta k/k$ of Technical Specification 5.3.d.
- The lowest subcriticality margin of the core with the most reactive shim blade and regulating blade fully withdrawn is 0.055 $\Delta k/k$, which is greater than 0.02 $\Delta k/k$ of the Technical Specification 3.1.b.
- The excess reactivity of the cold, clean, minimum burnup core with cold, fresh, base target assembly loading is 0.072 $\Delta k/k$, which is less than 0.098 $\Delta k/k$ referenced to the cold, clean, critical core in Technical Specification 3.1.a.
- A single target assembly insertion into the MURR pool adds 0.31% Δk to the MURR core, which is lower than allowed reactivity worth of each secured removable experiment, 0.6% Δk (Technical Specification: 3.8.a).

7 REFERENCES

- [ASME 2011] *Materials. Part D, Properties (Metric)*, New York, American Society of Mechanical Engineers, 2011.
- [ATI 2016] Reactor Grade Zirconium Alloys for Nuclear Waste Disposal, <https://www.atimetals.com>, 2016.
- [Bateman 1910] Bateman, H., "Solution of a System of Differential Equations Occurring in the Theory of Radioactive Transformation," Proc. Cambridge Phil. Soc., 1910.
- [Bolin 2016] Bolin, J., Private Communication, General Atomics, May 2016.
- [Briesmeister, 2000] Briesmeister, J. F., Ed., "MCNP™ – A General Monte Carlo N-Particle Transport Code," LA-13709-M, Los Alamos National Laboratory, March 2000.
- [Chiger 2016] Chiger, H., Private Communication, General Atomics, May 2016.
- [Choi 2011] Choi, H., "Sensitivity Analysis of Core Characteristics to In-Core Irradiation of 99Mo Target Rods in a 2 MW TRIGA Reactor," PC-000603, General Atomics, Feb. 2011.
- [Choi 2015a] Choi, H., "Neutronics Design and Analysis of MURR Fission Moly Target," GA-D28032, General Atomics, Jan. 2015.
- [Choi 2015b] Choi, H., "Verification of Physics Design Model for Mass Production of 99Mo in a Nuclear Reactor," ASME 2015 Verification and Validation Symposium, Las Vegas, May 2015.
- [Conlin 2013] Conlin, J. L. et al., "Continuous Energy Neutron Cross Section Data Tables Based upon ENDF/B-VII.1," LA-UR-13-20137, Los Alamos National Laboratory, Feb. 2013.
- [Croff 1980] Croff, A. G., "A User's Manual for the ORIGEN2 Computer Code," ORNL/TM-7175, Oak Ridge national Laboratory, July 1980.
- [Deen 2003] Deen, J. R., et al., "WIMS-ANL User Manual, Rev. 5," ANL/TD/TM99-07, Argonne National Laboratory, 2003.
- [Dionne 2008] Dionne, B., Stillman, J., Stevens, J., "Applicability of WIMS-ANL to Generate Cross Sections for Very High Density UMo Fuel in Proposed LEU

- Fuel Assembly," Proc. 2008 International Meeting on Reduced Enrichment for Research and Test Reactors, Washington, D.C., Oct. 5-9, 2008.
- [Durkee 2012] Durkee Jr., J. W., et al., "The MCNP6 Delayed-Particle Feature," LA-UR-12-00283, Los Alamos National Laboratory, March 2012.
- [Foyto 2014] Foyto, L. et al., "Accident Analyses for the Conversion of the University of Missouri Research Reactor from Highly-Enriched to Low-Enriched Uranium," 35th Int. Mtg. on Reduced Enrichment for Research and Test Reactors, RERTR 2014, Vienna, Austria, Oct. 2014.
- [GA 2015] "Monthly Technical Progress Report for the Month Ending 31 July 2015," GA-C28171 (7/15), General Atomics, August 2015.
- [Goorley 2013a] Goorley, J. T. et al., "Initial MCNP6 Release Overview – MCNP6 version 1.0," LA-UR-13-22934, Los Alamos National Laboratory, April 2013.
- [Goorley 2013b] Goorley, J. T. et al., "Features of MCNP6," Joint International Conference on Supercomputing in Nuclear Applications and Monte Carlo 2013 (SNA + MC2013), Paris, France, October 27-31, 2013.
- [Hanan 1998] Hanan, N. A. et al., "The Use of WIMS-ANL Lumped Fission Product Cross Sections for Burned Core Analysis with the MCNP Monte Carlo Code," Proc. 1998 International Meeting on Reduced Enrichment for Research and Test Reactors, São Paulo, Brazil, Oct. 18-23, 1998.
- [Kiedrowski 2010] Kiedrowski, B. C. et al., "MCNP5-1.60 Feature Enhancement & Manual Clarifications," LA-UR-10-06217, Los Alamos national Laboratory, 2010.
- [Kim 2005] Kim, S. S. et al., "Advanced Test Reactor: Serpentine Arrangement of Highly Enriched Water-Moderated Uranium-Aluminide Fuel Plates Reflected by Beryllium," NEA/NSC/DOC/(95)03/II, Volume II, Nuclear Energy Agency, September 2005.
- [LANL 2003] "MCNP – A General Monte Carlo N-Particle Transport Core, Version 5," LA-UR-03-1987, Los Alamos National Laboratory, April 2003.
- [Lawrence 1983] Lawrence, R. D., "The DIF3D Nodal Neutronics Option for Two- and Three-Dimensional Diffusion-Theory Calculations in Hexagonal Geometry," ANL-83-1, Argonne National Laboratory, March 1983.

Attachment 6

MO-99 Target Assembly Nuclear Design for Once-Through Operation

30441R00031/B

- [Marshall 2013] Marshall, F. M., "The Advanced Test Reactor National Scientific User Facility Overview," IAEA, June 2013.
- [McKibben 2006] McKibben, J. C. et al., "Current Status of the Missouri University Research Reactor HEU to LEU Conversion Feasibility Study," 2006 Int. RERTR Meeting, Cape Town, South Africa, Oct. 29 – Nov. 2, 2006.
- [McKibben 2009] McKibben, J. C., et al., "Feasibility Analyses for HEU to LEU Fuel Conversion of the University of Missouri Research Reactor (MURR)," MURR Technical Data Report No. 0125, September 2009.
- [Mosteller 2002] Mosteller, R. D., "Validation Suites for MCNP," LA-UR-02-0878, Los Alamos National Laboratory, 2002.
- [Mosteller 2010] Mosteller, R. D., "An Expanded Criticality Validation Suites for MCNP," LA-UR-10-06230, Los Alamos National Laboratory, 2010.
- [Motojima 1977] Motojima, K. et al., "Volatilization Process for Separation of Molybdenum-99 from Irradiated Uranium," United States Patent 4,017,583, April 12, 1977.
- [MURR 2006] "Missouri University Research Reactor Technical Specifications," Docket 50-186, License R-103, University of Missouri, Columbia, August 2006.
- [Nakagawa 2003] Nakagawa, T., Ed., "The JENDL-3.3 Fission Product Yield Data Library," IAEA-NDS-138, International Atomic Energy Agency, January 2003.
- [NEA 2010] "International Handbook of Evaluated Reactor Physics Benchmark Experiments," NEA/NSC/DOC/(2006)1, Nuclear Energy Agency, March 2010.
- [NRC 1997] "Standard review plan for dry cask storage systems," U.S. Nuclear Regulatory Commission, Jan. 1997.
- [NRC 1999] "Safety evaluation by the office of nuclear reactor regulation supporting amendment No. 31 to amended facility operating license No. R-37," Docket No. 50-20, Nuclear Regulatory Commission, Dec. 1999.
- [Olson 2001] Olson, A. P., A User's Guide for the REBUS-PC Code, Version 1.4, ANL/RERTR/TM-32, Argonne National Laboratory, 2001

- [Parker 2015] Parker, E. M. et al., "Y-12 Standard Specification Low Enriched Uranium Metal Supply for ⁹⁹Mo Isotope Production," Y/PM-462, National Nuclear Security Administration, August 2015.
- [Parsons 2012] Parsons, D. K., Conlin, J. L., "Release of Continuous Representation for S(α,β) ACE Data," LA-UR-12-00800, Los Alamos National Laboratory, Feb. 2012.
- [Pelowitz 2013] Pelowitz, D. B., Ed., "MCNP6™ User's Manual Version 1.0," LA-CP-13-00634, Los Alamos National Laboratory, May 2013.
- [Peters 2012a] Peters, N. J., Kutikkad, K., "Improvements to Predictions of the Estimated Critical Blade Positions Due to Control Blade Depletion Corrections at MURR," 34th Int. Mtg. on Reduced Enrichment for Research and Test Reactors, RERTR 2012, Warsaw, Poland, Oct. 2012.
- [Peters 2012b] Peters, N., Kutikkad, K., "MURR Control Blade Depletion Study Report," MURR Technical Data Report No. 134, June 2012.
- [Peters 2013] Peters, N. J., Kutikkad, K., "Validation for Computational Methods and Calculations at MURR (Draft)," University of Missouri Research Reactor, December 2013.
- [Peters 2016] Peters N. J., Private Communication, University of Missouri Research Reactor, May 2016.
- [Rosenbaum 1978] Rosenbaum, H. S. et al., "Process for Separating Fission Product Molybdenum from an Irradiated Target Material," United States Patent 4,123,498, Oct. 31, 1978.
- [Stillman 2012] Stillman, J. A. et al., "Technical Basis in Support of the Conversion of the University of Missouri Research Reactor (MURR) Core from Highly-Enriched to Low-Enriched Uranium – Core Neutron Physics," ANL/RERTR/TM-12-30, Argonne National laboratory, September 2012.
- [Stillman 2013] Stillman, J. A., "Conceptual Design Parameters for MURR LEU U-Mo Fuel Conversion Design Demonstration Experiment," ANL/RERTR/TM-12-28 Revision 1, Argonne National laboratory, March 2013.
- [Trellue 1999] Trellue, H. R., Poston, D. I., "User's Manual, Version 2.0 for MonteBurns, Version 5B," LA-UR-99-4999, Los Alamos National Laboratory, 1999.

- [Whalen 1992] Whalen, D. J. et al., "MCNP: Neutron Benchmark Problems," LA-12212, Los Alamos National Laboratory, 1992.
- [Whipple 2009] Whipple, C., et al., "Medical Isotope Production without Highly Enriched Uranium," The National Academies Press, Washington, D.C., 2009.
- [White 2000] White, M. C., "Development and Implementation of Photonuclear Cross-Section Data for Mutually Coupled Neutron-Photon Transport Calculations in the Monte Carlo N-Particle (MCNP) Radiation Transport Code," LA-13744-T, Los Alamos National Laboratory, July 2000.
- [White 2003] White, M. C., "Photoatomic Data Library MCPLIB04: A New Photoatomic Library Based On Data from ENDF/B-VI Release 8," LA-UR-03-1019, Los Alamos National Laboratory, February 2003.
- [Xu 2006] Xu, Z., et al, "MCODE, Version 2.2 – An MCNP-ORIGEN Depletion Program," Center for Advanced Nuclear Energy Systems (CANES), Nuclear Science & Engineering Department, Massachusetts Institute of Technology, Cambridge, MA, February 2006.

APPENDIX A MURR FUEL ELEMENT PEAKING FACTORS



Table A-1. MURR fuel element 1 peaking factor for the maximum burnup core (CB=44 cm)

Axial node	Fuel plate number											
	1	2	3	4	5	6	7	8	9	10	11	12
24	0.940	0.771	0.664	0.610	0.551	0.516	0.487	0.469	0.448	0.427	0.410	0.401
23	0.963	0.747	0.632	0.560	0.505	0.461	0.423	0.403	0.378	0.363	0.352	0.338
22	1.110	0.870	0.734	0.649	0.579	0.536	0.488	0.470	0.446	0.422	0.409	0.399
21	1.275	1.008	0.844	0.750	0.676	0.627	0.580	0.551	0.522	0.507	0.482	0.462
20	1.438	1.153	0.960	0.861	0.765	0.702	0.653	0.625	0.595	0.571	0.549	0.535
19	1.610	1.284	1.077	0.952	0.858	0.796	0.746	0.701	0.670	0.647	0.619	0.613
18	1.790	1.419	1.197	1.059	0.964	0.893	0.835	0.790	0.749	0.721	0.699	0.678
17	1.985	1.580	1.344	1.188	1.074	0.999	0.929	0.878	0.847	0.808	0.788	0.765
16	2.152	1.722	1.462	1.305	1.178	1.085	1.025	0.975	0.936	0.893	0.874	0.854
15	2.319	1.864	1.587	1.392	1.280	1.182	1.108	1.052	1.006	0.973	0.948	0.940
14	2.473	1.981	1.675	1.472	1.340	1.257	1.190	1.130	1.084	1.062	1.019	1.010
13	2.558	2.050	1.742	1.564	1.412	1.316	1.238	1.198	1.139	1.115	1.096	1.071
12	2.592	2.102	1.791	1.593	1.453	1.354	1.281	1.229	1.183	1.155	1.129	1.110
11	2.636	2.122	1.813	1.611	1.478	1.386	1.301	1.249	1.211	1.184	1.148	1.143
10	2.652	2.150	1.817	1.625	1.496	1.379	1.313	1.261	1.214	1.197	1.165	1.154
9	2.704	2.165	1.839	1.628	1.492	1.389	1.311	1.255	1.217	1.178	1.163	1.141
8	2.663	2.129	1.809	1.599	1.461	1.350	1.269	1.230	1.186	1.152	1.133	1.116
7	2.564	2.032	1.734	1.555	1.419	1.316	1.253	1.197	1.148	1.124	1.098	1.078
6	2.448	1.947	1.673	1.480	1.351	1.246	1.178	1.132	1.091	1.068	1.038	1.020
5	2.283	1.826	1.550	1.371	1.255	1.157	1.101	1.057	1.032	1.000	0.979	0.959
4	2.061	1.653	1.418	1.255	1.147	1.067	1.013	0.959	0.933	0.906	0.894	0.885
3	1.878	1.498	1.280	1.135	1.034	0.963	0.907	0.862	0.838	0.821	0.796	0.788
2	1.679	1.342	1.148	1.013	0.936	0.852	0.811	0.770	0.750	0.730	0.716	0.705
1	1.715	1.430	1.274	1.154	1.075	1.019	0.979	0.943	0.915	0.897	0.887	0.880
Plate	2.046	1.640	1.396	1.240	1.130	1.049	0.989	0.945	0.909	0.883	0.861	0.846
Axial	1.338	1.338	1.335	1.330	1.340	1.342	1.345	1.352	1.356	1.373	1.371	1.381

Axial node	Fuel plate number											
	13	14	15	16	17	18	19	20	21	22	23	24
24	0.388	0.374	0.364	0.352	0.339	0.329	0.318	0.303	0.293	0.288	0.278	0.279
23	0.328	0.320	0.312	0.306	0.301	0.292	0.283	0.278	0.270	0.265	0.265	0.275
22	0.389	0.380	0.367	0.355	0.347	0.334	0.328	0.319	0.317	0.313	0.309	0.313
21	0.448	0.438	0.429	0.416	0.401	0.393	0.376	0.372	0.370	0.356	0.361	0.374
20	0.519	0.503	0.492	0.473	0.460	0.453	0.441	0.436	0.423	0.418	0.421	0.427
19	0.596	0.574	0.565	0.550	0.534	0.520	0.516	0.501	0.491	0.479	0.479	0.485
18	0.659	0.639	0.630	0.613	0.605	0.578	0.568	0.560	0.555	0.549	0.546	0.564
17	0.746	0.725	0.711	0.694	0.682	0.665	0.650	0.642	0.629	0.628	0.639	0.667
16	0.838	0.819	0.800	0.783	0.777	0.767	0.759	0.761	0.766	0.788	0.823	0.904
15	0.920	0.903	0.896	0.892	0.885	0.898	0.910	0.934	0.973	1.049	1.151	1.351
14	0.991	0.985	0.979	0.981	0.993	1.002	1.030	1.080	1.146	1.250	1.406	1.696
13	1.062	1.050	1.052	1.055	1.058	1.079	1.102	1.155	1.242	1.371	1.567	1.899
12	1.093	1.092	1.091	1.088	1.103	1.132	1.168	1.217	1.299	1.433	1.647	2.010
11	1.133	1.111	1.114	1.118	1.129	1.154	1.197	1.260	1.349	1.475	1.694	2.072
10	1.140	1.124	1.118	1.134	1.150	1.175	1.211	1.266	1.358	1.508	1.716	2.091
9	1.133	1.118	1.127	1.135	1.150	1.166	1.212	1.265	1.364	1.499	1.711	2.101
8	1.109	1.102	1.107	1.118	1.124	1.148	1.189	1.252	1.336	1.470	1.689	2.072
7	1.067	1.066	1.071	1.075	1.099	1.097	1.151	1.213	1.292	1.433	1.642	2.006
6	1.012	1.014	1.014	1.022	1.044	1.054	1.086	1.142	1.229	1.369	1.560	1.912
5	0.960	0.952	0.954	0.957	0.975	0.989	1.025	1.072	1.153	1.277	1.467	1.791
4	0.872	0.862	0.861	0.859	0.875	0.902	0.936	0.989	1.065	1.180	1.362	1.658
3	0.775	0.764	0.777	0.778	0.796	0.815	0.844	0.886	0.960	1.060	1.227	1.514
2	0.697	0.694	0.696	0.705	0.725	0.726	0.755	0.800	0.856	0.954	1.113	1.378
1	0.872	0.868	0.857	0.872	0.872	0.871	0.891	0.922	0.975	1.052	1.181	1.412
Plate	0.834	0.822	0.818	0.816	0.820	0.825	0.842	0.870	0.916	0.990	1.108	1.319
Axial	1.386	1.385	1.396	1.409	1.421	1.443	1.459	1.473	1.508	1.542	1.569	1.613

Table A-2. MURR fuel element 2 peaking factor for the maximum burnup core (CB=44 cm)

Axial node	Fuel plate number											
	1	2	3	4	5	6	7	8	9	10	11	12
24	0.790	0.683	0.625	0.552	0.518	0.487	0.467	0.447	0.423	0.408	0.398	0.382
23	0.811	0.678	0.588	0.525	0.475	0.435	0.412	0.391	0.377	0.351	0.343	0.334
22	0.917	0.762	0.671	0.594	0.539	0.507	0.472	0.444	0.421	0.410	0.398	0.383
21	1.048	0.888	0.776	0.703	0.632	0.589	0.556	0.521	0.507	0.489	0.470	0.451
20	1.117	0.973	0.869	0.782	0.724	0.668	0.625	0.600	0.572	0.548	0.535	0.514
19	1.250	1.093	0.983	0.886	0.812	0.754	0.705	0.674	0.649	0.623	0.605	0.586
18	1.333	1.182	1.046	0.958	0.885	0.827	0.774	0.749	0.721	0.681	0.667	0.646
17	1.477	1.303	1.167	1.064	0.987	0.923	0.859	0.829	0.788	0.759	0.740	0.719
16	1.571	1.400	1.263	1.153	1.073	0.996	0.942	0.900	0.862	0.846	0.819	0.800
15	1.700	1.519	1.380	1.241	1.151	1.080	1.019	0.987	0.953	0.929	0.898	0.876
14	1.755	1.570	1.420	1.308	1.213	1.139	1.087	1.040	0.999	0.973	0.958	0.943
13	1.833	1.640	1.505	1.379	1.276	1.193	1.138	1.093	1.055	1.038	1.015	0.998
12	1.849	1.689	1.544	1.412	1.320	1.232	1.169	1.114	1.084	1.076	1.043	1.035
11	1.893	1.695	1.542	1.414	1.314	1.252	1.193	1.149	1.113	1.096	1.076	1.065
10	1.916	1.708	1.564	1.436	1.338	1.262	1.195	1.156	1.119	1.103	1.094	1.065
9	1.905	1.711	1.553	1.434	1.329	1.243	1.181	1.148	1.124	1.100	1.071	1.057
8	1.913	1.701	1.539	1.403	1.316	1.234	1.183	1.136	1.104	1.082	1.056	1.048
7	1.853	1.658	1.508	1.367	1.279	1.204	1.141	1.093	1.050	1.037	1.020	1.011
6	1.826	1.612	1.448	1.322	1.224	1.152	1.097	1.054	1.020	0.991	0.979	0.960
5	1.725	1.509	1.360	1.239	1.142	1.081	1.027	0.979	0.952	0.926	0.916	0.903
4	1.631	1.431	1.271	1.150	1.064	0.994	0.946	0.912	0.883	0.860	0.844	0.834
3	1.456	1.264	1.131	1.020	0.940	0.879	0.836	0.796	0.783	0.766	0.747	0.737
2	1.359	1.164	1.021	0.929	0.854	0.799	0.761	0.730	0.704	0.690	0.676	0.668
1	1.381	1.229	1.120	1.050	0.994	0.947	0.923	0.885	0.857	0.846	0.841	0.819
Plate	1.698	1.499	1.351	1.231	1.141	1.070	1.015	0.974	0.941	0.918	0.898	0.881
Axial	1.267	1.281	1.299	1.309	1.316	1.324	1.321	1.332	1.341	1.349	1.367	1.357

Axial node	Fuel plate number											
	13	14	15	16	17	18	19	20	21	22	23	24
24	0.372	0.358	0.350	0.339	0.322	0.303	0.291	0.277	0.261	0.244	0.234	0.222
23	0.324	0.312	0.298	0.290	0.284	0.277	0.268	0.252	0.240	0.231	0.222	0.212
22	0.370	0.360	0.350	0.342	0.329	0.315	0.303	0.290	0.283	0.264	0.251	0.236
21	0.438	0.432	0.419	0.404	0.392	0.376	0.361	0.346	0.331	0.314	0.295	0.275
20	0.503	0.480	0.469	0.453	0.437	0.426	0.402	0.387	0.367	0.344	0.320	0.299
19	0.563	0.550	0.539	0.515	0.498	0.485	0.462	0.447	0.424	0.402	0.377	0.346
18	0.619	0.609	0.589	0.571	0.555	0.536	0.518	0.492	0.470	0.437	0.407	0.374
17	0.695	0.683	0.659	0.651	0.632	0.608	0.589	0.572	0.545	0.522	0.478	0.455
16	0.778	0.758	0.747	0.732	0.729	0.711	0.701	0.688	0.673	0.663	0.653	0.636
15	0.864	0.851	0.848	0.844	0.847	0.848	0.856	0.873	0.903	0.940	0.999	1.078
14	0.936	0.916	0.920	0.930	0.939	0.956	0.981	1.012	1.067	1.142	1.235	1.362
13	0.989	0.984	0.982	0.989	1.004	1.025	1.064	1.100	1.169	1.249	1.368	1.515
12	1.022	1.011	1.022	1.030	1.049	1.077	1.111	1.157	1.235	1.327	1.443	1.594
11	1.045	1.050	1.045	1.052	1.079	1.105	1.135	1.190	1.261	1.354	1.473	1.631
10	1.057	1.056	1.056	1.064	1.088	1.114	1.157	1.208	1.279	1.379	1.504	1.666
9	1.049	1.046	1.051	1.059	1.075	1.106	1.138	1.196	1.272	1.363	1.498	1.664
8	1.032	1.028	1.032	1.039	1.062	1.082	1.131	1.181	1.261	1.358	1.503	1.666
7	0.994	0.998	0.997	1.004	1.021	1.048	1.094	1.144	1.207	1.319	1.441	1.608
6	0.959	0.954	0.955	0.975	0.988	1.003	1.039	1.096	1.174	1.270	1.409	1.595
5	0.898	0.896	0.886	0.898	0.921	0.948	0.973	1.018	1.084	1.188	1.316	1.490
4	0.831	0.829	0.825	0.838	0.862	0.868	0.907	0.951	1.024	1.126	1.244	1.422
3	0.730	0.733	0.739	0.746	0.751	0.776	0.815	0.849	0.914	1.000	1.113	1.282
2	0.669	0.663	0.660	0.666	0.685	0.701	0.735	0.767	0.825	0.913	1.031	1.200
1	0.825	0.816	0.816	0.821	0.830	0.837	0.859	0.889	0.935	0.993	1.085	1.227
Plate	0.868	0.859	0.854	0.853	0.859	0.867	0.883	0.906	0.945	0.998	1.071	1.172
Axial	1.366	1.380	1.388	1.399	1.421	1.443	1.470	1.496	1.519	1.551	1.577	1.596

Table A-3. MURR fuel element 3 peaking factor for the maximum burnup core (CB=44 cm)

Axial node	Fuel plate number											
	1	2	3	4	5	6	7	8	9	10	11	12
24	0.901	0.760	0.687	0.619	0.578	0.546	0.518	0.496	0.472	0.459	0.449	0.436
23	0.933	0.767	0.655	0.576	0.524	0.485	0.452	0.429	0.412	0.400	0.383	0.376
22	1.053	0.863	0.746	0.664	0.610	0.560	0.528	0.508	0.485	0.473	0.454	0.442
21	1.200	0.982	0.861	0.776	0.699	0.651	0.622	0.595	0.568	0.545	0.536	0.521
20	1.308	1.101	0.964	0.869	0.799	0.745	0.705	0.682	0.652	0.630	0.610	0.600
19	1.439	1.214	1.066	0.975	0.898	0.848	0.799	0.756	0.738	0.717	0.707	0.689
18	1.567	1.334	1.181	1.081	0.998	0.923	0.886	0.848	0.817	0.794	0.773	0.764
17	1.761	1.499	1.319	1.200	1.107	1.042	0.982	0.940	0.912	0.886	0.875	0.858
16	1.885	1.624	1.429	1.297	1.203	1.128	1.052	1.006	0.990	0.950	0.941	0.924
15	2.050	1.755	1.554	1.389	1.281	1.205	1.138	1.080	1.046	1.030	1.013	0.998
14	2.136	1.834	1.620	1.453	1.343	1.273	1.194	1.151	1.115	1.087	1.063	1.052
13	2.241	1.925	1.690	1.537	1.414	1.314	1.233	1.192	1.166	1.132	1.109	1.089
12	2.255	1.946	1.713	1.563	1.435	1.356	1.276	1.229	1.195	1.158	1.135	1.116
11	2.306	1.964	1.741	1.572	1.459	1.366	1.301	1.256	1.207	1.177	1.141	1.121
10	2.322	1.981	1.751	1.584	1.462	1.369	1.316	1.265	1.216	1.178	1.155	1.140
9	2.288	1.971	1.728	1.563	1.442	1.358	1.285	1.238	1.197	1.176	1.147	1.125
8	2.310	1.947	1.717	1.549	1.423	1.334	1.272	1.216	1.171	1.146	1.127	1.108
7	2.216	1.896	1.666	1.490	1.376	1.287	1.214	1.165	1.121	1.101	1.079	1.060
6	2.144	1.806	1.575	1.425	1.317	1.228	1.156	1.105	1.075	1.050	1.023	1.012
5	1.968	1.670	1.454	1.316	1.207	1.140	1.064	1.033	0.986	0.968	0.947	0.933
4	1.820	1.540	1.347	1.225	1.119	1.036	0.985	0.955	0.920	0.893	0.867	0.853
3	1.653	1.372	1.205	1.081	0.992	0.929	0.879	0.838	0.811	0.790	0.781	0.776
2	1.510	1.248	1.081	0.970	0.890	0.820	0.785	0.749	0.728	0.712	0.697	0.687
1	1.563	1.340	1.207	1.088	1.035	0.981	0.950	0.930	0.899	0.886	0.868	0.861
Plate	1.767	1.499	1.318	1.190	1.098	1.028	0.973	0.935	0.903	0.880	0.861	0.847
Axial	1.301	1.309	1.315	1.317	1.319	1.318	1.338	1.340	1.333	1.325	1.327	1.332

Axial node	Fuel plate number											
	13	14	15	16	17	18	19	20	21	22	23	24
24	0.421	0.412	0.402	0.387	0.375	0.365	0.353	0.344	0.333	0.325	0.319	0.326
23	0.369	0.358	0.349	0.340	0.334	0.332	0.326	0.319	0.317	0.320	0.327	0.339
22	0.436	0.419	0.414	0.403	0.401	0.391	0.389	0.377	0.375	0.373	0.385	0.404
21	0.512	0.502	0.498	0.486	0.481	0.476	0.478	0.479	0.477	0.485	0.501	0.538
20	0.580	0.582	0.574	0.568	0.562	0.573	0.575	0.586	0.597	0.623	0.669	0.738
19	0.686	0.676	0.663	0.665	0.666	0.666	0.675	0.693	0.710	0.757	0.834	0.945
18	0.756	0.750	0.745	0.736	0.742	0.751	0.760	0.775	0.807	0.864	0.935	1.055
17	0.835	0.823	0.823	0.818	0.826	0.831	0.847	0.880	0.917	0.972	1.068	1.203
16	0.906	0.898	0.898	0.895	0.911	0.911	0.935	0.970	1.023	1.093	1.203	1.361
15	0.991	0.979	0.978	0.973	0.991	1.015	1.049	1.078	1.151	1.250	1.391	1.611
14	1.037	1.047	1.033	1.037	1.060	1.075	1.116	1.175	1.250	1.356	1.523	1.754
13	1.089	1.072	1.083	1.087	1.107	1.127	1.174	1.227	1.316	1.433	1.605	1.869
12	1.112	1.098	1.101	1.119	1.138	1.175	1.207	1.263	1.349	1.472	1.651	1.916
11	1.108	1.111	1.112	1.127	1.145	1.174	1.221	1.283	1.358	1.481	1.669	1.944
10	1.128	1.128	1.122	1.139	1.160	1.193	1.228	1.287	1.369	1.505	1.683	1.943
9	1.117	1.111	1.113	1.125	1.145	1.164	1.209	1.271	1.365	1.473	1.643	1.914
8	1.095	1.090	1.091	1.090	1.105	1.132	1.173	1.234	1.318	1.435	1.604	1.873
7	1.044	1.040	1.041	1.044	1.066	1.096	1.126	1.186	1.264	1.388	1.553	1.802
6	1.003	0.997	0.993	1.005	1.017	1.048	1.082	1.131	1.199	1.326	1.484	1.725
5	0.934	0.923	0.918	0.929	0.941	0.961	0.996	1.041	1.113	1.223	1.375	1.612
4	0.851	0.844	0.851	0.861	0.870	0.886	0.916	0.968	1.026	1.123	1.277	1.507
3	0.761	0.759	0.760	0.761	0.768	0.786	0.815	0.861	0.933	1.020	1.157	1.377
2	0.678	0.673	0.674	0.684	0.707	0.719	0.736	0.777	0.839	0.934	1.064	1.275
1	0.846	0.838	0.840	0.825	0.849	0.859	0.875	0.903	0.955	1.024	1.130	1.306
Plate	0.837	0.830	0.828	0.829	0.840	0.854	0.877	0.912	0.964	1.042	1.157	1.334
Axial	1.334	1.344	1.342	1.360	1.367	1.383	1.387	1.397	1.406	1.430	1.440	1.443

Table A-4. MURR fuel element 4 peaking factor for the maximum burnup core (CB=44 cm)

Axial node	Fuel plate number											
	1	2	3	4	5	6	7	8	9	10	11	12
24	0.834	0.734	0.676	0.622	0.590	0.550	0.534	0.512	0.496	0.487	0.471	0.458
23	0.846	0.724	0.647	0.580	0.541	0.501	0.477	0.460	0.444	0.427	0.412	0.402
22	0.955	0.835	0.738	0.677	0.623	0.574	0.551	0.522	0.508	0.493	0.486	0.471
21	1.085	0.961	0.851	0.778	0.732	0.678	0.647	0.631	0.602	0.585	0.567	0.562
20	1.148	1.018	0.928	0.854	0.806	0.762	0.737	0.704	0.684	0.671	0.654	0.645
19	1.260	1.137	1.045	0.970	0.914	0.863	0.825	0.802	0.785	0.774	0.756	0.742
18	1.335	1.207	1.122	1.053	0.992	0.939	0.902	0.867	0.849	0.841	0.822	0.816
17	1.470	1.356	1.244	1.162	1.089	1.034	0.997	0.962	0.929	0.920	0.908	0.900
16	1.563	1.437	1.318	1.232	1.165	1.112	1.064	1.015	0.994	0.970	0.960	0.959
15	1.654	1.534	1.413	1.309	1.242	1.174	1.126	1.093	1.075	1.046	1.025	1.018
14	1.701	1.571	1.463	1.359	1.272	1.207	1.164	1.126	1.115	1.095	1.066	1.059
13	1.762	1.638	1.535	1.416	1.341	1.262	1.206	1.171	1.148	1.119	1.095	1.094
12	1.801	1.665	1.541	1.444	1.361	1.287	1.247	1.200	1.163	1.142	1.130	1.120
11	1.821	1.684	1.558	1.463	1.367	1.296	1.243	1.203	1.179	1.150	1.138	1.127
10	1.835	1.682	1.566	1.466	1.375	1.306	1.265	1.209	1.180	1.157	1.143	1.119
9	1.812	1.686	1.561	1.436	1.360	1.293	1.238	1.190	1.161	1.137	1.117	1.101
8	1.837	1.682	1.547	1.441	1.354	1.271	1.228	1.179	1.153	1.122	1.099	1.084
7	1.771	1.615	1.492	1.382	1.293	1.228	1.164	1.118	1.104	1.075	1.057	1.051
6	1.769	1.598	1.445	1.350	1.244	1.172	1.120	1.080	1.046	1.034	1.017	1.004
5	1.641	1.469	1.336	1.231	1.147	1.080	1.041	1.001	0.975	0.943	0.942	0.929
4	1.560	1.385	1.253	1.145	1.061	0.996	0.957	0.931	0.904	0.877	0.868	0.855
3	1.410	1.252	1.129	1.036	0.966	0.908	0.870	0.828	0.805	0.779	0.772	0.760
2	1.305	1.137	1.021	0.941	0.873	0.808	0.778	0.740	0.721	0.710	0.692	0.687
1	1.334	1.209	1.122	1.042	0.989	0.952	0.910	0.892	0.866	0.857	0.847	0.834
Plate	1.473	1.336	1.226	1.136	1.066	1.006	0.966	0.931	0.908	0.888	0.873	0.863
Axial	1.241	1.256	1.272	1.284	1.284	1.292	1.303	1.293	1.294	1.297	1.303	1.301

Axial node	Fuel plate number											
	13	14	15	16	17	18	19	20	21	22	23	24
24	0.447	0.430	0.424	0.412	0.400	0.383	0.374	0.357	0.336	0.318	0.306	0.290
23	0.393	0.382	0.377	0.365	0.357	0.351	0.343	0.333	0.319	0.309	0.304	0.298
22	0.454	0.453	0.439	0.435	0.423	0.421	0.407	0.399	0.383	0.370	0.362	0.353
21	0.547	0.545	0.537	0.540	0.534	0.520	0.520	0.516	0.517	0.523	0.526	0.546
20	0.638	0.637	0.638	0.634	0.641	0.639	0.652	0.669	0.692	0.730	0.773	0.844
19	0.738	0.739	0.742	0.756	0.753	0.773	0.791	0.823	0.861	0.923	1.001	1.114
18	0.804	0.806	0.815	0.824	0.831	0.851	0.884	0.921	0.961	1.024	1.101	1.215
17	0.891	0.894	0.903	0.911	0.923	0.944	0.978	1.016	1.071	1.153	1.248	1.367
16	0.952	0.943	0.952	0.968	0.976	1.008	1.040	1.085	1.150	1.239	1.334	1.462
15	1.000	1.008	1.019	1.029	1.044	1.077	1.117	1.169	1.245	1.339	1.446	1.592
14	1.045	1.041	1.050	1.079	1.097	1.120	1.158	1.219	1.300	1.392	1.501	1.639
13	1.087	1.089	1.104	1.116	1.140	1.167	1.216	1.272	1.345	1.449	1.561	1.702
12	1.110	1.106	1.111	1.125	1.147	1.179	1.226	1.282	1.364	1.462	1.574	1.722
11	1.118	1.126	1.125	1.149	1.170	1.196	1.237	1.296	1.381	1.476	1.596	1.727
10	1.110	1.120	1.141	1.140	1.173	1.202	1.245	1.300	1.373	1.479	1.598	1.742
9	1.096	1.100	1.104	1.118	1.148	1.181	1.227	1.277	1.360	1.456	1.573	1.716
8	1.075	1.078	1.089	1.102	1.121	1.158	1.199	1.261	1.337	1.437	1.557	1.711
7	1.038	1.031	1.036	1.052	1.067	1.103	1.147	1.198	1.279	1.377	1.494	1.647
6	0.996	0.999	1.003	1.008	1.033	1.057	1.098	1.151	1.225	1.322	1.447	1.613
5	0.916	0.916	0.918	0.931	0.950	0.981	1.021	1.068	1.139	1.227	1.338	1.497
4	0.847	0.852	0.854	0.861	0.876	0.905	0.942	0.988	1.059	1.145	1.267	1.430
3	0.756	0.762	0.763	0.766	0.783	0.803	0.839	0.883	0.942	1.023	1.137	1.286
2	0.679	0.678	0.676	0.683	0.698	0.712	0.751	0.790	0.845	0.926	1.040	1.183
1	0.835	0.825	0.830	0.844	0.837	0.851	0.873	0.897	0.944	1.002	1.081	1.189
Plate	0.854	0.853	0.857	0.865	0.876	0.895	0.924	0.961	1.013	1.083	1.168	1.281
Axial	1.305	1.314	1.326	1.323	1.332	1.336	1.341	1.347	1.357	1.360	1.362	1.354

Table A-5. MURR fuel element 5 peaking factor for the maximum burnup core (CB=44 cm)

Axial node	Fuel plate number											
	1	2	3	4	5	6	7	8	9	10	11	12
24	1.064	0.885	0.787	0.712	0.659	0.627	0.598	0.578	0.570	0.557	0.544	0.528
23	1.097	0.875	0.747	0.658	0.598	0.564	0.537	0.509	0.491	0.477	0.464	0.457
22	1.260	1.010	0.859	0.768	0.698	0.653	0.620	0.595	0.572	0.561	0.539	0.530
21	1.431	1.152	0.992	0.880	0.815	0.760	0.729	0.689	0.674	0.661	0.645	0.639
20	1.596	1.312	1.130	1.006	0.927	0.866	0.817	0.797	0.778	0.758	0.737	0.736
19	1.781	1.453	1.245	1.113	1.029	0.977	0.927	0.894	0.876	0.860	0.852	0.840
18	1.987	1.626	1.399	1.255	1.154	1.083	1.035	1.000	0.965	0.942	0.934	0.928
17	2.182	1.784	1.536	1.366	1.262	1.183	1.129	1.093	1.053	1.029	1.027	1.016
16	2.364	1.935	1.668	1.491	1.368	1.274	1.208	1.172	1.135	1.102	1.091	1.080
15	2.538	2.064	1.770	1.583	1.451	1.357	1.303	1.243	1.219	1.194	1.165	1.144
14	2.691	2.165	1.862	1.666	1.535	1.433	1.360	1.299	1.265	1.229	1.214	1.199
13	2.766	2.245	1.926	1.705	1.564	1.467	1.403	1.349	1.310	1.276	1.254	1.230
12	2.824	2.266	1.946	1.741	1.607	1.501	1.423	1.369	1.335	1.292	1.289	1.260
11	2.844	2.305	1.978	1.761	1.618	1.508	1.433	1.375	1.355	1.315	1.301	1.285
10	2.861	2.299	1.962	1.759	1.613	1.513	1.443	1.385	1.344	1.314	1.282	1.266
9	2.845	2.294	1.951	1.744	1.589	1.497	1.423	1.369	1.318	1.281	1.272	1.249
8	2.785	2.241	1.912	1.703	1.562	1.460	1.372	1.325	1.280	1.244	1.235	1.216
7	2.682	2.148	1.834	1.645	1.498	1.397	1.320	1.276	1.226	1.203	1.177	1.163
6	2.538	2.037	1.749	1.556	1.426	1.331	1.253	1.200	1.163	1.143	1.114	1.113
5	2.349	1.889	1.601	1.426	1.311	1.224	1.152	1.120	1.088	1.053	1.036	1.033
4	2.153	1.738	1.468	1.319	1.206	1.123	1.065	1.017	0.998	0.973	0.965	0.943
3	1.926	1.537	1.309	1.163	1.083	1.004	0.954	0.913	0.878	0.856	0.839	0.832
2	1.726	1.386	1.172	1.049	0.957	0.895	0.847	0.809	0.788	0.765	0.750	0.739
1	1.757	1.468	1.298	1.191	1.105	1.050	1.003	0.982	0.958	0.942	0.938	0.924
Plate Axial	1.839	1.488	1.276	1.140	1.047	0.981	0.931	0.896	0.871	0.849	0.836	0.825
Axial	1.319	1.314	1.315	1.310	1.310	1.308	1.314	1.311	1.319	1.314	1.319	1.320

Axial node	Fuel plate number											
	13	14	15	16	17	18	19	20	21	22	23	24
24	0.520	0.511	0.506	0.498	0.491	0.488	0.479	0.485	0.489	0.505	0.532	0.595
23	0.452	0.445	0.442	0.441	0.438	0.438	0.437	0.446	0.463	0.495	0.541	0.622
22	0.520	0.520	0.523	0.517	0.514	0.522	0.528	0.537	0.561	0.590	0.641	0.744
21	0.626	0.622	0.614	0.619	0.622	0.621	0.633	0.654	0.683	0.719	0.787	0.910
20	0.731	0.731	0.731	0.726	0.734	0.738	0.754	0.784	0.822	0.878	0.967	1.142
19	0.831	0.822	0.826	0.818	0.834	0.851	0.868	0.902	0.958	1.031	1.147	1.354
18	0.919	0.918	0.926	0.920	0.932	0.942	0.968	1.013	1.067	1.149	1.289	1.525
17	0.998	0.997	0.995	1.007	1.020	1.044	1.069	1.110	1.169	1.264	1.420	1.684
16	1.077	1.072	1.076	1.082	1.095	1.117	1.144	1.192	1.258	1.366	1.541	1.826
15	1.141	1.138	1.142	1.148	1.156	1.180	1.213	1.272	1.349	1.470	1.660	1.977
14	1.190	1.195	1.197	1.196	1.219	1.249	1.284	1.348	1.432	1.563	1.804	2.170
13	1.218	1.222	1.219	1.244	1.263	1.296	1.351	1.407	1.519	1.670	1.914	2.324
12	1.248	1.257	1.255	1.272	1.287	1.317	1.365	1.436	1.541	1.713	1.959	2.396
11	1.264	1.264	1.268	1.275	1.292	1.325	1.373	1.453	1.565	1.730	1.987	2.417
10	1.258	1.263	1.261	1.278	1.301	1.320	1.377	1.453	1.561	1.731	1.989	2.441
9	1.245	1.236	1.235	1.238	1.270	1.302	1.352	1.410	1.529	1.704	1.956	2.388
8	1.208	1.199	1.209	1.218	1.236	1.269	1.316	1.383	1.492	1.642	1.895	2.309
7	1.153	1.150	1.163	1.171	1.188	1.225	1.257	1.329	1.436	1.588	1.836	2.223
6	1.108	1.106	1.098	1.110	1.127	1.153	1.199	1.252	1.350	1.498	1.726	2.105
5	1.020	1.015	1.014	1.030	1.046	1.066	1.114	1.179	1.262	1.395	1.605	1.963
4	0.929	0.928	0.924	0.943	0.953	0.973	1.015	1.074	1.155	1.277	1.469	1.808
3	0.835	0.825	0.827	0.837	0.849	0.872	0.906	0.954	1.036	1.160	1.344	1.652
2	0.737	0.739	0.734	0.752	0.765	0.782	0.814	0.860	0.931	1.042	1.205	1.495
1	0.926	0.918	0.915	0.913	0.922	0.929	0.949	0.992	1.051	1.129	1.260	1.506
Plate Axial	0.818	0.816	0.816	0.822	0.832	0.849	0.875	0.916	0.978	1.071	1.218	1.469
Axial	1.310	1.314	1.317	1.319	1.325	1.324	1.334	1.345	1.357	1.370	1.385	1.409

Table A-6. MURR fuel element 6 peaking factor for the maximum burnup core (CB=44 cm)

Axial node	Fuel plate number											
	1	2	3	4	5	6	7	8	9	10	11	12
24	0.868	0.758	0.691	0.641	0.588	0.557	0.531	0.512	0.498	0.487	0.475	0.462
23	0.889	0.754	0.662	0.597	0.551	0.509	0.476	0.454	0.435	0.427	0.417	0.406
22	0.992	0.853	0.751	0.682	0.637	0.597	0.561	0.531	0.515	0.502	0.482	0.477
21	1.124	0.976	0.864	0.787	0.726	0.695	0.653	0.626	0.613	0.598	0.581	0.575
20	1.216	1.064	0.966	0.892	0.826	0.774	0.740	0.714	0.698	0.676	0.667	0.655
19	1.348	1.194	1.088	0.990	0.931	0.878	0.844	0.812	0.792	0.785	0.769	0.760
18	1.435	1.294	1.182	1.087	1.017	0.968	0.930	0.901	0.873	0.855	0.848	0.838
17	1.588	1.419	1.300	1.198	1.125	1.070	1.035	1.000	0.969	0.948	0.934	0.920
16	1.673	1.509	1.372	1.267	1.191	1.134	1.078	1.050	1.014	0.997	0.989	0.981
15	1.778	1.620	1.463	1.351	1.263	1.205	1.154	1.113	1.086	1.061	1.041	1.033
14	1.834	1.652	1.518	1.400	1.328	1.257	1.199	1.151	1.120	1.095	1.085	1.077
13	1.886	1.720	1.577	1.471	1.375	1.301	1.240	1.205	1.168	1.143	1.125	1.109
12	1.909	1.729	1.595	1.471	1.389	1.327	1.265	1.213	1.193	1.163	1.151	1.129
11	1.899	1.749	1.598	1.488	1.390	1.323	1.269	1.234	1.205	1.178	1.157	1.149
10	1.945	1.771	1.613	1.504	1.405	1.332	1.268	1.234	1.199	1.177	1.162	1.146
9	1.945	1.766	1.618	1.484	1.386	1.313	1.262	1.227	1.177	1.159	1.134	1.127
8	1.962	1.765	1.612	1.486	1.379	1.300	1.232	1.197	1.168	1.148	1.131	1.103
7	1.903	1.705	1.544	1.426	1.317	1.249	1.193	1.141	1.116	1.084	1.082	1.060
6	1.888	1.666	1.508	1.360	1.279	1.192	1.132	1.104	1.066	1.048	1.031	1.021
5	1.748	1.534	1.379	1.259	1.179	1.109	1.057	1.012	0.992	0.964	0.946	0.939
4	1.662	1.437	1.287	1.173	1.085	1.030	0.975	0.944	0.917	0.901	0.890	0.878
3	1.462	1.294	1.157	1.053	0.977	0.913	0.872	0.841	0.818	0.798	0.779	0.776
2	1.346	1.173	1.047	0.951	0.882	0.830	0.785	0.758	0.729	0.711	0.703	0.690
1	1.369	1.221	1.129	1.056	1.008	0.968	0.929	0.909	0.891	0.869	0.866	0.857
Plate	1.516	1.353	1.229	1.130	1.056	1.000	0.953	0.921	0.896	0.877	0.863	0.852
Axial	1.250	1.264	1.273	1.286	1.286	1.288	1.286	1.294	1.299	1.298	1.300	1.303

Axial node	Fuel plate number											
	13	14	15	16	17	18	19	20	21	22	23	24
24	0.449	0.438	0.428	0.422	0.400	0.386	0.368	0.354	0.338	0.326	0.311	0.301
23	0.397	0.385	0.384	0.372	0.358	0.351	0.345	0.336	0.326	0.321	0.312	0.309
22	0.459	0.454	0.449	0.439	0.434	0.421	0.413	0.407	0.393	0.378	0.368	0.362
21	0.561	0.555	0.547	0.539	0.534	0.536	0.532	0.534	0.529	0.540	0.548	0.567
20	0.644	0.644	0.643	0.649	0.641	0.655	0.667	0.679	0.715	0.755	0.807	0.900
19	0.759	0.746	0.757	0.755	0.766	0.783	0.805	0.838	0.882	0.954	1.036	1.171
18	0.830	0.827	0.834	0.836	0.845	0.865	0.898	0.933	0.995	1.058	1.161	1.300
17	0.912	0.905	0.915	0.921	0.938	0.962	0.992	1.042	1.109	1.197	1.317	1.468
16	0.974	0.980	0.983	0.995	1.009	1.040	1.075	1.131	1.193	1.294	1.420	1.580
15	1.033	1.041	1.038	1.058	1.070	1.107	1.142	1.200	1.274	1.389	1.528	1.716
14	1.071	1.071	1.079	1.091	1.120	1.148	1.192	1.253	1.327	1.442	1.582	1.770
13	1.104	1.106	1.115	1.129	1.162	1.190	1.230	1.296	1.381	1.497	1.641	1.823
12	1.130	1.135	1.139	1.151	1.175	1.211	1.261	1.327	1.409	1.528	1.667	1.864
11	1.137	1.147	1.157	1.172	1.195	1.233	1.272	1.344	1.420	1.539	1.683	1.868
10	1.134	1.138	1.153	1.164	1.194	1.213	1.263	1.331	1.424	1.543	1.691	1.884
9	1.124	1.130	1.139	1.152	1.166	1.204	1.252	1.314	1.396	1.515	1.663	1.846
8	1.096	1.109	1.112	1.119	1.143	1.176	1.223	1.280	1.375	1.501	1.642	1.841
7	1.061	1.057	1.056	1.078	1.098	1.127	1.163	1.225	1.307	1.413	1.565	1.756
6	1.013	1.014	1.013	1.035	1.046	1.077	1.116	1.190	1.275	1.376	1.527	1.727
5	0.930	0.930	0.932	0.944	0.971	0.995	1.041	1.094	1.169	1.272	1.409	1.599
4	0.868	0.869	0.875	0.881	0.898	0.929	0.962	1.011	1.087	1.184	1.324	1.520
3	0.763	0.774	0.773	0.781	0.802	0.820	0.860	0.909	0.974	1.061	1.187	1.362
2	0.689	0.690	0.696	0.701	0.715	0.745	0.772	0.812	0.874	0.964	1.085	1.263
1	0.854	0.847	0.854	0.854	0.864	0.881	0.896	0.934	0.979	1.038	1.125	1.270
Plate	0.845	0.845	0.848	0.855	0.867	0.888	0.915	0.957	1.013	1.090	1.192	1.331
Axial	1.300	1.311	1.318	1.325	1.331	1.342	1.342	1.357	1.359	1.368	1.371	1.367

Table A-7. MURR fuel element 7 peaking factor for the maximum burnup core (CB=44 cm)

Axial node	Fuel plate number											
	1	2	3	4	5	6	7	8	9	10	11	12
24	0.906	0.766	0.682	0.619	0.573	0.539	0.521	0.497	0.479	0.465	0.448	0.434
23	0.925	0.756	0.655	0.586	0.533	0.488	0.458	0.437	0.415	0.402	0.382	0.377
22	1.045	0.867	0.758	0.670	0.608	0.569	0.529	0.507	0.482	0.463	0.456	0.442
21	1.199	1.005	0.873	0.783	0.714	0.666	0.636	0.594	0.574	0.558	0.540	0.536
20	1.342	1.127	0.983	0.877	0.812	0.755	0.714	0.683	0.659	0.639	0.628	0.604
19	1.501	1.260	1.113	1.001	0.912	0.859	0.818	0.783	0.754	0.734	0.713	0.698
18	1.627	1.385	1.214	1.097	1.016	0.950	0.889	0.861	0.834	0.802	0.783	0.773
17	1.802	1.526	1.349	1.205	1.114	1.049	0.999	0.960	0.916	0.891	0.875	0.859
16	1.941	1.648	1.458	1.304	1.199	1.136	1.077	1.028	0.996	0.971	0.947	0.935
15	2.072	1.759	1.539	1.400	1.294	1.204	1.144	1.104	1.067	1.035	1.016	1.001
14	2.139	1.831	1.619	1.459	1.356	1.274	1.208	1.163	1.121	1.091	1.067	1.056
13	2.215	1.906	1.686	1.517	1.405	1.323	1.256	1.204	1.157	1.139	1.113	1.095
12	2.258	1.947	1.721	1.560	1.428	1.351	1.292	1.238	1.188	1.155	1.136	1.127
11	2.266	1.976	1.738	1.589	1.459	1.376	1.302	1.252	1.204	1.178	1.147	1.144
10	2.303	1.972	1.744	1.581	1.462	1.382	1.313	1.252	1.215	1.187	1.167	1.139
9	2.296	1.952	1.736	1.566	1.451	1.350	1.292	1.237	1.203	1.182	1.143	1.133
8	2.283	1.942	1.717	1.541	1.436	1.347	1.271	1.221	1.179	1.151	1.127	1.108
7	2.208	1.881	1.663	1.492	1.381	1.301	1.230	1.168	1.136	1.102	1.085	1.062
6	2.137	1.793	1.574	1.426	1.318	1.229	1.169	1.123	1.081	1.055	1.026	1.011
5	2.001	1.677	1.470	1.319	1.216	1.135	1.076	1.035	1.008	0.971	0.959	0.938
4	1.848	1.549	1.343	1.215	1.116	1.042	0.995	0.941	0.918	0.899	0.875	0.870
3	1.655	1.383	1.206	1.083	0.997	0.931	0.884	0.845	0.817	0.798	0.780	0.776
2	1.511	1.255	1.081	0.974	0.898	0.831	0.789	0.768	0.745	0.716	0.700	0.693
1	1.538	1.311	1.184	1.092	1.028	0.993	0.936	0.912	0.895	0.892	0.874	0.857
Plate	1.759	1.492	1.313	1.184	1.093	1.026	0.973	0.933	0.902	0.878	0.859	0.845
Axial	1.285	1.300	1.304	1.317	1.313	1.322	1.324	1.318	1.323	1.327	1.334	1.329

Axial node	Fuel plate number											
	13	14	15	16	17	18	19	20	21	22	23	24
24	0.422	0.412	0.402	0.389	0.382	0.365	0.357	0.349	0.335	0.336	0.330	0.337
23	0.365	0.356	0.356	0.346	0.335	0.330	0.326	0.324	0.322	0.320	0.326	0.340
22	0.430	0.422	0.418	0.407	0.405	0.393	0.390	0.382	0.384	0.384	0.388	0.407
21	0.521	0.508	0.497	0.499	0.481	0.481	0.473	0.476	0.482	0.490	0.512	0.544
20	0.598	0.591	0.583	0.573	0.569	0.577	0.583	0.593	0.613	0.637	0.678	0.764
19	0.687	0.676	0.675	0.675	0.672	0.679	0.683	0.703	0.723	0.773	0.850	0.960
18	0.760	0.747	0.749	0.751	0.745	0.754	0.760	0.788	0.821	0.867	0.945	1.075
17	0.841	0.831	0.823	0.830	0.839	0.842	0.854	0.880	0.927	0.986	1.086	1.227
16	0.916	0.909	0.903	0.895	0.915	0.927	0.943	0.981	1.031	1.109	1.220	1.397
15	0.989	0.986	0.977	0.981	1.000	1.011	1.054	1.098	1.178	1.268	1.415	1.649
14	1.046	1.044	1.028	1.049	1.058	1.082	1.117	1.163	1.254	1.367	1.531	1.776
13	1.083	1.081	1.073	1.083	1.105	1.140	1.176	1.237	1.327	1.452	1.620	1.882
12	1.127	1.119	1.109	1.122	1.146	1.175	1.216	1.283	1.355	1.487	1.666	1.939
11	1.135	1.132	1.128	1.138	1.163	1.188	1.230	1.295	1.384	1.517	1.692	1.957
10	1.133	1.133	1.136	1.151	1.158	1.189	1.233	1.298	1.381	1.504	1.696	1.981
9	1.117	1.105	1.116	1.128	1.149	1.173	1.219	1.277	1.349	1.490	1.671	1.935
8	1.094	1.086	1.092	1.101	1.110	1.146	1.188	1.247	1.334	1.455	1.623	1.892
7	1.056	1.036	1.052	1.058	1.075	1.103	1.141	1.198	1.283	1.391	1.561	1.821
6	1.006	0.999	1.001	1.012	1.027	1.044	1.083	1.147	1.216	1.329	1.496	1.757
5	0.935	0.931	0.934	0.945	0.955	0.972	1.005	1.059	1.133	1.239	1.387	1.642
4	0.856	0.857	0.855	0.861	0.877	0.904	0.939	0.982	1.053	1.147	1.301	1.540
3	0.770	0.765	0.772	0.771	0.786	0.799	0.835	0.878	0.943	1.046	1.186	1.404
2	0.685	0.684	0.686	0.689	0.702	0.720	0.758	0.800	0.859	0.946	1.083	1.305
1	0.852	0.845	0.837	0.847	0.859	0.867	0.884	0.922	0.964	1.035	1.142	1.325
Plate	0.835	0.828	0.826	0.830	0.839	0.853	0.877	0.914	0.967	1.046	1.162	1.344
Axial	1.333	1.342	1.349	1.360	1.360	1.368	1.379	1.393	1.404	1.424	1.433	1.447

Table A-8. MURR fuel element 8 peaking factor for the maximum burnup core (CB=44 cm)

Axial node	Fuel plate number											
	1	2	3	4	5	6	7	8	9	10	11	12
24	0.760	0.663	0.605	0.553	0.518	0.486	0.462	0.445	0.429	0.415	0.400	0.390
23	0.783	0.665	0.586	0.515	0.475	0.435	0.406	0.386	0.372	0.363	0.345	0.334
22	0.867	0.749	0.657	0.596	0.538	0.504	0.471	0.447	0.423	0.409	0.396	0.383
21	1.003	0.865	0.771	0.696	0.636	0.594	0.558	0.530	0.502	0.482	0.464	0.454
20	1.070	0.939	0.847	0.764	0.713	0.657	0.614	0.589	0.571	0.539	0.522	0.508
19	1.197	1.057	0.936	0.858	0.796	0.737	0.709	0.672	0.648	0.621	0.598	0.584
18	1.261	1.143	1.033	0.936	0.881	0.827	0.781	0.749	0.709	0.675	0.663	0.645
17	1.412	1.259	1.152	1.057	0.981	0.913	0.865	0.828	0.799	0.770	0.744	0.718
16	1.463	1.340	1.220	1.128	1.057	0.996	0.939	0.902	0.860	0.836	0.811	0.791
15	1.586	1.438	1.321	1.212	1.142	1.064	1.018	0.975	0.944	0.910	0.885	0.873
14	1.621	1.491	1.384	1.280	1.203	1.132	1.072	1.038	0.998	0.964	0.947	0.932
13	1.691	1.553	1.425	1.326	1.245	1.178	1.125	1.082	1.046	1.015	0.995	0.990
12	1.713	1.574	1.455	1.354	1.275	1.203	1.149	1.114	1.085	1.058	1.038	1.027
11	1.732	1.609	1.484	1.373	1.298	1.226	1.173	1.140	1.098	1.085	1.057	1.048
10	1.753	1.636	1.502	1.387	1.300	1.241	1.195	1.150	1.113	1.093	1.069	1.062
9	1.761	1.627	1.499	1.393	1.303	1.242	1.176	1.136	1.106	1.079	1.058	1.046
8	1.787	1.620	1.486	1.377	1.307	1.223	1.169	1.123	1.080	1.061	1.053	1.034
7	1.734	1.584	1.443	1.332	1.250	1.181	1.123	1.085	1.059	1.029	1.009	0.990
6	1.731	1.553	1.415	1.303	1.218	1.145	1.078	1.039	1.012	0.997	0.969	0.962
5	1.615	1.440	1.307	1.200	1.124	1.063	1.008	0.958	0.941	0.911	0.892	0.878
4	1.557	1.381	1.231	1.141	1.059	0.984	0.935	0.904	0.883	0.854	0.847	0.828
3	1.380	1.218	1.102	0.998	0.931	0.864	0.829	0.797	0.770	0.750	0.744	0.736
2	1.268	1.113	0.996	0.910	0.851	0.793	0.742	0.710	0.695	0.676	0.667	0.662
1	1.303	1.176	1.085	1.007	0.963	0.917	0.883	0.874	0.854	0.835	0.818	0.819
Plate	1.623	1.463	1.332	1.225	1.147	1.077	1.024	0.985	0.953	0.926	0.905	0.891
Axial	1.260	1.279	1.290	1.301	1.304	1.319	1.335	1.335	1.336	1.350	1.351	1.364

Axial node	Fuel plate number											
	13	14	15	16	17	18	19	20	21	22	23	24
24	0.374	0.365	0.344	0.336	0.318	0.308	0.293	0.280	0.263	0.249	0.233	0.217
23	0.323	0.308	0.305	0.295	0.281	0.273	0.264	0.256	0.244	0.234	0.222	0.213
22	0.371	0.359	0.349	0.339	0.324	0.315	0.305	0.287	0.277	0.265	0.248	0.229
21	0.438	0.420	0.407	0.394	0.384	0.372	0.357	0.343	0.328	0.307	0.288	0.269
20	0.493	0.478	0.455	0.444	0.434	0.416	0.401	0.384	0.364	0.341	0.313	0.285
19	0.568	0.540	0.529	0.511	0.496	0.481	0.466	0.444	0.423	0.393	0.364	0.334
18	0.618	0.595	0.578	0.563	0.548	0.525	0.508	0.483	0.460	0.427	0.394	0.354
17	0.701	0.678	0.657	0.638	0.616	0.601	0.575	0.557	0.538	0.510	0.470	0.430
16	0.770	0.757	0.737	0.722	0.716	0.700	0.681	0.675	0.657	0.642	0.625	0.603
15	0.857	0.841	0.833	0.828	0.832	0.835	0.845	0.864	0.888	0.930	0.976	1.022
14	0.919	0.912	0.913	0.917	0.933	0.946	0.966	1.000	1.046	1.118	1.204	1.297
13	0.974	0.975	0.973	0.987	1.005	1.016	1.061	1.098	1.149	1.229	1.324	1.440
12	1.013	1.021	1.012	1.021	1.034	1.062	1.095	1.142	1.207	1.281	1.374	1.502
11	1.030	1.025	1.034	1.050	1.061	1.082	1.114	1.175	1.234	1.311	1.419	1.546
10	1.049	1.040	1.047	1.059	1.075	1.089	1.141	1.180	1.255	1.347	1.455	1.576
9	1.037	1.031	1.035	1.046	1.063	1.090	1.126	1.173	1.242	1.333	1.432	1.564
8	1.030	1.023	1.029	1.034	1.050	1.081	1.118	1.176	1.239	1.333	1.445	1.590
7	0.982	0.986	0.987	0.996	1.011	1.047	1.080	1.128	1.201	1.290	1.402	1.538
6	0.946	0.951	0.949	0.959	0.975	1.007	1.037	1.088	1.154	1.246	1.365	1.532
5	0.873	0.874	0.879	0.889	0.907	0.921	0.958	1.011	1.074	1.167	1.278	1.426
4	0.824	0.811	0.818	0.831	0.857	0.868	0.906	0.947	1.009	1.100	1.222	1.379
3	0.732	0.732	0.740	0.746	0.754	0.777	0.809	0.846	0.914	1.000	1.104	1.253
2	0.661	0.664	0.659	0.671	0.680	0.704	0.733	0.774	0.824	0.905	1.024	1.170
1	0.819	0.802	0.799	0.814	0.822	0.832	0.854	0.882	0.920	0.981	1.065	1.188
Plate	0.877	0.867	0.861	0.862	0.866	0.874	0.891	0.915	0.949	0.998	1.060	1.142
Axial	1.368	1.373	1.391	1.406	1.419	1.425	1.464	1.475	1.513	1.544	1.570	1.593

Table A-9. MURR fuel element 1 peaking factor for the extreme burnup core (CB=30 cm)

Axial node	Fuel plate number											
	1	2	3	4	5	6	7	8	9	10	11	12
24	0.846	0.699	0.602	0.545	0.513	0.472	0.449	0.426	0.409	0.394	0.383	0.370
23	0.864	0.688	0.589	0.511	0.466	0.434	0.393	0.369	0.351	0.338	0.323	0.313
22	0.994	0.799	0.666	0.588	0.525	0.484	0.457	0.429	0.410	0.391	0.371	0.361
21	1.137	0.925	0.775	0.680	0.614	0.560	0.530	0.502	0.476	0.459	0.436	0.427
20	1.295	1.024	0.877	0.772	0.702	0.649	0.604	0.576	0.547	0.529	0.518	0.498
19	1.467	1.168	0.999	0.871	0.789	0.739	0.699	0.656	0.629	0.602	0.575	0.550
18	1.647	1.299	1.112	0.987	0.895	0.831	0.771	0.728	0.700	0.668	0.637	0.614
17	1.802	1.447	1.233	1.090	0.988	0.902	0.853	0.802	0.773	0.738	0.701	0.689
16	1.991	1.592	1.351	1.179	1.068	0.995	0.929	0.873	0.824	0.803	0.782	0.754
15	2.154	1.727	1.464	1.296	1.164	1.072	1.003	0.937	0.899	0.870	0.837	0.807
14	2.317	1.862	1.567	1.375	1.244	1.152	1.073	1.003	0.970	0.928	0.894	0.875
13	2.446	1.960	1.681	1.475	1.336	1.229	1.149	1.095	1.033	1.003	0.961	0.928
12	2.553	2.067	1.761	1.544	1.396	1.294	1.213	1.155	1.104	1.068	1.031	1.001
11	2.641	2.152	1.840	1.628	1.475	1.371	1.274	1.223	1.175	1.122	1.085	1.063
10	2.794	2.226	1.888	1.696	1.544	1.427	1.349	1.278	1.224	1.185	1.149	1.131
9	2.886	2.317	1.990	1.754	1.601	1.496	1.394	1.334	1.282	1.246	1.205	1.180
8	2.945	2.364	2.006	1.785	1.620	1.505	1.423	1.355	1.315	1.276	1.241	1.217
7	2.930	2.353	1.996	1.777	1.619	1.512	1.431	1.356	1.310	1.266	1.231	1.217
6	2.852	2.293	1.962	1.739	1.587	1.478	1.385	1.334	1.285	1.253	1.219	1.193
5	2.722	2.209	1.877	1.646	1.521	1.394	1.330	1.265	1.229	1.191	1.164	1.152
4	2.541	2.041	1.732	1.538	1.400	1.306	1.241	1.187	1.137	1.097	1.080	1.070
3	2.282	1.850	1.581	1.400	1.256	1.171	1.117	1.067	1.035	1.009	0.974	0.965
2	2.072	1.678	1.422	1.255	1.155	1.083	1.019	0.968	0.937	0.920	0.892	0.886
1	2.175	1.814	1.581	1.443	1.355	1.287	1.226	1.198	1.158	1.145	1.115	1.098
Plate	2.184	1.759	1.499	1.326	1.207	1.121	1.055	1.003	0.963	0.933	0.902	0.883
Axial	1.404	1.399	1.393	1.401	1.397	1.405	1.413	1.408	1.420	1.425	1.432	1.435

Axial node	Fuel plate number											
	13	14	15	16	17	18	19	20	21	22	23	24
24	0.359	0.346	0.334	0.323	0.311	0.309	0.291	0.282	0.269	0.260	0.257	0.259
23	0.308	0.298	0.286	0.280	0.270	0.262	0.260	0.250	0.245	0.239	0.238	0.242
22	0.353	0.348	0.338	0.325	0.317	0.307	0.299	0.295	0.286	0.280	0.282	0.283
21	0.417	0.404	0.387	0.382	0.376	0.360	0.350	0.341	0.333	0.325	0.322	0.326
20	0.481	0.457	0.450	0.436	0.423	0.410	0.404	0.392	0.387	0.377	0.370	0.376
19	0.535	0.517	0.502	0.485	0.477	0.470	0.452	0.440	0.429	0.421	0.418	0.416
18	0.593	0.577	0.573	0.563	0.536	0.524	0.505	0.499	0.478	0.468	0.464	0.463
17	0.668	0.642	0.632	0.614	0.597	0.580	0.561	0.546	0.529	0.518	0.513	0.514
16	0.735	0.700	0.682	0.676	0.646	0.634	0.615	0.595	0.582	0.570	0.558	0.568
15	0.795	0.770	0.739	0.716	0.702	0.687	0.668	0.643	0.633	0.614	0.605	0.613
14	0.851	0.829	0.804	0.774	0.756	0.732	0.716	0.700	0.686	0.669	0.656	0.661
13	0.908	0.889	0.855	0.837	0.821	0.798	0.771	0.752	0.738	0.722	0.713	0.724
12	0.967	0.945	0.923	0.903	0.876	0.853	0.834	0.816	0.802	0.791	0.785	0.804
11	1.027	1.001	0.975	0.956	0.941	0.932	0.914	0.901	0.892	0.893	0.907	0.958
10	1.099	1.081	1.063	1.051	1.040	1.030	1.036	1.052	1.080	1.113	1.197	1.346
9	1.159	1.146	1.135	1.132	1.142	1.145	1.163	1.209	1.274	1.358	1.524	1.802
8	1.201	1.182	1.178	1.179	1.193	1.216	1.247	1.297	1.370	1.487	1.678	2.013
7	1.201	1.204	1.196	1.196	1.206	1.231	1.258	1.307	1.399	1.530	1.728	2.081
6	1.178	1.168	1.174	1.178	1.181	1.203	1.242	1.290	1.389	1.513	1.725	2.083
5	1.127	1.118	1.123	1.130	1.134	1.166	1.184	1.240	1.333	1.470	1.671	2.017
4	1.053	1.042	1.045	1.057	1.061	1.082	1.115	1.170	1.244	1.375	1.580	1.920
3	0.954	0.952	0.951	0.956	0.966	0.980	1.018	1.065	1.147	1.264	1.453	1.771
2	0.869	0.865	0.859	0.868	0.881	0.899	0.927	0.975	1.046	1.161	1.340	1.638
1	1.090	1.082	1.073	1.077	1.071	1.091	1.113	1.139	1.211	1.291	1.427	1.690
Plate	0.864	0.848	0.836	0.828	0.821	0.820	0.822	0.833	0.858	0.898	0.972	1.109
Axial	1.447	1.478	1.489	1.504	1.530	1.563	1.594	1.635	1.697	1.773	1.850	1.955

Table A-10. MURR fuel element 2 peaking factor for the extreme burnup core (CB=30 cm)

Axial node	Fuel plate number											
	1	2	3	4	5	6	7	8	9	10	11	12
24	0.713	0.610	0.546	0.509	0.470	0.444	0.419	0.406	0.394	0.383	0.363	0.351
23	0.724	0.619	0.535	0.471	0.429	0.404	0.367	0.351	0.335	0.324	0.306	0.298
22	0.811	0.689	0.604	0.545	0.494	0.463	0.436	0.404	0.386	0.374	0.360	0.353
21	0.930	0.798	0.696	0.633	0.573	0.533	0.502	0.480	0.457	0.440	0.418	0.406
20	1.007	0.881	0.774	0.705	0.649	0.597	0.569	0.538	0.516	0.489	0.473	0.461
19	1.129	0.988	0.881	0.795	0.731	0.680	0.641	0.607	0.584	0.552	0.538	0.526
18	1.226	1.084	0.966	0.883	0.800	0.754	0.704	0.675	0.644	0.626	0.601	0.585
17	1.379	1.215	1.087	0.980	0.904	0.843	0.791	0.755	0.725	0.693	0.673	0.646
16	1.458	1.297	1.161	1.065	0.974	0.914	0.857	0.816	0.782	0.746	0.719	0.701
15	1.591	1.404	1.263	1.150	1.060	0.988	0.941	0.891	0.847	0.820	0.786	0.759
14	1.688	1.491	1.341	1.223	1.131	1.061	1.002	0.946	0.911	0.873	0.839	0.809
13	1.802	1.589	1.430	1.313	1.207	1.135	1.071	1.020	0.980	0.943	0.903	0.878
12	1.871	1.662	1.499	1.378	1.284	1.203	1.134	1.074	1.039	0.992	0.956	0.924
11	1.950	1.740	1.579	1.440	1.334	1.259	1.188	1.136	1.087	1.043	1.022	0.984
10	2.045	1.808	1.644	1.501	1.396	1.310	1.252	1.177	1.133	1.116	1.077	1.053
9	2.097	1.869	1.686	1.544	1.448	1.347	1.291	1.226	1.186	1.155	1.131	1.108
8	2.188	1.933	1.748	1.595	1.485	1.390	1.324	1.272	1.229	1.189	1.167	1.139
7	2.149	1.899	1.727	1.581	1.465	1.375	1.318	1.251	1.224	1.189	1.166	1.144
6	2.173	1.926	1.717	1.557	1.448	1.370	1.299	1.250	1.202	1.175	1.150	1.139
5	2.068	1.802	1.624	1.478	1.370	1.287	1.231	1.189	1.146	1.117	1.093	1.073
4	2.001	1.735	1.546	1.415	1.307	1.235	1.180	1.121	1.073	1.056	1.034	1.016
3	1.809	1.566	1.388	1.262	1.172	1.115	1.058	1.012	0.976	0.951	0.927	0.919
2	1.686	1.451	1.302	1.170	1.083	1.010	0.966	0.930	0.886	0.864	0.850	0.831
1	1.731	1.539	1.410	1.318	1.245	1.186	1.143	1.111	1.092	1.065	1.053	1.035
Plate	1.840	1.617	1.452	1.324	1.226	1.151	1.092	1.042	1.003	0.971	0.944	0.921
Axial	1.374	1.381	1.392	1.392	1.399	1.395	1.401	1.411	1.416	1.415	1.428	1.435

Axial node	Fuel plate number											
	13	14	15	16	17	18	19	20	21	22	23	24
24	0.344	0.327	0.320	0.300	0.296	0.284	0.271	0.252	0.241	0.227	0.215	0.199
23	0.292	0.283	0.277	0.267	0.258	0.250	0.241	0.229	0.217	0.209	0.198	0.191
22	0.339	0.328	0.316	0.307	0.303	0.287	0.280	0.265	0.248	0.237	0.226	0.206
21	0.401	0.391	0.375	0.365	0.356	0.347	0.326	0.312	0.293	0.280	0.266	0.245
20	0.449	0.440	0.423	0.409	0.397	0.381	0.363	0.347	0.332	0.310	0.286	0.264
19	0.514	0.493	0.477	0.466	0.452	0.429	0.411	0.389	0.373	0.353	0.326	0.297
18	0.561	0.541	0.524	0.515	0.486	0.472	0.452	0.433	0.409	0.380	0.350	0.319
17	0.630	0.602	0.583	0.562	0.547	0.528	0.507	0.483	0.451	0.421	0.387	0.354
16	0.681	0.656	0.629	0.617	0.588	0.564	0.544	0.521	0.493	0.456	0.418	0.376
15	0.736	0.712	0.693	0.672	0.644	0.616	0.595	0.568	0.536	0.496	0.461	0.412
14	0.788	0.761	0.737	0.720	0.689	0.673	0.639	0.604	0.570	0.535	0.490	0.435
13	0.848	0.820	0.796	0.771	0.744	0.718	0.689	0.650	0.611	0.570	0.529	0.477
12	0.897	0.872	0.856	0.832	0.801	0.772	0.736	0.705	0.664	0.623	0.569	0.524
11	0.952	0.938	0.913	0.888	0.855	0.842	0.819	0.779	0.756	0.712	0.675	0.627
10	1.028	1.014	0.996	0.979	0.963	0.959	0.952	0.948	0.948	0.950	0.965	0.987
9	1.084	1.071	1.069	1.074	1.084	1.083	1.101	1.120	1.173	1.233	1.310	1.425
8	1.123	1.115	1.126	1.128	1.138	1.163	1.193	1.237	1.298	1.380	1.498	1.656
7	1.128	1.134	1.126	1.132	1.143	1.170	1.205	1.246	1.319	1.424	1.555	1.736
6	1.120	1.115	1.109	1.119	1.139	1.159	1.207	1.255	1.336	1.445	1.579	1.787
5	1.072	1.058	1.061	1.065	1.082	1.110	1.146	1.198	1.277	1.373	1.517	1.720
4	1.006	1.001	1.000	1.003	1.026	1.052	1.099	1.143	1.218	1.318	1.471	1.661
3	0.911	0.905	0.907	0.908	0.922	0.947	0.990	1.043	1.111	1.216	1.355	1.557
2	0.823	0.825	0.829	0.839	0.853	0.873	0.910	0.958	1.028	1.119	1.249	1.449
1	1.025	1.017	1.023	1.029	1.043	1.051	1.077	1.104	1.152	1.230	1.332	1.505
Plate	0.903	0.887	0.875	0.865	0.857	0.854	0.854	0.856	0.869	0.890	0.926	0.982
Axial	1.444	1.478	1.488	1.513	1.540	1.583	1.632	1.694	1.776	1.875	1.971	2.102

Table A-11. MURR fuel element 3 peaking factor for the extreme burnup core (CB=30 cm)

Axial node	Fuel plate number											
	1	2	3	4	5	6	7	8	9	10	11	12
24	0.794	0.672	0.591	0.539	0.505	0.474	0.451	0.433	0.423	0.409	0.392	0.379
23	0.817	0.678	0.577	0.515	0.468	0.437	0.399	0.372	0.367	0.354	0.337	0.325
22	0.929	0.774	0.666	0.589	0.533	0.492	0.466	0.446	0.428	0.412	0.393	0.382
21	1.059	0.876	0.764	0.677	0.620	0.579	0.541	0.512	0.493	0.475	0.462	0.450
20	1.158	0.977	0.850	0.760	0.707	0.657	0.615	0.588	0.566	0.549	0.533	0.511
19	1.283	1.089	0.955	0.861	0.800	0.749	0.696	0.666	0.645	0.618	0.600	0.581
18	1.410	1.204	1.059	0.953	0.889	0.821	0.779	0.741	0.706	0.691	0.671	0.656
17	1.615	1.349	1.192	1.086	1.005	0.937	0.870	0.837	0.812	0.781	0.753	0.733
16	1.763	1.507	1.329	1.202	1.106	1.030	0.971	0.931	0.894	0.858	0.834	0.809
15	1.956	1.649	1.452	1.318	1.211	1.133	1.070	1.024	0.984	0.945	0.919	0.897
14	2.110	1.782	1.571	1.417	1.308	1.217	1.145	1.096	1.061	1.008	1.006	0.979
13	2.247	1.903	1.670	1.503	1.391	1.291	1.226	1.177	1.134	1.103	1.086	1.057
12	2.338	1.999	1.766	1.591	1.482	1.379	1.300	1.239	1.196	1.161	1.141	1.106
11	2.428	2.060	1.838	1.647	1.526	1.436	1.352	1.303	1.261	1.217	1.186	1.176
10	2.535	2.150	1.898	1.721	1.574	1.473	1.407	1.354	1.294	1.255	1.232	1.215
9	2.562	2.178	1.913	1.731	1.613	1.500	1.435	1.380	1.329	1.295	1.262	1.236
8	2.628	2.225	1.959	1.767	1.622	1.524	1.440	1.397	1.340	1.311	1.272	1.249
7	2.586	2.182	1.913	1.725	1.598	1.507	1.422	1.368	1.314	1.286	1.269	1.252
6	2.526	2.148	1.882	1.697	1.555	1.464	1.389	1.336	1.286	1.251	1.232	1.208
5	2.401	2.032	1.778	1.599	1.484	1.386	1.337	1.277	1.222	1.195	1.170	1.137
4	2.285	1.903	1.667	1.491	1.377	1.297	1.225	1.176	1.145	1.114	1.078	1.070
3	2.070	1.735	1.506	1.354	1.255	1.168	1.092	1.056	1.031	1.000	0.971	0.960
2	1.911	1.596	1.386	1.235	1.144	1.061	1.008	0.966	0.927	0.897	0.889	0.881
1	1.972	1.707	1.511	1.398	1.310	1.243	1.209	1.170	1.137	1.120	1.099	1.086
Plate	1.873	1.584	1.391	1.254	1.159	1.084	1.025	0.984	0.949	0.920	0.899	0.880
Axial	1.390	1.392	1.396	1.396	1.386	1.393	1.391	1.406	1.399	1.411	1.401	1.408

Axial node	Fuel plate number											
	13	14	15	16	17	18	19	20	21	22	23	24
24	0.369	0.358	0.344	0.329	0.317	0.310	0.297	0.285	0.280	0.273	0.266	0.268
23	0.317	0.310	0.298	0.289	0.281	0.277	0.270	0.268	0.260	0.255	0.260	0.266
22	0.372	0.359	0.351	0.338	0.330	0.324	0.315	0.309	0.306	0.300	0.297	0.304
21	0.427	0.426	0.415	0.403	0.391	0.382	0.378	0.362	0.360	0.355	0.356	0.354
20	0.498	0.484	0.474	0.458	0.448	0.441	0.430	0.422	0.414	0.404	0.404	0.400
19	0.564	0.547	0.532	0.530	0.517	0.506	0.492	0.479	0.476	0.468	0.459	0.461
18	0.637	0.621	0.613	0.599	0.581	0.569	0.555	0.538	0.524	0.517	0.511	0.513
17	0.714	0.693	0.679	0.665	0.656	0.637	0.620	0.614	0.597	0.587	0.576	0.581
16	0.795	0.775	0.754	0.734	0.721	0.716	0.700	0.691	0.678	0.663	0.663	0.670
15	0.877	0.859	0.845	0.823	0.821	0.817	0.814	0.808	0.815	0.828	0.855	0.896
14	0.963	0.946	0.931	0.919	0.920	0.918	0.917	0.924	0.950	0.991	1.052	1.148
13	1.035	1.018	1.012	1.001	1.002	1.006	1.015	1.030	1.056	1.108	1.187	1.317
12	1.091	1.087	1.067	1.067	1.068	1.087	1.081	1.110	1.136	1.213	1.302	1.446
11	1.152	1.131	1.129	1.120	1.124	1.134	1.158	1.185	1.224	1.298	1.402	1.573
10	1.192	1.181	1.170	1.175	1.186	1.194	1.233	1.275	1.333	1.421	1.561	1.768
9	1.227	1.220	1.213	1.224	1.232	1.245	1.282	1.348	1.421	1.527	1.690	1.942
8	1.236	1.232	1.234	1.244	1.260	1.282	1.322	1.380	1.445	1.565	1.747	2.014
7	1.241	1.225	1.222	1.228	1.238	1.267	1.299	1.360	1.440	1.556	1.739	2.000
6	1.204	1.194	1.189	1.196	1.206	1.224	1.267	1.318	1.408	1.533	1.715	1.986
5	1.134	1.123	1.126	1.132	1.145	1.166	1.197	1.259	1.334	1.450	1.628	1.900
4	1.059	1.056	1.053	1.058	1.066	1.095	1.122	1.181	1.258	1.375	1.553	1.813
3	0.947	0.944	0.942	0.947	0.961	0.981	1.013	1.071	1.147	1.252	1.416	1.661
2	0.877	0.872	0.858	0.865	0.882	0.901	0.936	0.971	1.046	1.157	1.304	1.557
1	1.072	1.055	1.058	1.057	1.062	1.077	1.096	1.124	1.186	1.272	1.391	1.589
Plate	0.867	0.855	0.846	0.842	0.843	0.848	0.859	0.880	0.912	0.964	1.045	1.173
Axial	1.418	1.428	1.444	1.463	1.482	1.497	1.525	1.554	1.570	1.607	1.655	1.700

Table A-12. MURR fuel element 4 peaking factor for the extreme burnup core (CB=30 cm)

Axial node	Fuel plate number											
	1	2	3	4	5	6	7	8	9	10	11	12
24	0.713	0.635	0.580	0.546	0.503	0.476	0.455	0.449	0.430	0.413	0.400	0.390
23	0.748	0.639	0.569	0.515	0.467	0.431	0.411	0.393	0.375	0.364	0.348	0.338
22	0.831	0.715	0.638	0.580	0.537	0.498	0.477	0.451	0.431	0.417	0.407	0.393
21	0.938	0.833	0.735	0.683	0.630	0.588	0.556	0.530	0.511	0.494	0.482	0.463
20	0.995	0.891	0.807	0.740	0.694	0.650	0.619	0.594	0.570	0.556	0.540	0.526
19	1.111	0.992	0.909	0.847	0.793	0.757	0.719	0.683	0.657	0.641	0.621	0.607
18	1.170	1.073	0.996	0.925	0.868	0.823	0.781	0.746	0.725	0.714	0.695	0.672
17	1.340	1.226	1.129	1.045	0.982	0.930	0.891	0.861	0.833	0.804	0.782	0.760
16	1.442	1.325	1.228	1.136	1.072	1.022	0.973	0.938	0.904	0.885	0.869	0.840
15	1.583	1.464	1.359	1.267	1.199	1.127	1.082	1.044	1.010	0.993	0.972	0.946
14	1.661	1.541	1.439	1.350	1.278	1.215	1.166	1.128	1.094	1.069	1.049	1.029
13	1.792	1.666	1.554	1.443	1.381	1.316	1.253	1.210	1.168	1.156	1.135	1.128
12	1.844	1.717	1.617	1.505	1.430	1.366	1.310	1.274	1.242	1.204	1.199	1.179
11	1.925	1.804	1.682	1.581	1.482	1.428	1.369	1.337	1.294	1.267	1.245	1.233
10	2.003	1.873	1.749	1.647	1.541	1.475	1.415	1.367	1.332	1.292	1.274	1.269
9	2.053	1.906	1.771	1.655	1.567	1.482	1.406	1.367	1.339	1.309	1.290	1.269
8	2.095	1.937	1.785	1.669	1.580	1.492	1.436	1.398	1.349	1.323	1.297	1.280
7	2.083	1.912	1.754	1.630	1.538	1.447	1.388	1.356	1.315	1.276	1.274	1.253
6	2.099	1.913	1.746	1.614	1.512	1.441	1.377	1.320	1.282	1.261	1.242	1.233
5	1.999	1.785	1.626	1.516	1.418	1.339	1.272	1.243	1.211	1.178	1.164	1.146
4	1.933	1.713	1.562	1.437	1.338	1.260	1.207	1.169	1.133	1.104	1.091	1.082
3	1.741	1.550	1.415	1.303	1.216	1.139	1.088	1.055	1.019	0.996	0.983	0.978
2	1.643	1.459	1.306	1.196	1.105	1.044	1.000	0.967	0.930	0.907	0.886	0.883
1	1.692	1.526	1.433	1.346	1.273	1.218	1.175	1.143	1.119	1.103	1.089	1.077
Plate	1.530	1.393	1.283	1.192	1.120	1.061	1.015	0.982	0.951	0.929	0.913	0.898
Axial	1.346	1.364	1.365	1.373	1.384	1.379	1.388	1.397	1.391	1.397	1.394	1.398
Axial node	Fuel plate number											
	13	14	15	16	17	18	19	20	21	22	23	24
24	0.378	0.369	0.356	0.346	0.337	0.317	0.307	0.291	0.276	0.259	0.247	0.232
23	0.327	0.319	0.312	0.305	0.296	0.285	0.279	0.269	0.256	0.247	0.234	0.223
22	0.382	0.373	0.356	0.348	0.343	0.330	0.319	0.309	0.295	0.283	0.265	0.247
21	0.445	0.435	0.428	0.414	0.405	0.396	0.384	0.370	0.351	0.333	0.315	0.297
20	0.509	0.495	0.482	0.471	0.464	0.449	0.431	0.419	0.395	0.375	0.352	0.319
19	0.593	0.577	0.553	0.548	0.535	0.513	0.499	0.485	0.460	0.438	0.410	0.373
18	0.659	0.640	0.626	0.610	0.601	0.572	0.557	0.534	0.505	0.479	0.443	0.402
17	0.736	0.716	0.703	0.692	0.682	0.662	0.644	0.612	0.584	0.550	0.511	0.466
16	0.822	0.807	0.800	0.780	0.764	0.743	0.722	0.708	0.684	0.649	0.615	0.564
15	0.939	0.922	0.904	0.895	0.893	0.886	0.893	0.891	0.886	0.895	0.895	0.907
14	1.024	1.027	1.006	1.013	1.021	1.034	1.044	1.074	1.094	1.137	1.197	1.262
13	1.107	1.108	1.106	1.111	1.123	1.138	1.177	1.213	1.263	1.317	1.388	1.481
12	1.172	1.167	1.169	1.180	1.203	1.227	1.265	1.297	1.358	1.428	1.508	1.610
11	1.226	1.221	1.218	1.230	1.254	1.280	1.320	1.366	1.432	1.515	1.614	1.741
10	1.250	1.253	1.264	1.279	1.299	1.317	1.374	1.422	1.511	1.613	1.717	1.855
9	1.265	1.263	1.278	1.291	1.316	1.351	1.398	1.464	1.540	1.619	1.744	1.894
8	1.274	1.275	1.291	1.292	1.330	1.358	1.403	1.474	1.551	1.656	1.787	1.951
7	1.255	1.245	1.256	1.271	1.284	1.326	1.373	1.435	1.509	1.625	1.746	1.911
6	1.213	1.211	1.214	1.232	1.254	1.292	1.339	1.408	1.491	1.606	1.744	1.928
5	1.135	1.145	1.145	1.158	1.176	1.204	1.245	1.308	1.384	1.496	1.630	1.810
4	1.073	1.071	1.076	1.082	1.096	1.138	1.176	1.230	1.311	1.419	1.566	1.754
3	0.970	0.956	0.963	0.978	0.991	1.022	1.056	1.105	1.178	1.283	1.412	1.589
2	0.874	0.874	0.879	0.885	0.896	0.927	0.963	1.010	1.087	1.182	1.311	1.496
1	1.061	1.071	1.065	1.066	1.074	1.082	1.115	1.145	1.191	1.262	1.364	1.504
Plate	0.886	0.880	0.877	0.878	0.884	0.893	0.911	0.933	0.964	1.008	1.063	1.137
Axial	1.410	1.421	1.444	1.444	1.475	1.492	1.511	1.549	1.578	1.611	1.649	1.684

Table A-13. MURR fuel element 5 peaking factor for the extreme burnup core (CB=30 cm)

Axial node	Fuel plate number											
	1	2	3	4	5	6	7	8	9	10	11	12
24	0.932	0.769	0.677	0.615	0.577	0.550	0.524	0.504	0.483	0.465	0.461	0.449
23	0.960	0.760	0.647	0.574	0.517	0.493	0.459	0.439	0.415	0.409	0.398	0.389
22	1.093	0.889	0.758	0.662	0.609	0.573	0.534	0.503	0.491	0.475	0.470	0.458
21	1.259	1.014	0.868	0.779	0.709	0.652	0.624	0.598	0.575	0.561	0.547	0.533
20	1.420	1.147	0.981	0.868	0.814	0.756	0.724	0.690	0.668	0.649	0.624	0.621
19	1.590	1.285	1.102	0.997	0.927	0.873	0.828	0.783	0.763	0.741	0.723	0.706
18	1.806	1.448	1.253	1.126	1.039	0.975	0.932	0.897	0.861	0.827	0.819	0.804
17	2.018	1.642	1.422	1.262	1.163	1.088	1.027	0.991	0.958	0.935	0.912	0.900
16	2.241	1.832	1.589	1.406	1.300	1.203	1.150	1.108	1.070	1.045	1.023	0.995
15	2.462	1.999	1.725	1.550	1.421	1.331	1.269	1.221	1.187	1.158	1.125	1.102
14	2.657	2.171	1.870	1.669	1.537	1.450	1.354	1.313	1.271	1.242	1.222	1.210
13	2.824	2.297	1.984	1.784	1.649	1.550	1.466	1.410	1.374	1.342	1.321	1.291
12	2.951	2.399	2.085	1.862	1.708	1.606	1.534	1.470	1.436	1.412	1.387	1.374
11	3.082	2.505	2.178	1.948	1.780	1.673	1.598	1.532	1.487	1.445	1.423	1.417
10	3.173	2.563	2.221	1.992	1.830	1.716	1.634	1.572	1.525	1.491	1.480	1.466
9	3.222	2.608	2.236	2.010	1.855	1.734	1.660	1.600	1.538	1.513	1.489	1.460
8	3.231	2.619	2.253	2.018	1.845	1.720	1.651	1.583	1.526	1.499	1.482	1.467
7	3.192	2.581	2.221	1.976	1.819	1.699	1.609	1.562	1.513	1.486	1.453	1.426
6	3.081	2.487	2.145	1.895	1.749	1.631	1.552	1.491	1.444	1.415	1.394	1.380
5	2.885	2.322	1.999	1.783	1.650	1.540	1.446	1.402	1.352	1.325	1.298	1.280
4	2.675	2.162	1.843	1.650	1.505	1.407	1.339	1.289	1.259	1.228	1.209	1.188
3	2.400	1.968	1.679	1.506	1.364	1.283	1.211	1.164	1.126	1.101	1.081	1.068
2	2.195	1.773	1.510	1.345	1.233	1.147	1.089	1.051	1.014	0.992	0.982	0.962
1	2.256	1.882	1.665	1.524	1.437	1.369	1.326	1.281	1.247	1.233	1.206	1.193
Plate	1.873	1.520	1.310	1.172	1.079	1.011	0.961	0.925	0.895	0.875	0.860	0.847
Axial	1.395	1.393	1.390	1.392	1.390	1.386	1.396	1.399	1.389	1.397	1.399	1.401

Axial node	Fuel plate number											
	13	14	15	16	17	18	19	20	21	22	23	24
24	0.439	0.432	0.418	0.419	0.413	0.410	0.410	0.401	0.405	0.412	0.437	0.484
23	0.383	0.375	0.368	0.361	0.359	0.363	0.366	0.372	0.378	0.396	0.433	0.495
22	0.456	0.446	0.440	0.438	0.433	0.431	0.437	0.440	0.447	0.474	0.507	0.570
21	0.530	0.527	0.518	0.512	0.513	0.498	0.510	0.514	0.527	0.547	0.590	0.666
20	0.611	0.601	0.593	0.590	0.587	0.580	0.592	0.596	0.616	0.643	0.688	0.774
19	0.695	0.684	0.671	0.677	0.672	0.672	0.680	0.686	0.707	0.734	0.802	0.896
18	0.796	0.782	0.772	0.767	0.759	0.761	0.770	0.781	0.803	0.838	0.906	1.014
17	0.893	0.883	0.867	0.857	0.865	0.863	0.866	0.876	0.914	0.944	1.017	1.147
16	0.993	0.977	0.961	0.973	0.970	0.962	0.973	0.992	1.018	1.069	1.153	1.312
15	1.091	1.084	1.077	1.077	1.080	1.084	1.100	1.135	1.167	1.238	1.354	1.559
14	1.196	1.187	1.185	1.180	1.189	1.204	1.232	1.263	1.313	1.414	1.550	1.813
13	1.285	1.271	1.272	1.276	1.275	1.304	1.338	1.377	1.450	1.546	1.713	1.989
12	1.373	1.354	1.342	1.360	1.358	1.372	1.408	1.453	1.543	1.644	1.826	2.144
11	1.415	1.406	1.393	1.393	1.415	1.442	1.481	1.533	1.623	1.739	1.937	2.268
10	1.445	1.441	1.430	1.439	1.461	1.481	1.521	1.586	1.667	1.802	2.032	2.411
9	1.464	1.450	1.456	1.459	1.476	1.498	1.555	1.617	1.726	1.884	2.121	2.553
8	1.436	1.441	1.452	1.457	1.470	1.509	1.562	1.631	1.738	1.911	2.173	2.629
7	1.412	1.414	1.408	1.426	1.454	1.483	1.542	1.614	1.730	1.901	2.165	2.636
6	1.355	1.366	1.360	1.367	1.392	1.416	1.472	1.563	1.675	1.837	2.099	2.551
5	1.283	1.283	1.284	1.296	1.322	1.341	1.394	1.471	1.585	1.736	1.984	2.405
4	1.181	1.179	1.180	1.193	1.213	1.236	1.280	1.347	1.458	1.610	1.848	2.251
3	1.060	1.060	1.060	1.073	1.088	1.124	1.160	1.230	1.318	1.462	1.677	2.054
2	0.955	0.951	0.957	0.964	0.985	1.014	1.055	1.111	1.196	1.326	1.531	1.875
1	1.192	1.187	1.182	1.186	1.196	1.216	1.243	1.284	1.345	1.445	1.608	1.913
Plate	0.840	0.835	0.830	0.833	0.840	0.851	0.874	0.905	0.955	1.029	1.150	1.361
Axial	1.409	1.404	1.418	1.416	1.420	1.434	1.444	1.457	1.471	1.501	1.527	1.566

Table A-14. MURR fuel element 6 peaking factor for the extreme burnup core (CB=30 cm)

Axial node	Fuel plate number											
	1	2	3	4	5	6	7	8	9	10	11	12
24	0.748	0.658	0.586	0.544	0.507	0.483	0.459	0.443	0.434	0.420	0.404	0.395
23	0.777	0.659	0.578	0.512	0.478	0.448	0.416	0.394	0.377	0.361	0.348	0.334
22	0.852	0.732	0.655	0.600	0.534	0.498	0.478	0.448	0.442	0.426	0.415	0.393
21	0.998	0.849	0.768	0.690	0.636	0.594	0.557	0.541	0.516	0.496	0.483	0.472
20	1.065	0.923	0.834	0.758	0.704	0.669	0.634	0.611	0.587	0.572	0.554	0.540
19	1.199	1.061	0.949	0.872	0.803	0.763	0.728	0.697	0.672	0.647	0.636	0.609
18	1.317	1.163	1.043	0.955	0.886	0.841	0.809	0.770	0.740	0.724	0.709	0.690
17	1.468	1.299	1.180	1.082	1.019	0.950	0.901	0.863	0.836	0.814	0.792	0.770
16	1.587	1.411	1.282	1.183	1.109	1.052	0.994	0.972	0.928	0.895	0.869	0.851
15	1.739	1.560	1.423	1.311	1.217	1.148	1.103	1.061	1.027	1.001	0.978	0.969
14	1.860	1.645	1.520	1.406	1.305	1.247	1.193	1.138	1.119	1.091	1.079	1.062
13	1.944	1.753	1.607	1.492	1.405	1.324	1.281	1.232	1.203	1.179	1.152	1.136
12	2.020	1.817	1.678	1.561	1.463	1.385	1.334	1.287	1.260	1.235	1.222	1.202
11	2.098	1.880	1.730	1.621	1.533	1.452	1.397	1.341	1.311	1.281	1.263	1.258
10	2.176	1.957	1.802	1.673	1.559	1.493	1.429	1.388	1.350	1.313	1.305	1.294
9	2.234	2.016	1.840	1.692	1.598	1.499	1.447	1.390	1.364	1.341	1.327	1.312
8	2.285	2.045	1.865	1.724	1.610	1.517	1.458	1.411	1.381	1.344	1.330	1.314
7	2.251	2.005	1.817	1.684	1.572	1.496	1.434	1.374	1.343	1.318	1.305	1.286
6	2.262	2.003	1.820	1.662	1.543	1.450	1.388	1.359	1.310	1.276	1.260	1.247
5	2.119	1.887	1.694	1.564	1.456	1.383	1.310	1.266	1.233	1.198	1.179	1.172
4	2.035	1.774	1.606	1.476	1.366	1.280	1.217	1.184	1.158	1.133	1.111	1.094
3	1.873	1.618	1.454	1.327	1.226	1.160	1.105	1.077	1.039	1.022	1.001	0.984
2	1.697	1.496	1.318	1.195	1.116	1.055	1.000	0.958	0.932	0.917	0.897	0.887
1	1.740	1.560	1.426	1.348	1.271	1.228	1.199	1.173	1.140	1.123	1.098	1.095
Plate	1.598	1.417	1.287	1.186	1.106	1.046	1.001	0.966	0.939	0.916	0.900	0.886
Axial	1.359	1.372	1.379	1.383	1.384	1.378	1.385	1.390	1.398	1.394	1.405	1.410

Axial node	Fuel plate number											
	13	14	15	16	17	18	19	20	21	22	23	24
24	0.376	0.365	0.359	0.346	0.339	0.323	0.309	0.294	0.280	0.265	0.247	0.235
23	0.327	0.321	0.312	0.303	0.299	0.288	0.281	0.273	0.264	0.247	0.239	0.231
22	0.385	0.372	0.363	0.357	0.354	0.338	0.323	0.315	0.303	0.286	0.270	0.254
21	0.453	0.437	0.432	0.422	0.411	0.399	0.388	0.376	0.362	0.348	0.329	0.308
20	0.526	0.515	0.496	0.483	0.474	0.460	0.445	0.429	0.407	0.387	0.367	0.341
19	0.597	0.587	0.575	0.557	0.545	0.534	0.513	0.494	0.476	0.451	0.420	0.393
18	0.675	0.657	0.643	0.626	0.601	0.588	0.563	0.543	0.520	0.492	0.466	0.426
17	0.758	0.750	0.726	0.703	0.680	0.667	0.652	0.627	0.600	0.570	0.536	0.505
16	0.840	0.821	0.815	0.794	0.783	0.759	0.748	0.732	0.701	0.677	0.648	0.611
15	0.941	0.931	0.917	0.919	0.912	0.916	0.911	0.915	0.922	0.936	0.949	0.980
14	1.047	1.038	1.032	1.036	1.045	1.059	1.075	1.112	1.150	1.199	1.274	1.384
13	1.126	1.120	1.124	1.139	1.148	1.162	1.201	1.244	1.293	1.377	1.479	1.626
12	1.186	1.193	1.189	1.201	1.214	1.240	1.285	1.335	1.400	1.489	1.609	1.768
11	1.236	1.241	1.250	1.256	1.278	1.311	1.361	1.415	1.491	1.585	1.735	1.906
10	1.284	1.285	1.296	1.312	1.328	1.362	1.402	1.462	1.548	1.669	1.830	2.046
9	1.304	1.298	1.310	1.320	1.344	1.375	1.423	1.493	1.589	1.699	1.862	2.089
8	1.309	1.302	1.298	1.322	1.339	1.371	1.422	1.496	1.589	1.727	1.894	2.125
7	1.265	1.271	1.279	1.300	1.317	1.357	1.387	1.458	1.556	1.682	1.843	2.075
6	1.251	1.236	1.242	1.255	1.288	1.309	1.359	1.428	1.526	1.649	1.821	2.062
5	1.169	1.164	1.164	1.180	1.199	1.237	1.283	1.348	1.429	1.560	1.718	1.941
4	1.087	1.084	1.098	1.109	1.123	1.150	1.201	1.259	1.349	1.466	1.635	1.878
3	0.976	0.972	0.981	0.987	1.005	1.039	1.077	1.133	1.218	1.341	1.500	1.715
2	0.881	0.882	0.887	0.903	0.918	0.941	0.980	1.042	1.116	1.231	1.383	1.597
1	1.093	1.093	1.093	1.099	1.097	1.122	1.149	1.182	1.246	1.329	1.445	1.615
Plate	0.875	0.869	0.867	0.869	0.873	0.884	0.901	0.927	0.964	1.017	1.089	1.193
Axial	1.422	1.424	1.437	1.447	1.464	1.479	1.502	1.534	1.567	1.615	1.653	1.694

Table A-15. MURR fuel element 7 peaking factor for the extreme burnup core (CB=30 cm)

Axial node	Fuel plate number											
	1	2	3	4	5	6	7	8	9	10	11	12
24	0.789	0.669	0.600	0.546	0.500	0.471	0.452	0.432	0.414	0.410	0.394	0.383
23	0.830	0.676	0.578	0.511	0.461	0.426	0.397	0.375	0.361	0.348	0.337	0.328
22	0.928	0.759	0.654	0.582	0.539	0.495	0.464	0.437	0.415	0.403	0.390	0.381
21	1.058	0.879	0.757	0.670	0.624	0.574	0.539	0.520	0.494	0.480	0.461	0.451
20	1.178	0.974	0.855	0.763	0.696	0.661	0.624	0.589	0.565	0.542	0.533	0.514
19	1.325	1.109	0.971	0.878	0.808	0.755	0.710	0.673	0.648	0.620	0.592	0.584
18	1.482	1.251	1.094	0.996	0.909	0.841	0.792	0.758	0.724	0.696	0.674	0.660
17	1.649	1.409	1.222	1.102	1.016	0.943	0.894	0.841	0.807	0.784	0.760	0.733
16	1.809	1.516	1.347	1.200	1.097	1.025	0.972	0.922	0.888	0.859	0.838	0.819
15	1.961	1.651	1.466	1.307	1.204	1.113	1.067	1.009	0.975	0.942	0.917	0.889
14	2.106	1.802	1.579	1.422	1.298	1.211	1.141	1.092	1.054	1.021	0.993	0.977
13	2.239	1.892	1.665	1.514	1.396	1.291	1.217	1.170	1.133	1.094	1.064	1.045
12	2.322	1.985	1.749	1.590	1.450	1.355	1.285	1.229	1.198	1.166	1.136	1.113
11	2.398	2.059	1.815	1.643	1.514	1.418	1.353	1.293	1.248	1.212	1.179	1.165
10	2.494	2.134	1.880	1.696	1.571	1.476	1.393	1.351	1.305	1.254	1.233	1.217
9	2.557	2.166	1.907	1.721	1.588	1.496	1.433	1.381	1.334	1.292	1.269	1.247
8	2.612	2.221	1.939	1.771	1.623	1.530	1.446	1.386	1.346	1.309	1.285	1.245
7	2.591	2.180	1.919	1.725	1.583	1.483	1.436	1.381	1.323	1.285	1.258	1.242
6	2.552	2.143	1.866	1.699	1.571	1.464	1.388	1.328	1.294	1.249	1.224	1.204
5	2.400	2.037	1.784	1.609	1.486	1.387	1.311	1.251	1.207	1.182	1.159	1.143
4	2.264	1.893	1.662	1.500	1.383	1.298	1.225	1.172	1.145	1.116	1.082	1.069
3	2.054	1.736	1.514	1.356	1.238	1.160	1.101	1.059	1.019	0.992	0.975	0.968
2	1.883	1.573	1.359	1.225	1.128	1.057	0.999	0.955	0.924	0.910	0.890	0.875
1	1.914	1.668	1.508	1.405	1.317	1.260	1.205	1.173	1.141	1.115	1.107	1.084
Plate	1.866	1.578	1.385	1.251	1.151	1.077	1.021	0.978	0.944	0.916	0.894	0.877
Axial	1.381	1.389	1.381	1.396	1.391	1.402	1.397	1.399	1.407	1.410	1.418	1.403

Axial node	Fuel plate number											
	13	14	15	16	17	18	19	20	21	22	23	24
24	0.370	0.360	0.352	0.344	0.329	0.319	0.311	0.295	0.287	0.277	0.272	0.270
23	0.320	0.307	0.303	0.294	0.288	0.280	0.272	0.268	0.262	0.263	0.263	0.276
22	0.367	0.361	0.348	0.342	0.338	0.328	0.321	0.314	0.311	0.304	0.298	0.309
21	0.435	0.423	0.411	0.407	0.396	0.385	0.373	0.366	0.360	0.359	0.349	0.359
20	0.494	0.480	0.469	0.458	0.447	0.444	0.433	0.422	0.414	0.407	0.402	0.405
19	0.569	0.555	0.538	0.523	0.515	0.503	0.488	0.479	0.474	0.468	0.462	0.465
18	0.640	0.622	0.607	0.591	0.580	0.565	0.554	0.541	0.525	0.524	0.510	0.514
17	0.708	0.696	0.678	0.666	0.652	0.636	0.626	0.614	0.604	0.587	0.581	0.587
16	0.790	0.774	0.761	0.743	0.722	0.715	0.701	0.692	0.678	0.676	0.670	0.679
15	0.880	0.865	0.849	0.841	0.828	0.820	0.810	0.815	0.823	0.836	0.856	0.910
14	0.959	0.953	0.936	0.931	0.925	0.915	0.917	0.938	0.962	1.000	1.071	1.178
13	1.032	1.018	1.015	1.012	1.017	1.015	1.019	1.030	1.079	1.116	1.204	1.328
12	1.093	1.080	1.071	1.070	1.065	1.073	1.086	1.109	1.148	1.212	1.302	1.454
11	1.151	1.134	1.135	1.138	1.139	1.146	1.161	1.198	1.238	1.315	1.420	1.591
10	1.200	1.196	1.191	1.183	1.186	1.200	1.222	1.273	1.349	1.442	1.570	1.793
9	1.237	1.223	1.219	1.225	1.231	1.253	1.292	1.339	1.425	1.533	1.696	1.956
8	1.241	1.239	1.232	1.242	1.265	1.285	1.318	1.367	1.451	1.590	1.758	2.036
7	1.240	1.227	1.224	1.226	1.245	1.277	1.314	1.366	1.453	1.576	1.746	2.026
6	1.193	1.190	1.184	1.193	1.208	1.238	1.274	1.326	1.414	1.546	1.730	2.014
5	1.137	1.129	1.125	1.135	1.152	1.174	1.212	1.261	1.356	1.458	1.653	1.916
4	1.060	1.058	1.052	1.064	1.077	1.102	1.140	1.201	1.273	1.382	1.559	1.832
3	0.951	0.958	0.955	0.958	0.971	1.005	1.042	1.080	1.160	1.262	1.428	1.692
2	0.867	0.851	0.868	0.864	0.891	0.910	0.946	0.988	1.065	1.163	1.325	1.586
1	1.073	1.074	1.075	1.072	1.081	1.097	1.118	1.154	1.206	1.294	1.425	1.642
Plate	0.864	0.854	0.847	0.844	0.845	0.850	0.861	0.881	0.918	0.970	1.050	1.185
Axial	1.418	1.432	1.435	1.452	1.478	1.491	1.510	1.530	1.563	1.618	1.651	1.695

Table A-16. MURR fuel element 8 peaking factor for the extreme burnup core (CB=30 cm)

Axial node	Fuel plate number											
	1	2	3	4	5	6	7	8	9	10	11	12
24	0.682	0.601	0.546	0.504	0.470	0.435	0.420	0.398	0.389	0.368	0.359	0.347
23	0.695	0.594	0.518	0.471	0.431	0.393	0.375	0.362	0.339	0.322	0.316	0.298
22	0.768	0.680	0.597	0.540	0.492	0.455	0.433	0.413	0.391	0.377	0.365	0.350
21	0.892	0.778	0.697	0.628	0.575	0.523	0.493	0.476	0.454	0.438	0.429	0.409
20	0.956	0.846	0.765	0.696	0.641	0.602	0.565	0.536	0.515	0.493	0.474	0.460
19	1.092	0.966	0.868	0.796	0.731	0.681	0.640	0.603	0.581	0.566	0.539	0.519
18	1.152	1.051	0.944	0.856	0.797	0.734	0.689	0.657	0.637	0.616	0.596	0.568
17	1.266	1.151	1.057	0.960	0.883	0.827	0.780	0.741	0.708	0.681	0.665	0.636
16	1.338	1.216	1.112	1.033	0.952	0.892	0.842	0.801	0.772	0.740	0.716	0.690
15	1.455	1.327	1.209	1.123	1.038	0.966	0.921	0.879	0.846	0.799	0.777	0.752
14	1.524	1.401	1.292	1.184	1.114	1.030	0.981	0.934	0.898	0.854	0.823	0.797
13	1.622	1.493	1.366	1.258	1.183	1.107	1.053	0.994	0.960	0.918	0.885	0.858
12	1.677	1.546	1.422	1.310	1.227	1.149	1.095	1.046	1.008	0.969	0.937	0.903
11	1.739	1.603	1.483	1.371	1.291	1.222	1.150	1.104	1.062	1.023	0.993	0.965
10	1.833	1.699	1.570	1.434	1.345	1.275	1.215	1.158	1.118	1.082	1.061	1.033
9	1.893	1.740	1.604	1.475	1.390	1.316	1.253	1.200	1.172	1.132	1.101	1.080
8	1.977	1.806	1.666	1.534	1.430	1.349	1.282	1.238	1.199	1.182	1.155	1.135
7	1.958	1.789	1.645	1.519	1.425	1.347	1.286	1.233	1.199	1.178	1.146	1.133
6	2.002	1.812	1.652	1.523	1.415	1.330	1.273	1.206	1.173	1.151	1.134	1.116
5	1.894	1.715	1.559	1.438	1.336	1.262	1.199	1.156	1.119	1.095	1.063	1.062
4	1.856	1.659	1.506	1.364	1.273	1.199	1.134	1.097	1.056	1.038	1.020	1.004
3	1.674	1.485	1.339	1.239	1.145	1.087	1.034	0.986	0.959	0.937	0.909	0.907
2	1.586	1.396	1.247	1.131	1.048	0.991	0.936	0.911	0.877	0.852	0.835	0.824
1	1.633	1.486	1.367	1.280	1.232	1.161	1.131	1.093	1.069	1.056	1.036	1.027
Plate	1.739	1.575	1.436	1.319	1.230	1.154	1.097	1.050	1.014	0.983	0.956	0.934
Axial	1.366	1.366	1.377	1.380	1.380	1.387	1.392	1.400	1.404	1.428	1.433	1.443

Axial node	Fuel plate number											
	13	14	15	16	17	18	19	20	21	22	23	24
24	0.340	0.327	0.317	0.307	0.294	0.281	0.269	0.261	0.241	0.223	0.208	0.194
23	0.283	0.279	0.275	0.265	0.256	0.248	0.239	0.230	0.220	0.209	0.200	0.188
22	0.339	0.326	0.316	0.306	0.296	0.280	0.276	0.261	0.249	0.234	0.223	0.202
21	0.397	0.380	0.367	0.365	0.346	0.329	0.320	0.308	0.292	0.274	0.254	0.233
20	0.442	0.428	0.416	0.403	0.383	0.370	0.356	0.336	0.318	0.297	0.268	0.247
19	0.502	0.483	0.469	0.460	0.439	0.421	0.406	0.390	0.365	0.345	0.318	0.284
18	0.555	0.540	0.519	0.496	0.482	0.465	0.445	0.420	0.397	0.369	0.334	0.295
17	0.612	0.594	0.577	0.558	0.545	0.514	0.498	0.469	0.436	0.410	0.375	0.330
16	0.667	0.645	0.627	0.610	0.587	0.562	0.537	0.509	0.476	0.439	0.396	0.352
15	0.728	0.701	0.676	0.661	0.637	0.615	0.585	0.555	0.521	0.483	0.434	0.383
14	0.775	0.760	0.722	0.698	0.681	0.648	0.622	0.593	0.548	0.507	0.456	0.406
13	0.834	0.801	0.776	0.753	0.724	0.698	0.670	0.635	0.597	0.558	0.504	0.445
12	0.878	0.856	0.831	0.803	0.777	0.748	0.715	0.683	0.641	0.596	0.540	0.483
11	0.939	0.916	0.892	0.871	0.843	0.827	0.798	0.767	0.734	0.688	0.637	0.579
10	1.011	0.995	0.984	0.962	0.951	0.942	0.938	0.933	0.923	0.921	0.916	0.910
9	1.060	1.057	1.056	1.049	1.051	1.066	1.080	1.111	1.145	1.196	1.257	1.323
8	1.118	1.100	1.102	1.111	1.122	1.145	1.173	1.214	1.275	1.348	1.441	1.546
7	1.105	1.107	1.112	1.111	1.123	1.150	1.185	1.230	1.297	1.377	1.479	1.605
6	1.098	1.097	1.097	1.113	1.124	1.162	1.191	1.244	1.310	1.397	1.517	1.677
5	1.043	1.041	1.037	1.060	1.077	1.098	1.141	1.191	1.251	1.348	1.466	1.616
4	0.993	0.986	0.985	0.998	1.016	1.034	1.084	1.133	1.205	1.297	1.428	1.597
3	0.899	0.908	0.902	0.911	0.921	0.944	0.992	1.028	1.095	1.187	1.304	1.459
2	0.817	0.816	0.815	0.822	0.836	0.860	0.900	0.947	1.011	1.110	1.227	1.401
1	1.018	1.015	1.012	1.009	1.017	1.036	1.056	1.092	1.141	1.203	1.298	1.434
Plate	0.913	0.898	0.885	0.876	0.867	0.863	0.865	0.868	0.875	0.891	0.914	0.949
Axial	1.454	1.464	1.492	1.509	1.538	1.598	1.635	1.702	1.777	1.861	1.970	2.097

APPENDIX B TARGET ASSEMBLY LINEAR POWER



Table B-1. Target assembly linear power for the maximum burnup core (CB=44 cm)

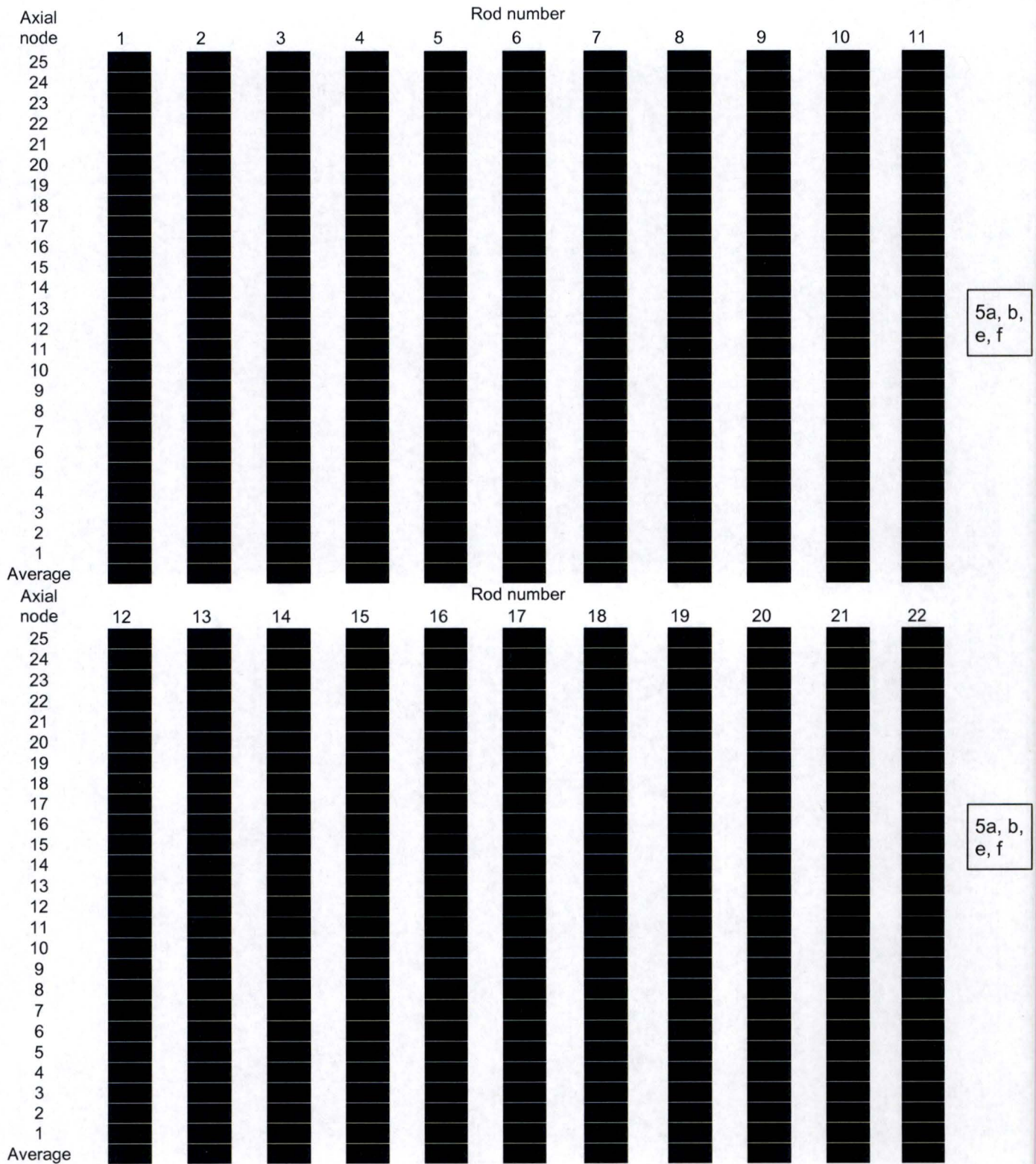


Table B-2. Target assembly linear power for the average burnup core (CB=40 cm)

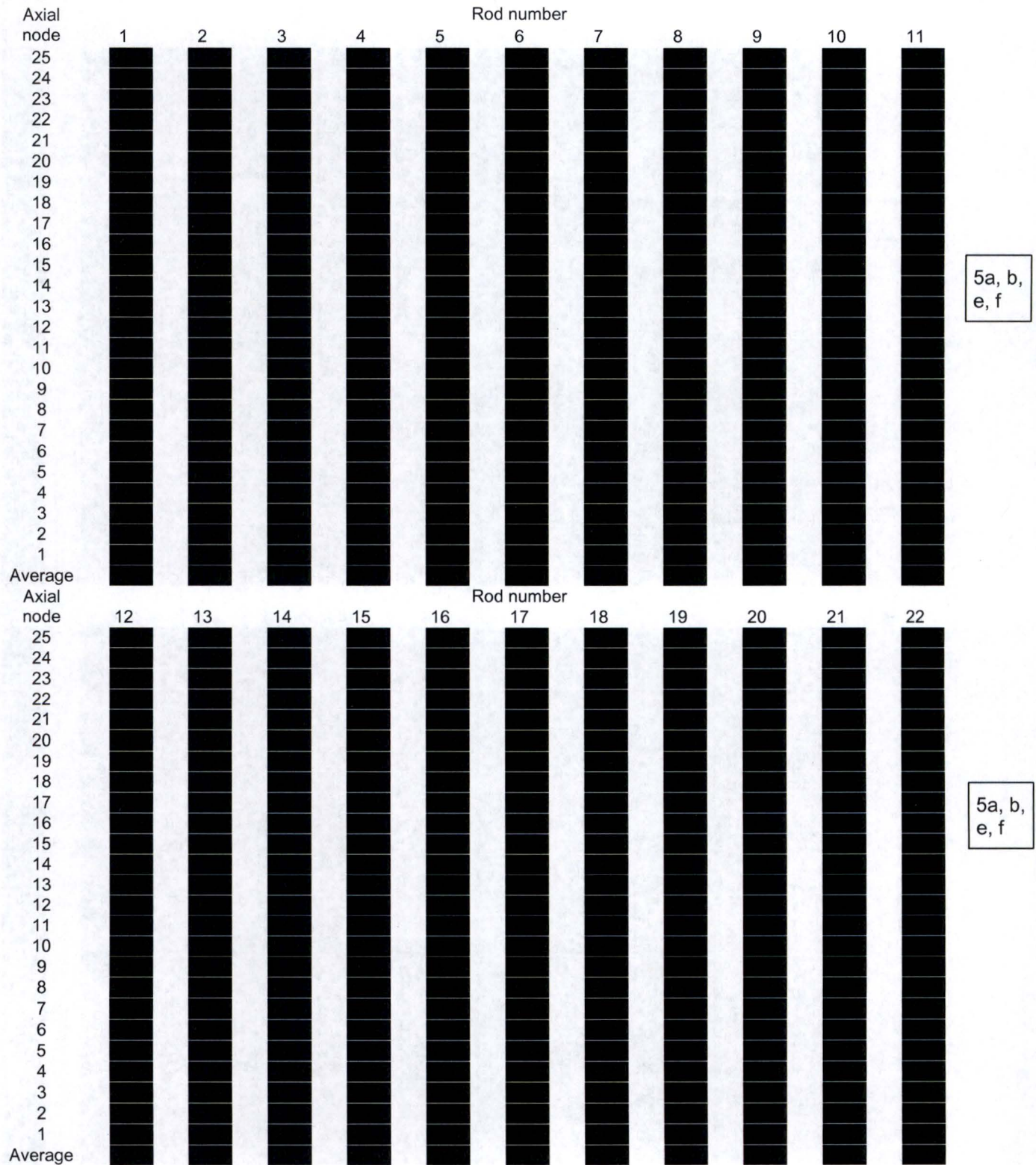


Table B-3. Target assembly linear power for the minimum burnup core (CB=30 cm)

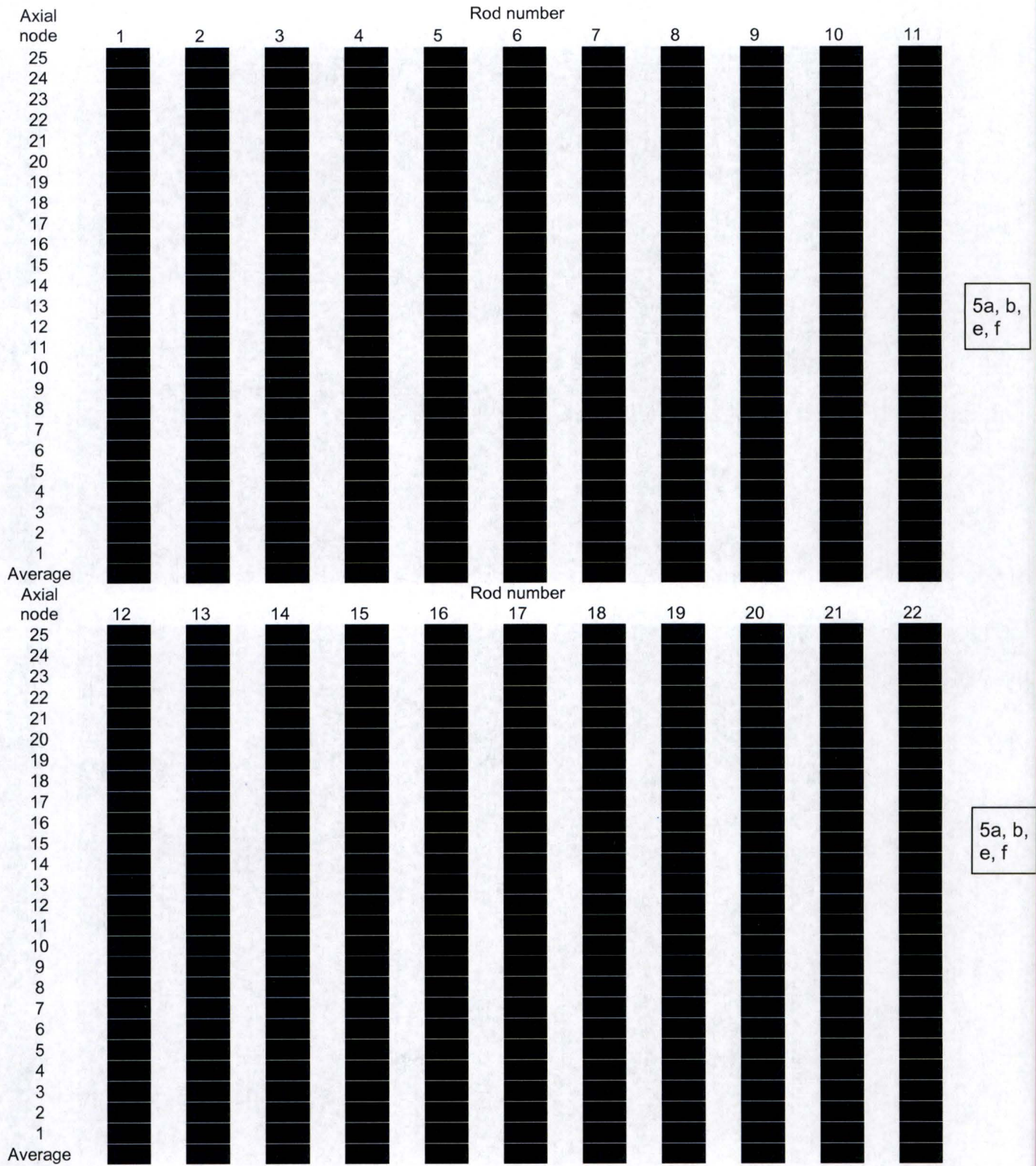
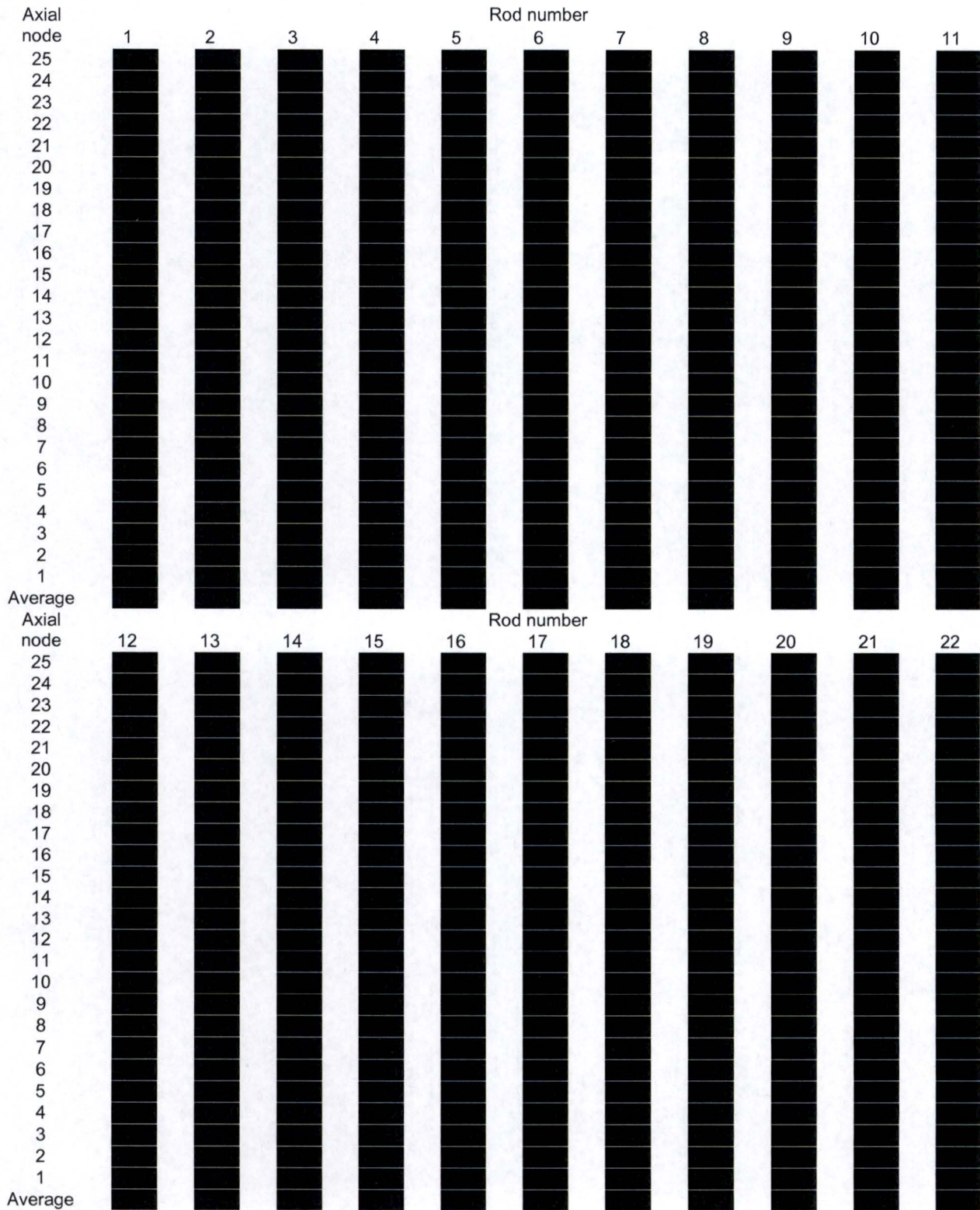


Table B-4. Target assembly linear power for the extreme burnup core (CB=30 cm)



5a, b,
e, f

5a, b,
e, f



GENERAL ATOMICS

P.O. BOX 85608 SAN DIEGO, CA 92186-5608 (858) 455-3000